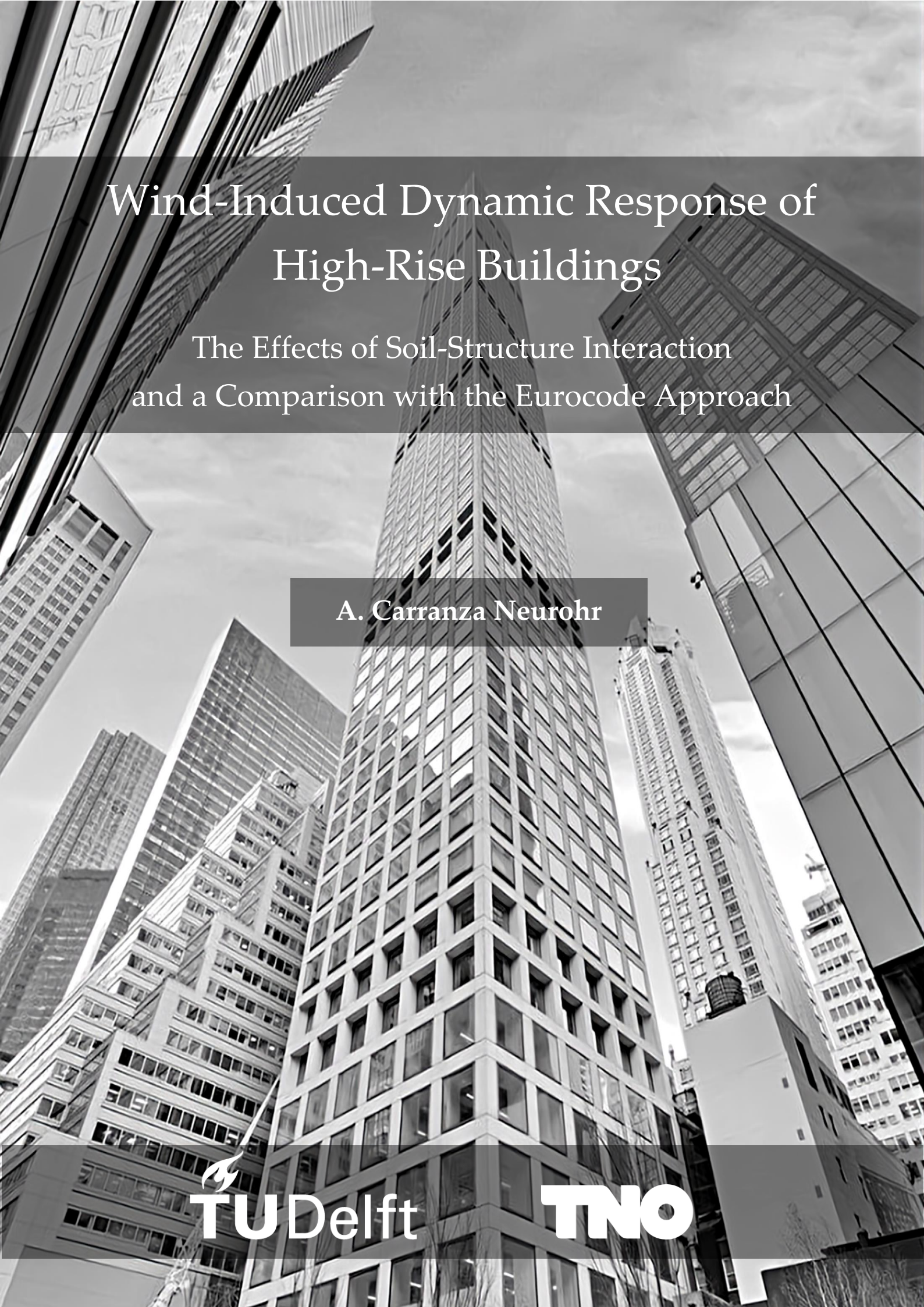

Wind-Induced Dynamic Response of High-Rise Buildings

The Effects of Soil-Structure Interaction and a Comparison with the Eurocode Approach

A. Carranza Neurohr

TU Delft

TNO

Wind-Induced Dynamic Response of High-Rise Buildings

The Effects of Soil-Structure Interaction and a Comparison with the Eurocode Approach

By

A. Carranza Neurohr

in partial fulfilment of the requirements for the degree of

Master of Science

in Civil Engineering

at the Delft University of Technology,
to be defended publicly on August 25, 2022, at 11:00 AM.

Faculty of Civil Engineering and Geosciences
Masters: Civil Engineering
Track: Structural Engineering
Specialisation: Structural Mechanics
Annotation: Structural Dynamics

In collaboration with:

Student number:	5215307	
Project duration:	November 15, 2021 - August 25, 2022	
Thesis committee:	Dr. Ir. K.N. van Dalen,	TU Delft, Chair
	Dr. Ir. S. Sánchez Gómez,	TU Delft, supervisor
	Ir. J.S. Hoving,	TU Delft, supervisor
	Ir. A.J. Bronkhorst	TNO, daily supervisor

Preface

This thesis was developed in order to meet the graduation requirements for the Delft University of Technology's Civil Engineering Master's program in Structural Engineering with a specialisation in Structural Mechanics. The study was carried out as a part of the HiViBe initiative, which studies the vibrations of high-rise buildings in the Netherlands. The HiViBe Project has many contributing partners from the building and research industry. For additional information on the HiViBe project, check the project's webpage[1]. This thesis was done in collaboration with TNO, Besix and Fugro.

During my work experience in structural engineering design, I have always gravitated toward high-rise building design. Even in my motivation letter to apply to the TU Delft, I had already stated that I wanted to do a thesis on the analysis and modelling of the dynamic behaviour of high-rise buildings. The dynamics courses I took during my MSc only reinforced my appreciation for the dynamic analysis of high-rise buildings. I contacted TNO, and was fortunate that they were working on the HiViBe research project, which studied the dynamic behaviour of high-rise buildings in the Netherlands. I was thrilled to work on the dynamics of high-rise buildings. However, my thesis topic would also require complex soil modelling, wind modelling and python programming; subjects and skills I had limited experience in my studies or work. After overcoming all these challenges and learning these new skills, I am glad I undertook this challenging thesis topic, which undoubtedly made me grow as a more well-rounded engineer.

I sincerely want to thank TNO and my colleagues at TNO. It was invaluable working on my thesis and having access to experts in any field that I encountered troubles. I especially want to thank Okke Bronkhorst and Davide Moretti for always taking their time to teach, help and advise me throughout the thesis process. I am also grateful that Karel van Dalen, Sergio Sánchez, and Jeroen Hoving were on my assessment committee. Their extensive knowledge gave me the guidance I needed to meet the high standards I had placed for myself. Additionally, the external advisors: Flip from Fugro and Xavier from Besix, provided important information and knowledge that helped ground the project to what is essential to the industry.

Last but most definitely not least, I would like to thank my family, which is of utmost importance when studying outside your country. Especially my mom and dad for always supporting me and being there for me. I am also grateful to my brothers Ale and Luigi, as well as my uncle Erich. As the structural engineers in my family, they always served as the first to hear about my crazy ideas regarding studies and thesis and were there to support me as I made some of my most crucial choices.

Andres Carranza Neurohr

Delft, August 2022

Abstract

In the Netherlands, there is an increasing need to create residential spaces in its already crowded cities to accommodate the growing population. Constructing high-rise buildings is one way to try to solve the issue. However, high-rise buildings are sensitive to wind-induced vibrations. The accurate prediction of the dynamic response is important in high-rise building design. In building design practice, calculating the dynamic response of high-rise buildings under wind loading typically involves simplifying the structure as a single degree of freedom system, characterised by the first eigenmode properties and subjected to a white noise spectrum. The damping and natural frequency of the building substantially impact its dynamic response. These parameters are challenging to predict with accuracy. Additionally, in the presence of soft soils, soil-structure interaction can play an important role in energy dissipation and influence the structure's natural frequency. In practice, soil-structure interaction is either disregarded or simplified.

In order to assess the effect of soil-structure interaction on the dynamic response of the building, this study models in a robust manner: the foundation, the tower structure, and the wind load. This newly developed model is addressed as the HF model. The investigation consists of a case study and a parametric study. Additionally, this study compares the predictions by the newly developed model with those obtained with a model as specified in the Eurocode. The case study provides a comparison between the models and the measured dynamic response of the New Orleans Tower. The parametric study looks into the influence of soil stiffness and material damping on the dynamic response of high-rise buildings. Furthermore, it investigates how these parameters affect the dynamic response of structures with various slenderness ratios.

The case study was used to demonstrate that the developed model accurately predicts the measured dynamic response of the New Orleans Tower in the along-wind direction. For all the examined dynamic properties, the error compared with the measurements was lower than 7%. In the case of the Eurocode model, the results demonstrate that, when using the natural frequency estimation recommended by the Eurocode, it provides a 30%–35% underestimation of the peak acceleration compared to measurements. This Eurocode model overestimates the natural frequency and overall damping, which causes it to underestimate peak acceleration. However, the natural frequency determined in the design phase of the New Orleans Tower was significantly lower than the value obtained with the recommended estimation method in the Eurocode. With this lower natural frequency, the peak acceleration is overestimated by around 50%. This underestimation of the natural frequency and overestimation of the damping provided acceptable conservative results. Although this showcases the importance of accurate predictions of both natural frequency and damping, having poor predictions that cancel out each other’s effects is not desirable.

The results from the parametric study support the findings from the case study. This shows that the case study’s findings apply to the more extensive range of building configurations investigated in the parametric study. In general, the Eurocode model, for slender structures on soft soil, overestimates the natural frequency and overall damping, which causes it to underestimate peak acceleration.

The parametric study revealed that the building's first natural frequency and global damping ratio are significantly influenced by the soil stiffness and soil material damping, which can

result in various effects on the peak acceleration. In the case of soil material damping, not considering it at all or considering a higher value could lead to 20% overestimation and 40% underestimation of peak acceleration, respectively. Soil stiffness had more intricate effects since it affected the natural frequency and the amount of energy dissipated by the soil radiation damping, the soil material damping and the structure material damping. For particular combinations of parameters, soil stiffness had up to a 40% increase in the peak accelerations compared to the fixed foundation.

The results of this research show that the soil stiffness and soil material damping, for the ranges of properties relevant to the Netherlands, significantly influence the accurate predictions of the wind-induced dynamic response of high-rise buildings. Especially, there was found a higher influence on the dynamic response for the extreme cases of high slenderness ratio structures on very soft soils.

Keywords: High-Rise Buildings, Wind-induced Dynamic Behaviour, Soil-Structure Interaction Effects, Stochastic Frequency Domain Dynamic Analysis, Modelling of Building in Soft Soils, SSI

Contents

List of Symbols

Symbol	Description	Units
A	Area of face perpendicular to wind direction	m^2
B	Width of the Structure	m
C_D	Drag coefficient	-
C_p	Local dynamic pressure coefficient	-
C_{pF}	Front pressure coefficient	-
C_{pB}	Back pressure coefficient	-
EI	Bending stiffness of the section	N m^2
f	Frequency	Hz
f_n	Natural frequency of clamped model	Hz
$f_{n,EC}$	Eurocode natural frequency approximation	Hz
$\widetilde{f_n}$	Natural frequency with SSI	Hz
f_0	Central frequency	Hz
g	Gravitational constant	m/s^2
H	Height of the structure	m
H_w	Lateral mechanical admittance	m/Hz
$H_{\dot{w}}$	Lateral mechanical mobility	m/s/Hz
$H_{\ddot{w}}$	Lateral mechanical accelerance	m/s^2/Hz
H_{tilt}	Tilt transfer function	m/s^2/Hz
H_a	Apparent acceleration transfer function	m/s^2/Hz
h	Height of the centre of mass for the mode shape	m
I_v	Wind turbulence intensity	-
K_z	Effective modal mass factor from Eurocode	-
K_s	Wind size reduction function from Eurocode	-
$\overline{\overline{K}}_d$	Complex dynamic stiffness matrix	-
$\widetilde{K}_{tt}$	Translational component of the dynamic stiffness matrix	N/m
$\widetilde{K}_{rr}$	Rotational component of the dynamic stiffness matrix	N m/rad
$\widetilde{K}_{tr}$	Coupling component of the dynamic stiffness matrix	N/rad
k	Structure's modal stiffness	N/m
k_x	Soil translational stiffness	N/m
k_{yy}	Soil rotational stiffness	N/rad
L_t	Characteristic length	m
M	Total mas of the building	kg
m_n	Modal effective mass	kg

n	Section number	-
q	Aerodynamic pressure	Pa
$S_{\tilde{v}\tilde{v}}$	Spectral density function at the natural frequency	N^2/Hz
T	Duration of the event	s
T_F	Period of fixed model	s
$\tilde{T}$	Period of model with SSI	s
t	Time variable	s
$\bar{v}$	Mean wind velocity	m/s
$\tilde{v}_{\parallel}$	Wind fluctuations parallel to the mean value	m/s
$\tilde{v}_{\perp}$	Wind fluctuations orthogonal to the mean value	m/s
v_b	Reference wind speed at 10 m of height	m/s
w	Deflection of the beam element	m
$\ddot{w}_e$	Expected acceleration	m/s^2
x	Horizontal coordinate, in direction of the wind	m
z	Vertical coordinate	m
z_0	Surface roughness length of surrounding terrain	m
z_s	Reference height of the structure	M
z_t	Characteristic roughness	m
ε	Beam strain	m/m
ζ	Global damping ratio	-
ζ_n	Modal damping ratio	-
ζ_s	Superstructure structural damping ratio	-
ζ_m	Soil material damping ratio	-
ζ_x	Soil radiation damping ratio from translation	-
ζ_{yy}	Soil radiation damping ratio from rotation	-
η	Imaginary stiffness damping coefficient	-
θ_H	Transfer function phase angle	rads
κ	Beam curvature	rads/m
ρ_a	Density of air	kg/m^3
σ_v	Wind speed fluctuations standard deviation	m/s
σ_a	Apparent acceleration standard deviation	m/s^2
ρA	Beam density area of the cross section	kg/m
Φ	Mode shape	-
ϕ	Beam rotation angle	rads
χ^2	Aerodynamic admittance	-
ω	Angular frequency = $2\pi f$	rads/s

$\mathcal{F}$	Fourier transform operator	-
$\mathcal{F}^{-1}$	Inverse Fourier transform operator	-
$\otimes$	Convolution operator	-

1

Introduction

1.1 Background

Due to the rise in population, the Netherlands must increase the number of residential spaces in already dense cities. One way to achieve this is to construct more high-rise buildings. Architectural requirements with respect to natural lighting set a limit on the platform area of high-rise buildings in the Netherlands. Increasing the height of the buildings with limited platform area leads to slender structures, which under wind loading are prone to a high dynamic response. These wind-induced vibrations of the building can present issues in comfort and structural safety.

In building design practice, the dynamic response of high-rise buildings under wind loading is generally calculated by simplifying the structure as a single degree of freedom system (SDOF), characterised by the first eigenmode properties, subjected to a white noise spectrum. This simplified approach assumes that the resonance response of the first vibration mode governs the maximum dynamic response of a high-rise building, which is a widely accepted assumption. But for this to be accurate, reliable modal properties of the first mode need to be calculated. The Eurocode EN 1991-1-4 [2] recommends procedures that approximate these modal properties such as the natural frequency, mode shapes, modal mass and modal damping, from the type of building. For high rise buildings the EN 1991-1-4 [2] gives the following approximations: natural frequency = 46/H, mode shapes are assumed linear, modal mass is the same as the total mass and modal damping is assigned from a table depending on the material of the structure. In this study, this model is addressed as the EC model.

The EC model presents a big limitation, primarily in the estimation of natural frequency and modal damping. In design practice, the properties such as the modal mass, mode shape and natural frequency are generally calculated from the undamped structure model, often modelled in FEM software. A study by Bronkhorst et al. [3] showed that even with the FEM models, it was common that natural frequencies were underestimated. The natural frequency is closely tied to the wind load calculations, where an underestimated natural frequency will result in a significant overestimation of the wind load and vice versa. Additionally, using this undamped FEM structure model still presents the limitation that it is unable to calculate the modal damping, which means that through this procedure the modal damping cannot be refined, so it ends up being estimated crudely, often just choosing them from tables in codes or empirical formulas. In the case of the estimation of the modal damping when the damping is low (such as in high-rise buildings that is around 0.5%-1.5%), an inaccurate estimate of this parameter has a large influence on the dynamic response.

Bronkhorst et al. [3] showed that the damping estimated by codes or with different empirical predictors can deviate significantly from the measured damping in Dutch high-rise buildings.

Tamura et al. [4] presented that there is a wide variation in the measured damping even on similar high-rise buildings. The spread of damping measurements of similar buildings was different by a factor of 5.7, meaning that if the upper and lower values of measured damping would be used to predict the wind induced acceleration calculations would differ by a factor of around 2.4. Similarly, using a common example of damping overestimation, Smith and Willford [5] showed that this could lead to a 72% increase in the dynamic response.

Soil-Structure Interaction (SSI) or Soil-Foundation-Structure Interaction (SFSI) refers to the mechanical processes that arise when the introduction of the deformability of the soil impacts the behaviour of the system. Gomez [6], [7] found that the damping contribution of the foundation plays an important role, and that this contribution depends on the ratio of the building and foundation stiffness. A smaller relative foundation stiffness, typically observed for buildings on soft soils, results in a larger contribution from the soil to the overall damping. Cruz and Miranda [8] showed that the observed decrease in overall damping with building aspect ratio can be attributed to SSI.

These studies have investigated the influence of SSI on the overall damping, but do not address the effect on the dynamic response, such as the peak acceleration. They also use simplified analytical models for the foundations that do not consider soil layers, soil material damping nor pile foundations. None of these studies corroborate if their models predicted reasonable results under wind loading, in terms of its dynamic response, such as the peak acceleration or the acceleration power spectrum. Finally, there has not been a comparison of the performance of the simplified approach of the Eurocode, to models including SSI.

1.2 Problem statement

An important aspect in the design of high-rise buildings is the accurate prediction of the dynamic response. This dynamic response is sensitive and heavily influenced by the damping and natural frequency of the system. Which are difficult parameters to accurately predict. Additionally, in the presence of soft soils, SSI can play an important role in the energy dissipation and in the natural frequency of the system. So in certain situations SSI should not be disregarded from the impact it may have on the dynamic response of the system.

In practice, SSI is either disregarded or simplified to elastic springs, none of which include the energy dissipated in the ground and foundations. This study looks to model the SSI, the towers structure and the wind load in a more robust way to be able to quantify the impact of this energy dissipation mechanism on the overall dynamic response of the system. Moreover, this study looks to compare the results to those simplified models used in practice and recommended by the Eurocode. This study also introduces a model that uses the procedures described by United States' National Institute of Standards and Technology (NIST)[9], which includes the effects of SSI on the calculation of natural frequency and modal damping. Nevertheless, these methodologies have been developed for seismic conditions, and have not been validated for high-rise buildings under wind loading. In this study, these procedures will be used to modify the natural frequency and modal damping of the EC model, this model is later introduced as the NIST model.

The **goal** of this study is:

Assessment of the influence of soil stiffness and soil material damping on the wind-induced dynamic response of high-rise buildings

1.3 Research questions

To accomplish the goal introduced in the problem statement section, 3 main research questions have been established.

1. How much impact does the soil material damping and soil stiffness have on the resonance frequency, the overall damping and the dynamic response?
2. How do the equivalent SDOF methods of the Eurocode compare with a more rigorous model, with respect to the overall damping, the first natural frequency and the dynamic response?
3. Does the methodologies used in seismic conditions to include the effect of SSI on a SDOF system, apply to high-rise buildings under wind loading?

To support the main research question, 5 sub questions were established.

1. Is the HF model an accurate model for predicting the dynamic response of high-rise buildings under wind loading?
2. How do simplified methods such as the EC model and NIST model compare with the measurements?

These first two questions are addressed in the Case Study in Chapter 4. The New Orleans Tower has synchronous measurements of both wind loading and acceleration of the tower, which provides the opportunity to validate the HF model. These measurements and results from the HF model are also compared with the results from the current and NIST models.

3. How much impact does the soil material damping have on the dynamic properties of the system?
4. How much impact does the soil stiffness have on the dynamic properties of the system?
5. How do simplified methods such as the EC model and NIST model compare with the more rigorous HF model, with respect to the overall damping, the resonance frequency and the dynamic response?

Questions 3–5 are addressed in the Parametric Study in Chapter 5. This section shows how for different structural configurations, the soil material damping properties and soil stiffness can have different effects on the overall damping, the first natural frequency and the dynamic response of the high-rise building. This study also includes the results of the EC model and NIST models, providing a comparison of the different methods.

1.4 Methodology

In the previous chapter, the research questions needed to achieve the objectives of the study were proposed. This chapter describes the methodology used to answer these research questions.

In the first part of the report after the introduction, is a literature review of the important aspects of high-rise buildings, regarding the dynamic response from wind loading. This section is found in chapter 2, and it focuses on assembling the most relevant information from theory and recent studies that explain the state-of-the-art knowledge on high-rise buildings under wind loading.

To study the dynamic behaviour of high-rise buildings under wind loading, a higher fidelity model was developed. The next section of the report concerns with introducing this High Fidelity (HF) model. This section is found in chapter 3, and it introduces the formulation of the three different sub-models of the HF model (the foundation, wind load, and tower structure models) and how they are assembled to form the HF model. This combination of the models is depicted in Figure 1.1. This chapter will also introduce the other models also used in this thesis, the model currently proposed by the Eurocode, and the modifications on the calculation of natural frequency and modal damping as described by NIST [9] to include effects of SSI.

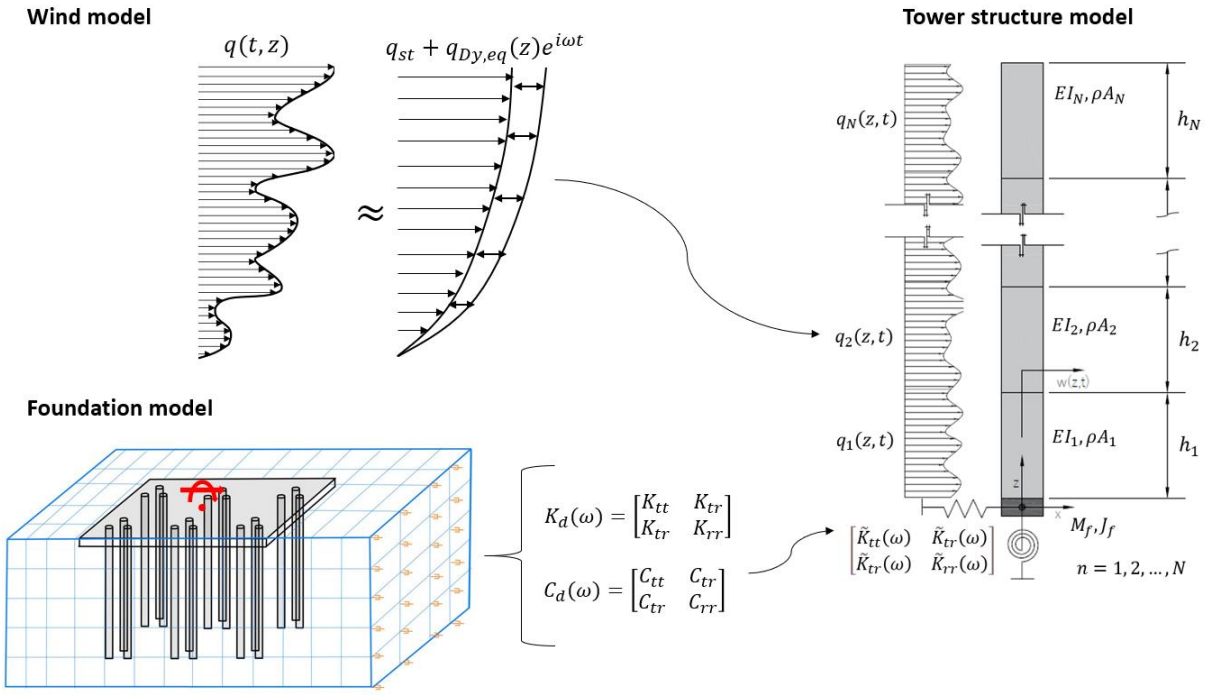

Figure 1.1 Depiction of the assembly of the three-part model (soils, wind and tower) to produce the HF model.

The foundation model was modelled in Dynaplile software, which is a 3D, Boundary Element Method (BEM) and Finite Element Method (FEM) model of the pile foundation and the soil. This model provides the influence of SSI through this foundation dynamic stiffness matrix, which can include material and radiation damping of the soil. The wind load model was programmed in Python, it has an accurate distribution of the mean and fluctuating wind speeds and loads throughout the height of the structure, including their coherence and stochastic nature. The tower model was also programmed in Python, and it computes an analytic solution to a segmented continuous Bernoulli beam model subjected to accurate wind loading and supported by a complex valued foundation dynamic stiffness matrix. The solution of this HF model is obtained through a stochastic frequency domain approach.

This model is first used in the New Orleans tower case study, where measurements of the wind loading and the acceleration response of the structure to the wind loading are used to validate the model. This Case Study is presented in Chapter 4. In this chapter, all the relevant characteristics and parameters from the New Orleans Tower are described. A soil profile of the soil layers and its properties is generated using information from CPT soil tests. The geometric and material properties of the foundation were obtained from the structural plans. The tower structure properties were obtained from a SCIA Engineer model, which was

developed by Besix for application in the HiViBe project [1]. The wind loads are determined from in-situ pressure measurements in the building façade of the New Orleans Tower at the 34th floor. These pressure measurements were obtained only at one floor height, so using the information on wind velocity and the wind theory, they are extrapolated to the complete building. The measurements were separated and grouped by their mean wind speed. Three groups are used: 10m/s to 12m/s, 12m/s to 14m/s, and 14m/s to 16m/s. In this chapter, the results of the HF sub-models and the main model are presented. As well as the results from the dynamic properties from the acceleration measurements, the EC model and the NIST model. The dynamic results presented and compared are the expected peak acceleration, the first natural frequency and the global damping ratio. This chapter serves as both a validation of the HF model as well as an initial comparison with the simplified EC and NIST models. This chapter provides a the discussion and conclusion of its own results.

Chapter 5 presents a parametric study, which investigates soil stiffness and soil material damping and how they affect the dynamic behaviour of the structure. This study was conducted with the three models of interest: the EC model, the NIST model and the HF model. This allows comparing and corroborating the results of the different models. The models in this chapter use system properties from those expected of high-rise buildings in the Netherlands. The base line model, that is subjected to the parametric variations, closely resembles the properties defined in the Case Study. In this chapter, properties such as shear wave velocity and soil material damping were studied for different building heights. The final results of this chapter present, for the three models of interest, the overall damping ratio, the resonance frequency and expected peak acceleration, at the highest point of the building. This chapter provides a the discussion and conclusion of its own results.

Finally, chapter 6 provides the general conclusions of the research. It focuses on answering the research questions. Followed by the recommendations about the conducted study. Lastly, it provides a summary and closing remarks of the study.

1.5 Scope

The study presented in this report answers the specific research questions and achieves the goal proposed in previous chapters under a certain scope. But the extent of this study is bounded by its assumptions and limitations. The assumptions are explained in detail in the body of the report. Some of the most important limitations are the following,

- The developed HF model is only representative for the following:
    - High-rise buildings that are slender enough, where the bending is the governing deformation mechanism,
    - deformations that are small enough that the linear model is an accurate representation,
    - and wind loading and deformation are in along-wind direction.
- The developed HF model was compared with measurements of a single building. Since the measurement set up of synchronous measurements of wind speed, wind pressure and acceleration needed for the validation is a very unique and uncommon measurement configuration, there was only access to the dataset of a single building. Some major characteristics of this building are the following:

  - reinforced concrete shear wall system
  - prefabricated concrete slabs
  - circular concrete pile foundations
  - cemented under soft soils
  - located in a dense urban area
  - and located in Rotterdam, Netherlands

- The magnitude of the events from the measurements is much lower than the one required the SLS. Which means that the models were only compared for lower magnitude events.
- The computational power and modelling complexity limited the inclusion of material nonlinearities (mainly from soil).
- Uncertainties in measurements such as soil CPT tests.
- The assumption of material and geometric properties of the structure and pile foundations from structural plans.

2

Important aspects of wind-induced response of high-rise buildings

This chapter focuses on the most relevant theory and recent studies that explain the state-of-the-art knowledge on high-rise buildings under wind loading. It starts by introducing the various relevant topics present in high-rise buildings under wind loading such as the frequency content of the systems, the amplitude dependency, the impact of damping on the acceleration, the expected displacements and strains, and the damping mechanisms. These sections serve as an introduction to concepts that are regularly referenced and discussed in the rest of the report. Following these sections, the relevance of SSI in the dynamic response of high-rise buildings is explored by looking into further details on the studies briefly mentioned in the introduction chapter. This chapter is accompanied by annex A and B, which cover subjects that were not deemed to be suitable for the body of the report, since they dive into more detail on the theory surrounding damping mechanisms, dynamic soil and SSI behaviour and modelling.

2.1 Resonance frequency and frequency content of the system

One of the main dynamic characteristics to be considered for a dynamic system is its frequency content. To solve a dynamics system, several assumptions need to be made, and knowing which frequencies are relevant in the system helps bound the problem so the correct models, parameters and assumptions can be chosen. Generally, what determines the frequency content of a system is a combination of the frequency content of the force and the sensitivity of the structure for certain frequencies.

For the case wind-induced vibrations, the force is the pressure exerted by the wind. The force is calculated using the wind velocity, this means that the wind velocity frequency content is related to the wind force frequency content. The wind frequency content can be obtained from the measurements, but also from theory. Some common spectra are the modified Kaimal, Davenport, Harris and Simiu (Vrouwenvelder [10]). The frequency spectra of the wind must be modified with the aerodynamic admittance, to determine the frequency spectra of the wind load. The aerodynamic admittance considers the geometry and spatial variation of the local wind pressure.

The sensitivity of the structure for certain frequencies is defined through the transfer function. In this study this transfer function will also be referenced as mechanical admittance. This transfer function is determined by the response of the system with respect to a unitary force. For high-rise buildings the natural frequency of the system and the resonance frequency are considered to be practically equal, since they are extremely underdamped systems.

Figure 2.1, shows a diagram representing the stochastic frequency domain analysis, which also depicts the frequency content of the system. This process is explained in greater detail in annex D.5. The typical relevant frequencies for wind induced vibration for high-rise buildings are between 10^{-2} Hz and 10 Hz.

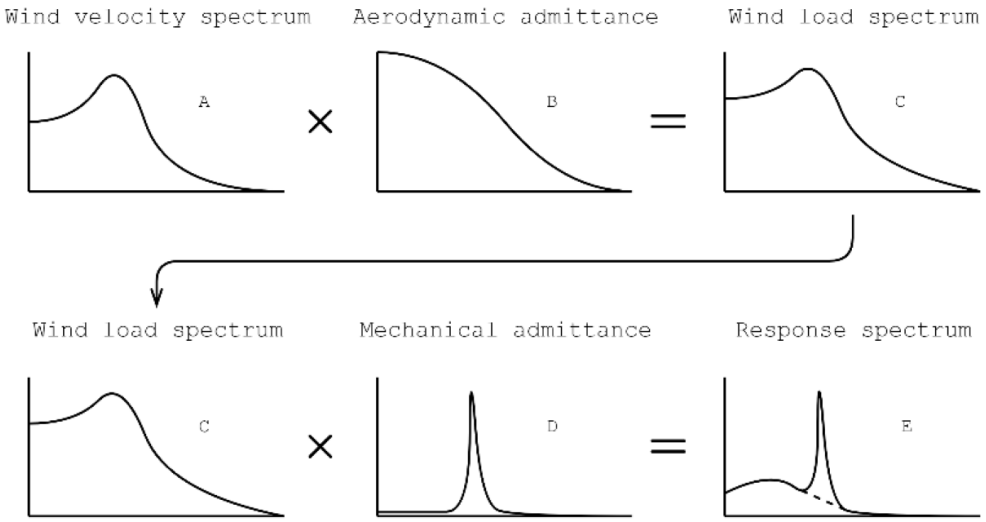

Figure 2.1 Representation of stochastic frequency domain analysis, for a high-rise building under wind loading. Taken from Y. Paauwe [11].

The diagrams show both axis in log scale, which means that the wind load magnitude is very sensitive to changes in frequency. This means that an accurate estimation of the peak frequency of the transfer function is imperative. This peak frequency would correspond to the resonance frequency of the system.

A study by Bronkhorst et al. [3] on 5 Dutch high rise buildings, showed that even with the FEM models, it was common that natural frequencies were underestimated. In Table 2.1, the results of this study are displayed. This table also includes the natural frequency calculations with the current Eurocode. It can be observed that the natural frequencies used in the structural design are on average 43% underestimated. An underestimation of the natural frequency would lead to an overestimation of the loads. The Eurocode approximation of the natural frequency on average has less error, but there is a wider spread of the errors, from 35% underestimation to 17% overestimation with respect to experimental results.

Table 2.1 Estimated natural frequencies compared to measurements

	Hight $[m]$	**Experimental** [Hz]	**Structural design** [Hz]	$\%\boldsymbol{E}$	**Eurocode** $[Hz]$	$\%\boldsymbol{E}$
New Erasmus MC	121	0.52	0.23	-56%	0.38	-27%
Montevideo	140	0.42	0.19	-55%	0.33	-22%
New Orleans	155	0.29	0.19	-34%	0.30	2%
JuBi tower	153	0.46	0.27	-41%	0.30	-35%
Oval tower	98	0.4	0.28	-30%	0.47	17%
		Average error		-43%		-13%

2.2 Impact of global damping on acceleration

For high-rise buildings, one of the most important results that needs to be accurately predicted to avoid are comfort issues are the peak accelerations. Figure 2.2 shows the influence of the damping on the peak acceleration determined by the value for damping given by NEN- EN 1991-1-4 [2] in the doted red line and in black the expected response at different damping levels. Since a small variation from the damping estimation significantly impacts the dynamic response, accurate damping estimation is of great importance. Especially for high-rise buildings where the damping is low where at these damping levels, the system is very sensitive, in other words, a small inaccuracy in the damping estimation can have a large influence on the dynamic response.

From the research by Bronkhorst et al. [3] on 12 Dutch high rise buildings that the damping estimated by codes or with different empirical predictors can deviate significantly from the measured damping in Dutch high-rise buildings. Tamura et al. [4] presented that there is a wide variation in the measured damping on even on similar high-rise buildings. If one was to use the results from measurements as a way to predict damping, this significant variation in damping for high-rise buildings, should be considered. Tamura et al. [4] showed that, if a $\pm\sigma$ from the mean measurement was calculated, the upper and lower bound damping ratios would be different by a factor of 5.7, which meant that the wind induced acceleration calculations would differ by a factor of around 2.4 times. Similarly, Smith and Willford [5] using a common example of damping overestimation, showed a 72% increase in the dynamic response. Because of this, Tamura [4] states that *"accurate evaluation of design damping ratio is a pressing need for tall building design"*.

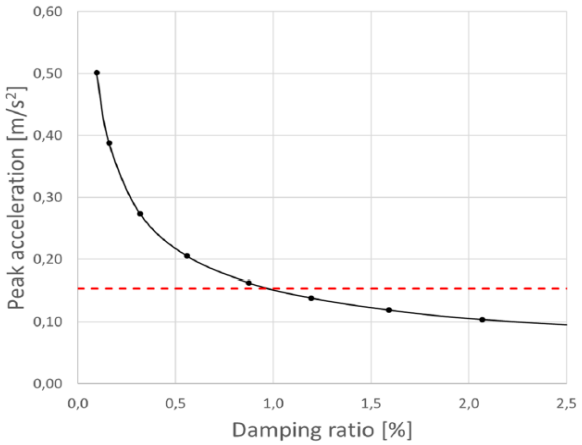

Figure 2.2 Peak acceleration level in a high-rise building at different damping ratios, the limit value according to NEN 6702 is specified by the dashed red line. Taken from Bronkhorst et al. [3]

2.3 Damping amplitude dependence

In this section, the amplitude dependence is treated in terms of the deformation of the structure as a whole, not on the local scale, such as when looking at the individual damping mechanisms. Results from experiments show that, for the same structure, the damping for tall structures changes at different amplitudes of movement. Additionally, this tendency is not constant: there is a tendency for the damping to increase at low amplitudes, then plateau at mid amplitudes and decrease at high amplitudes. This behaviour is illustrated in Figure 2.3,

where the amplitudes are divided into different design ranges of wind-induced vibrations. This information about the global damping is based on measurements, so since high amplitude events are rare, there are fewer measurements, so they have more uncertainty.

This amplitude dependency has been studied by Tamura [4]. Tamura defines a "tip drift ratio" as the ratio between the amplitude at the highest point of the building x_{HC} and the building height (H). At the critical tip drift ratio, the reduction of damping starts to occur. Results from measurements on a 200 m tall office building are shown in Figure 2.4, in this figure the critical tip drift ratio is marked with a dotted line. Tamura [4] found for 4 buildings ranging between 10 m and 100 m in height that the critical tip drift ratio was between 10^{-5} and 10^{-4}.

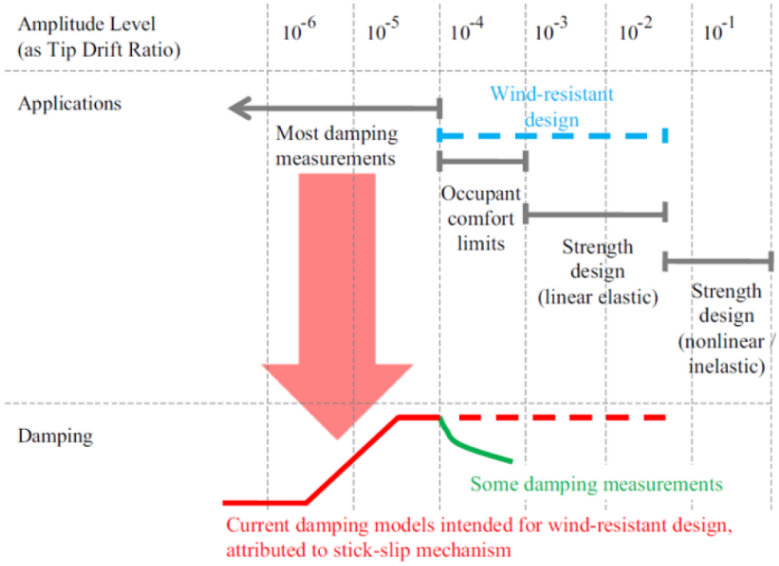

Figure 2.3 Variation of damping at different amplitude ranges, with expected amplitudes of wind induced deformations. Taken from Aquino and Tamura [12]

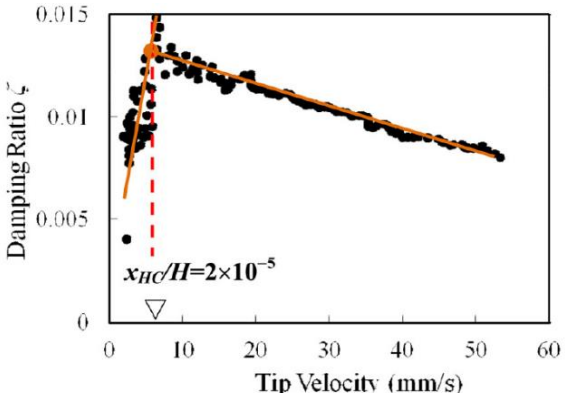

Figure 2.4 Change in damping ratio of the 200 m steel frame office building. Taken from Tamura [4]

With what has been presented in this section, it can be noted that there are big uncertainties in determining the correct damping, for example even though this critical tip drift ratio is an important parameter, the best approximations have an order of magnitude in variation. Smith and Willford [5] believe that understanding the critical tip-drift effect is of outmost importance since when calibrating damping models, the higher design amplitude behaviour is most likely different and cannot be verified from the low amplitude measurements. For this reason, there is a great interest in understanding what causes this reduction in damping so that it can be better predicted.

A proposed explanation by Tamura [4] for the tendency of the damping ratio to decrease at high amplitudes is the stick-slip mechanisms in the building. In a nutshell, after a certain amplitude is reached, most friction and yielding of the non-structural components have already reached the "slip" phase. This means that for every amount of extra deformation, the resistance of the structure remains the same. Tamura [4] recommends modelling the structure using the STICTION technique (i.e. a stick-slip model) developed by Wyatt (1977). In this model contact surface do not move at very low amplitudes and starts slipping at higher amplitudes. It is also important to mention that the stick slip model predicts the higher overall stiffness at lower amplitudes since, non-structural members contribute to the stiffness of the building at low amplitudes.

Using the stick-slip model, Tamura describes that:

i. At low amplitudes, many damping mechanisms that have stick-slip behaviour are still on the "stuck" phase so there is no dissipation due to slip.
ii. As the amplitude increases, some components start to slip and dissipate energy.
iii. At certain high amplitudes, most of these mechanisms have reach slip and the peak damping is reached.
iv. At higher amplitudes, the total amount of energy dissipation remains constant, but the energy of the system keeps increasing. Because of this, there is a drop in the relative damping as the amplitude increases.

All of these are in the small to large deformation range (10^{-6} to 10^{-2} tip drift ratio). At higher amplitudes, the structural elements are the ones that undergo non-linear behaviour (slip in connections, yielding, cracking and others) that leads to a second increase and peak of the damping. This study does not focus on those amplitudes since they are not suited for the case of continuous wind loading. These amplitudes of deformation are normally only allowed in extreme rare and short events like earthquakes or impacts.

2.4 Damping mechanisms present in wind-excited high-rise buildings

Numerous mechanisms are responsible for damping in high-rise buildings, the mechanisms that have the biggest effect on the dynamic behaviour are presented in this section. They can be grouped in different ways, in this chapter, the following division is used:

- Structural components
- Non-structural components
- Wind
- Foundation
- Auxiliary damping

All these mechanisms are addressed for the ranges with respect to the frequencies and amplitudes of strains and deformations expected from a slender high-rise building subjected to the wind loads and cemented in piles. It also considered both, the composition of the structure and soil, as is commonly found in high-rise buildings in the Netherlands.

Energy dissipation in damping is a complex phenomenon where the behaviour is normally simplified under some common idealised damping mechanism (relevant idealizations are

presented in the annex A). In this section, the damping mechanisms of a high-rise building are described by one or a combination of those idealised simpler mechanisms.

2.4.1 Structural components

Most of the time, the dissipation of energy of a structure is determined by the material of the main loadbearing structure. But a building's structure presents several sources of discreet energy dissipation mechanisms. They can be separated into material damping, slip on connections, and yielding of structural elements.

Material damping occurs from friction between molecules when under relative motion, the energy is dissipated through heat. The damping properties of different materials can be found experimentally through measurements in the laboratory. Common construction materials like steel and concrete have been widely studied and some common values for their damping ratios are 0.3% and 0.5% respectively (Smith and Willford [5]).

Connections such as steel-bolted connections and dry pre-cast concrete element connections are capable of having some slip without failure. These type of connections normally present elastic deformations before and after the slip, but during the slip phase, there will be an increase in displacement with no increase in the force. This means that the energy dissipation would be frictional and can be modelled through coulomb damping, which also means that they are partially amplitude dependent but not frequency dependent. Coulomb damping is further explained in the annexe A.1. The partial amplitude dependence is due to a dependency of the amplitude of the displacement during the slip phase, but it is displacement independent before and after the slip phase. The slip phase should not occur too frequently, since the friction in the slip phase will deteriorate the connection, if many cycles of deformation are expected. A windstorm achieving the SLS parameters may run for several hours, inducing thousands of cycles.

The yielding of structural components is also a big source of the energy dissipation capacity of a structure, yielding is present in both the elements and connections. The energy dissipation comes from the cyclical deformation in the plastic regime, which means that this type of damping can be simulated with the complex stiffness model presented on the annexe A.4. Cyclic plastic deformations lead to a degradation of stiffness and fatigue failure. This means that they are normally only acceptable in rare events of low duration, like earthquakes. Similar to slip, a windstorm could induce thousands of cycles, but in this case the deterioration would be due to fatigue, which leads to eventual failure. This means that in the range of the amplitudes typically induced by the wind, damping due to yielding is unlikely to occur since the deformations are well under the yielding of the elements.

2.4.2 Non-structural components

Non-structural components englobe a big group of elements, most notably: facades, partition walls, cladding, fixed furniture and mechanical and electrical shafts. These non-structural elements are fixed to the structure and when they deform, they will deform as well. They will present the same energy dissipating mechanisms as the structural components (material damping, slip on connections, and yielding or failure), but they are normally much weaker and can display this behaviour at smaller displacements (much earlier than the structural components), but without leading to failure of the structure. It is common to model these damping mechanisms with a stick and slip model. In these types of models, it will show the

behaviour of not offering any additional damping or resistance at larger deformations, where the non-structural components most likely have already given out.

Smith and Willford [5], who investigated damping mechanisms on buildings, state that studies found that non-structural components present a significant contribution to the damping, but they also point out that the taller the building, the less significant it becomes. This statement comes from the results of measurements showing that damping decreases with an increase in height. They attribute this to the structural elements of buildings getting stronger as the height increases, while the non-structural elements remain constant, so in relative terms, the damping due to non-structural elements is lower. Smith and Willford [5] back up this claim by showing that for high-rises and chimneys, the damping is very similar. Since chimneys have no non-structural elements, it leads to the conclusion that the non-structural elements have virtually no contribution to damping, in very high structures. This reduction in the importance of the damping of non-structural elements is significant to the overall damping since it is one of the major contributors to the damping of lower buildings, even at small deformations.

2.4.3 Wind

The flow of a fluid over a structure creates a drag force in the opposite direction of the relative motion between the wind flow and the structure. On the annexes A.3, the energy dissipation due to fluid structure interaction is described. But, for the case of wind-induced vibrations, the air is already moving at high velocities and the wind motion is much faster than the building vibrations, so the relative motion is almost always dominated by the wind. Because of this, studies on damping on high-rise buildings such as Gomez [6], [7] and Smith and Willford [5] consider aerodynamic damping to be negligible.

2.4.4 Foundation

The energy dissipation of the foundation is mostly associated with mechanisms in the soil, such as hysteretic behaviour, wave radiation, stiffness nonlinearities and friction. A general overview is given in this section, but these topics are further looked more into depth in the chapter on soil modelling.

The nonlinear plastic deformation of the soil when loaded cyclically create hysteretic loops that dissipate energy. The type of soil plays an important part in the hysteretic behaviour. This soil hysteretic damping becomes more important at higher amplitudes of motion, but for some soil types is also present at small strains. This means that the damping mechanism is amplitude dependant.

Radiation damping is an energy dissipation mechanism caused by the radiation of elastic waves to the soil. In this damping mechanism the energy is not changed from one form to another, but it has just fiscally moved. For this reason, it is also known as geometrical attenuation. An essential factor to consider when including this source of energy dissipation is looking at the surrounding soil and identify if there are objects or stiffness changes in the soil that can cause the reflection of the ground waves. Waves with different speeds will attenuate and propagate at different speeds; so, it is important to mention that radiated waves can be dispersive or non-dispersive depending on the type of wave, so they can have different radiative properties.

Finally, there are other sources of dissipation of energy that occur in the interface between soil and structure, these are friction and gapping. Friction occurs when the soil in contact with the foundation slips and there is a relative motion of the soil parallel to the surface of the foundation. Gapping occurs when the relative motion is perpendicular to the surface of the foundation and they lose contact, this happens because soil has practically no tension strength. Both mechanisms dissipate energy through different processes, but they are irrelevant to the magnitude of deformations expected in the soil from wind-induced vibrations.

2.4.5 Auxiliary damping

The damping mechanisms that are purposefully added to the structure to increase the amount of damping are commonly known as auxiliary or supplementary damping. Some of the most common types are Tuned Mass Dampers, Tuned Liquid Dampers, Friction dampers, Viscous and Visco-elastic dampers. Even though they work very differently, they are all able to increase the amount of damping to the building significantly. On a high-rise building where the intrinsic damping is around 1.5%-0.5% auxiliary damping could add an extra 5% of damping.

This is a very interesting concept because, as it has been stated in this report, there are difficulties in defining the correct damping of a high-rise building, and by adding a deliberate amount of damping will ensure that the damping of the structure is at higher levels. This does not mean that the damping predictions are more accurate but since at higher damping levels, the dynamic response is less susceptible to variation, so adding supplementary damping can increase the accuracy of the response. An example of this principle is presented Smith and Willford [5] whereby adding auxiliary damping, the variation of the dynamic response due to damping uncertainties went from 72% to 20%.

2.5 Relevance of SSI in dynamic response of high-rise buildings under wind loading

Soil-Structure Interaction (SSI) or Soil-Foundation-Structure Interaction (SFSI) refers to the mechanical processes that arise when the deformability of the soil impacts the behaviour of the system. Accounting for SSI changes the dynamic properties of the structure. This is caused by the added deformability of the system that yields an increase in the natural periods of the structure and a change in the shape of vibration modes. Another important factor is that the soil deformability introduces radiation energy dissipation and material damping from the hysteretic behaviour of the soil. Nevertheless, influence of including the SSI in a system is not guaranteed to be important for every system. The extra work needed to include SSI merits that there is a significant difference when including these more rigorous modelling techniques. For this reason, this section focuses on results from previous studies that provide arguments and evidence that SSI is relevant for modelling the wind induced motion of high-rise building on soft soils.

2.5.1 Period lengthening

One of the most notable effects of including SSI is period lengthening. Due to the flexible foundation, the natural period of the building increases, compared to the case with the fixed boundary condition. This is a topic covered by the United States' National Institute of Standards and Technology (NIST) [9], it explains how in seismic scenarios, an increase in the

period almost always means a decrease in the seismic demand. This is not strictly true for wind-induced vibrations since the wind load is normally characterized by a higher energy content at lower frequencies. In other words, a lower natural frequency is likely to result in a larger response. For this reason, the correct determination of the period of the system is of great importance.

This period lengthening effect has been shown to be of such importance that a study described by B. R. Ellis [13] presented measurements from a building, that even showed that a difference in water saturation height due to changing tides of a river nearby, created significant daily changes in the natural frequency and damping of the structure. It is important to clarify that a change in water saturation level because of tides might have a significant change in the local properties of the soil at the depth of the saturation boundary, but with respect of the overall properties of the soil, which is considered between 10 m to 30 m depth, it will have a small change. In other words, if a small change in the overall properties of the soil makes a substantial change in natural frequency, this implies that in the case studied by B. R. Ellis [13], the SSI parameters can have a large influence on the dynamic response. A study by J. Mercado and L. Arboleda [14] showd that the "period lengthening in structures is largely influenced by the predominant shear wave velocity of the supporting soil and the geometric configuration of the structure.".

The magnitude of the effect of this period lengthening depends on the difference in stiffness between the soil and the structure. NIST [9] uses a structure-to-soil stiffness ratio (h/(VsT)) as a parameter to determine this relative difference in stiffness. The higher the structure-to-soil stiffness ratio, the bigger the period lengthening effect, which means that slender structures only have a significant period lengthening effects if the soil is soft relative to the structure stiffness.

The change in the period comes hand in hand with a change in mode shapes, compared to the clamped model, because of the rocking and translation of the foundation. This is important when using simplified methods that assume the shape of the first natural period mode shape, since the mode shapes are not the same as the clamped model. A study on the effect of SSI on wind and induced tall buildings using macro-elements by Venanzi et al. [15] showed that a heavy structure (such as a high-rise building) in a relative soft soil has significant soil structure interaction, with significant changes to the mode shapes and natural frequencies.

2.5.2 Influence on damping

The aspect ratio (height over base with) of a structure has a large influence on the damping ratio. The dependence on slenderness was studied by Cruz and Miranda [8]. They showed that soil stiffness plays an important role in the tendency of the damping ratio to decrease with the slenderness of the structure. A decrease in shear wave velocity on squat structures increases the damping ratio, while for slender structures it decreases the damping ratio. Results from Cruz and Miranda [8], displayed in Figure 2.5, show that soils with low shear wave velocity properties (i.e. soft soils) show an important influence on the damping ratio with respect to the slenderness. From Figure 2.5, it can also be concluded that the damping ratio is quite sensitive to a variation in shear wave velocity for softer soils. This study suggests this effect is primarily driven by SSI. This means that soils in the Netherlands, which are normally soft soils, play an important role in determining the damping of the structure.

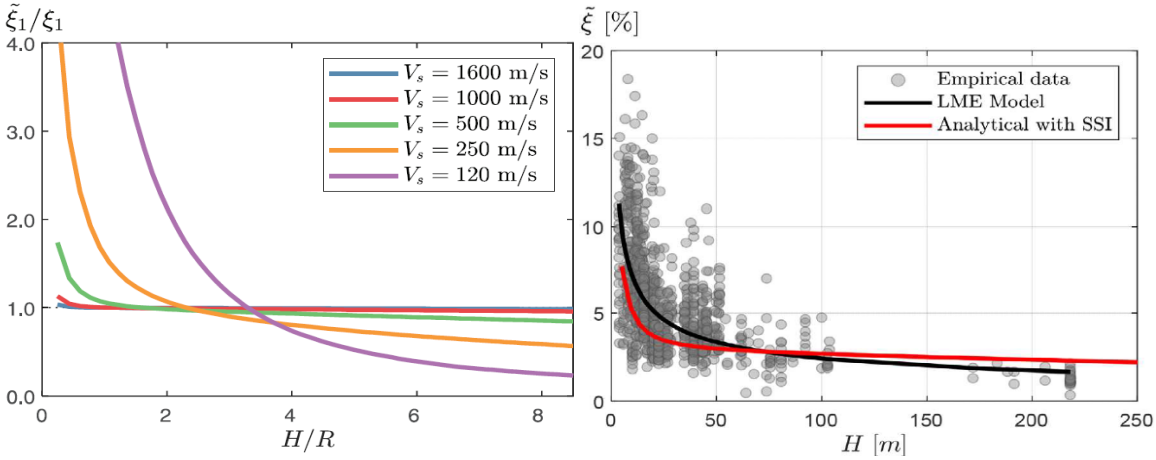

(a) (b)

Figure 2.5 Variation of damping ratio with respect to the height. Taken from Cruz, Miranda [8]. (a) For different shear wave velocity, (b) Comparison with measurements using mean shear wave velocity

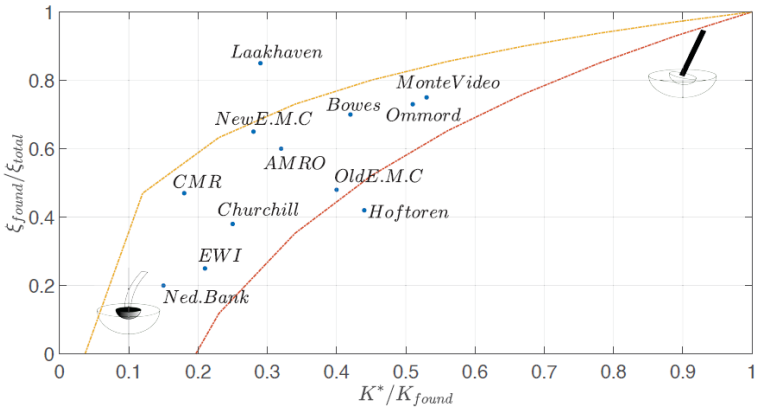

Figure 2.6 Influence of the foundation damping to the total damping for several buildings located in the Netherlands. Taken from Gomez [6]

Results from a study on small amplitude measurements of 205 Japanese buildings from Satake et al. [16] found that *"the main reason for the dependency between damping ratio and building height may be the effects of soil-structure interaction and radiational damping*". These results agree with the analytical results from Cruz and Miranda.

On this same topic, studies conducted by Gomez [6] show that the damping contribution of the soil increases when the ratio of foundation stiffness and superstructure stiffness decreases. These results can be observed in Figure 3 from which 12 buildings in the Netherlands are plotted with respect to their ratio of foundation stiffness to superstructure stiffness against the ratio between foundation damping and total damping.

Furthermore, using a half space description of the foundation and damping predictor models, Bronkhorst et al. [3] found that, to be able to match the estimated and measured damping ratio of 5 high-rise buildings on soft soils, the material damping of the soil plays an important role in the contribution of the overall damping of the structure. Neglection of this term resulted in an underestimation of the damping. This is interesting since in current practice the both the soil radiation damping and the soil material damping properties are not considered. Additionally, shows the importance of an accurate prediction of the natural frequency for obtaining a reliable estimate of the damping.

Smith and Willford [5], compiled the results of buildings up to 450 m tall. They observed that for buildings between 200 and 450 m tall, there was less variation in the damping ratio associated to different building material types (steel/concrete) for higher buildings compared to the large difference in the damping ratio found in shorter buildings for structures of different material types, this can be observed in Figure 2.7. These results show that for higher buildings, the structure plays less of an important role in the damping since it looks like varying the structure material type would not change the overall damping significantly. Consequently, other damping mechanisms, such as the ones introduced by SSI, perform a bigger role.

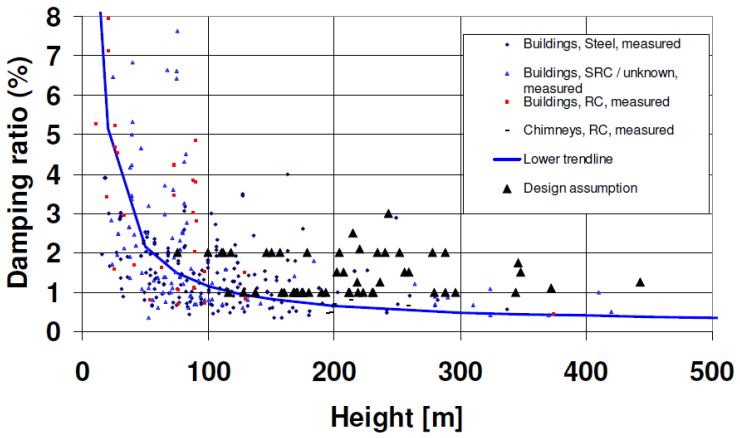

Figure 2.7 Damping ratio against height, showing measurement from different building types and also design assumptions. Taken from Smith and Willford [5]

It is interesting to point out that B. R. Ellis [13], even though he believes that the SSI effects are relevant, he comments that SSI becomes less important for tall buildings. He used the parameter of the ratio of translation of the roof compared with the base of the structure to quantify the influence of SSI. In a way, this ratio is similar to the ratio of foundation stiffness to structure stiffness used by Gomez [6], [7], but with the important difference that the translation of the roof cannot be just attributed to the structural stiffness but also to the translational stiffness and the rotational stiffness of the soil. This might have been an oversight because the rotational stiffness of the soil is of great relevant for high-rise building because due to the large height, a small rotation of the base can lead to big displacements at the roof. In other words, part of the horizontal translation of the roof would need to be attributed to SSI and cannot be exclusively attributed to the flexibility of the structure.

Nevertheless, these studies have some limitations. The studies only focus on the influence in damping but do not address the effect on the dynamic response, such as the peak acceleration. All these also use simplified analytical models for the foundations that do not consider soil layers, soil material damping nor pile foundations. Finally, none of these studies corroborate whether their models predicted reasonable results when subjected to wind loading, in terms of its dynamic response, such as peak acceleration or power density acceleration spectrum.

2.6 Expected displacements and strains

As has been introduced in this chapter, there are many sources of energy dissipation mechanisms in high-rise buildings, and they have big variations in behaviour and range of relevance. Because of this, it is of the utmost importance to be able to foresee what will be the expected behaviour of the different components on a high-rise building and the magnitude of

the relevant quantities that drive the energy dissipation. Some of the most relevant quantities are the expected magnitudes of strains and strain rate of the following: the soil (at different distances from the foundation) and the structural elements. Additionally, the displacement, rotation, velocity, and rotation rate of the foundation are relevant factors to consider.

Information regarding the magnitudes of the relevant factors previously mentioned, for high-rise buildings subjected to wind loads is not readily available. But it is commonly assumed that, for high-rise buildings subjected to wind loads, both the structure and the soil strains are normally small enough that they can still be modelled by linear behaviour, which narrows down the strains and deformations expected. As well as using the information on the expected frequency content of the vibrations mentioned in the previous section, this can give good approximations of the order of magnitude of the strain rates and velocities.

3

High-rise building models

As introduced in the methodology, this study uses 3 models of different complexities to predict the dynamic behaviour of high-rise buildings, for both the case study (chapter 4) and the parametric study (chapter 5). This chapter presents these 3 models and describes how they to predict the dynamic behaviour of high-rise buildings. More specifically the dynamic behaviour of an along-wind loading perpendicular to one of the main axes of the structure of a high-rise building and the building deflection along that same direction, as depicted by the diagram in Figure 3.1.

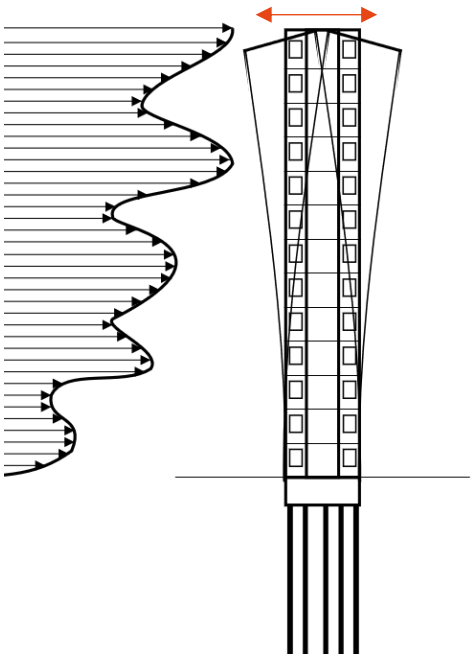

Figure 3.1 Diagram of dynamic behaviour of a high-rise building under wind loading. [17]

3.1 Eurocode (EC) model

The current practices for calculating the dynamic response of high-rise buildings under wind loading comes by simplifying the structure to a single degree of freedom system subjected to a white noise spectrum. This simplification is generally considered accurate enough because most of the dynamic response comes from the excitation of the first vibration mode of the structure. So, the properties of the equivalent single degree of freedom system of stiffness, height and mass come from the equivalent modal properties of modal stiffness, modal height and modal mass of the first vibration mode. With respect to the white noise, the magnitude of this constant is computed as the magnitude of the spectral density function at the natural

frequency, since this will be the frequency most excited by resonance in the structural admittance.

The response of a single degree of freedom subjected to a stochastic white noise load, can be separated into a background response and a resonant response. The acceleration measurements are overwhelmingly driven by the resonant response, so it is common to neglect the background response. For this formulation, the standard deviation of the acceleration can be approximated through SDOF the equation, Steenbergen et al. [18], [19]

$$\sigma_{\ddot{w}}(\mathrm{z}=\mathrm{H}) = \frac{A \cdot C_D \cdot \rho_a \cdot \bar{v}(z_s) \cdot I_v(z_s)}{m_n} \sqrt{\chi^2(f_n) \frac{S_L(z_s, f_n) \cdot \pi}{4 \cdot \zeta_n}}$$

with,

ρ_a = density of air [kg/m^3]
A = area of face perpendicular to wind direction [m^2]
H = Height of the structure [m]
C_D = Drag Coefficient
$\bar{v}(z_s)$ = mean wind velocity at reference height [m/s]
m_n = modal effective mass [kg]
ζ_n = Modal damping ratio
f_n = first natural frequency [Hz]
$I_v(z_s) = \frac{\sigma_v}{\bar{v}(z_s)}$
σ_v = wind fluctuations standard diviation [m/s]
$S_L(z_s, f_n) = \frac{S_{\tilde{v}\tilde{v}}(f_n) \cdot \sigma_v^2}{f_n}$
$S_{\tilde{v}\tilde{v}}(f_n)$ = the spectral density function at the natural frequency [N^2/Hz]
$\chi^2(f_n)$ = Aerodynamic admittance

This equation predicts the standard deviation of the acceleration at the highest point, to calculate the acceleration at different heights, the mode shape of the first mode is used.

$$\sigma_{\ddot{w}}(\mathrm{z}) = \frac{\sigma_{\ddot{w}}(\mathrm{z}=\mathrm{H})\Phi(z)}{\Phi(z=H)}$$

For the case of the Gaussian narrow banded process, when knowing the predominant frequency and the period (T) of the event, the expected peak response of high-rise buildings can be calculated using the next formula,

$$\ddot{w}_e(T) = \sigma_{\ddot{w}}(z)\left(\sqrt{2\ln(T \cdot f_0)} + \frac{0.6}{\sqrt{2\ln(T \cdot f_0)}}\right)$$

with,

$\ddot{w}_e(z, T)$ = expected acceleration at a certain z for an event of a period T
T = duration of the event [s]
f_0 = central frequency [Hz]

For this study the duration the wind event will always be 10 mins, T = 600s.

From Procedure 2 in the Eurocode [2][20], the formula for the standard deviation of the acceleration is the C.4. This formula written in the nomenclature in this study and with only z dependency would be:

$$\sigma_{\ddot{w}}(\mathrm{z}) = \frac{A \cdot C_D \cdot \rho_a \cdot \bar{v}(z_s) \cdot I_v(z_s)}{\frac{M}{K_z}} \sqrt{\mathrm{K_s}(f_n) \frac{S_L(z_s, f_n) \cdot \pi}{4 \cdot \zeta_n}} \frac{\Phi(z)}{\Phi(z = H)}$$

with,

M = Total mas of the building

K_z = effective modal mass factor (for linear mode shape = 1.5)

$\mathrm{K_s}(f_n)$ = size reduction function

$\frac{\Phi(z)}{\Phi(z=H)} = \frac{z}{H}$ for the linear mode shape approximation

In this study, this is addressed as the EC model.

If we compare the Eurocode equation to the theoretical equation for the stochastic response of a SDOF, the Eurocode approximations are the following:

$$f_n = \frac{46}{H} \qquad \frac{\Phi(z)}{\Phi(z = H)} = \frac{z}{H} \qquad m_n = \frac{M}{K_z} \qquad \chi(f_n) = \sqrt{\mathrm{K_s}(f_n)}$$

In design practice, the properties such as the natural frequency, the mode shape and the modal mass are often more accurately calculated from the undamped structure model, often modelled in FEM software. For the most part, in practice these models do not include SSI and if they are included, they are simplified to elastic springs, none of which include the energy dissipated in the ground and foundations.

Moreover, using this undamped structure model still presents the limitation that it is unable to calculate the modal damping, which means that through this procedure the modal damping cannot be refined. So, even if accurate modal properties are used or the standard Eurocode approximations, the global modal damping ends up being estimated crudely, often just choosing them from tables in codes or empirical formulas. In the Eurocode EN 1991-1-4 [2] it is found under Table F.2, where different structural damping values are assigned for different types of structures.

3.2 NIST model

The method for choosing the value for the modal damping ratio, explained in the previous section, is a big limitation for this simplified model. As has been introduced in section 2.5.2, the damping of high-rise buildings is strongly dependent on SSI, furthermore the dynamic response of high-rise buildings is strongly dependent on the overall damping. Also, the damping ratio is particularly low for high-rise buildings (about 0.5%-1.5%), which means that an inaccurate estimate of this parameter has a large influence on the dynamic response.

Additionally, the approximation for the natural frequency does not consider that the added flexibility of the soil will introduce period lengthening. As has been introduced in section 2.1, the wind load magnitude is very sensitive to changes in frequency, so the natural frequency needs to be accurately predicted. Additionally, the period lengthening effect means that the natural frequencies should be lower, so not including this effect would mean underestimating the wind load.

For this study, modifications to the EC model are proposed, to include the effects of SSI. This section introduces the procedures described by the NIST [9], which include the effects of SSI on the calculation of natural frequency and modal damping. In this study, the EC model with this modification is addressed as the NIST model.

These modifications, as introduced in the NIST [9] document, are normally applied in seismic engineering. Even though this model is meant to be used for seismic engineering, the properties of interest are the natural frequency (f_n) and the modal damping ratio (ζ_n). This procedure is meant to be able to include the effects of SSI on the calculation of natural frequency and modal damping.

The model is built from a single degree of freedom system, were the properties come from the modal properties of the multi-degree of freedom system. The procedure starts by calculating the period lengthening effect by comparing the period (T) of the model with a fixed base and the period ($\tilde{T}$) of the full model that also includes foundation rocking and translational stiffness. These models are shown in Figure 3.2. This period lengthening effect for this model can be expressed as,

$$\frac{\tilde{T}}{T} = \sqrt{1 + \frac{k}{k_x} + \frac{k \cdot h^2}{k_{yy}}}$$

with,

T = Period of clamped model [s]
$\tilde{T}$ = Period of model with SSI [s]
h = Height of the centre of mass for the mode shape [m]
k = Structure's modal stiffness [N/m]
k_x = Soil translational stiffness [N/m]
k_{yy} = Soil rotational stiffness [N/rad]

With the modified natural frequency calculated as,

$$\tilde{f_n} = f_n \left(\frac{\tilde{T}}{T}\right)^{-1}$$

with,

f_n = Natural frequency of clamped model [Hz]
$f_n = f_{n,EC} = 46/H$ Eurocode natural frequency approximation [Hz]
$\tilde{f_n}$ = Natural frequency with SSI [Hz]

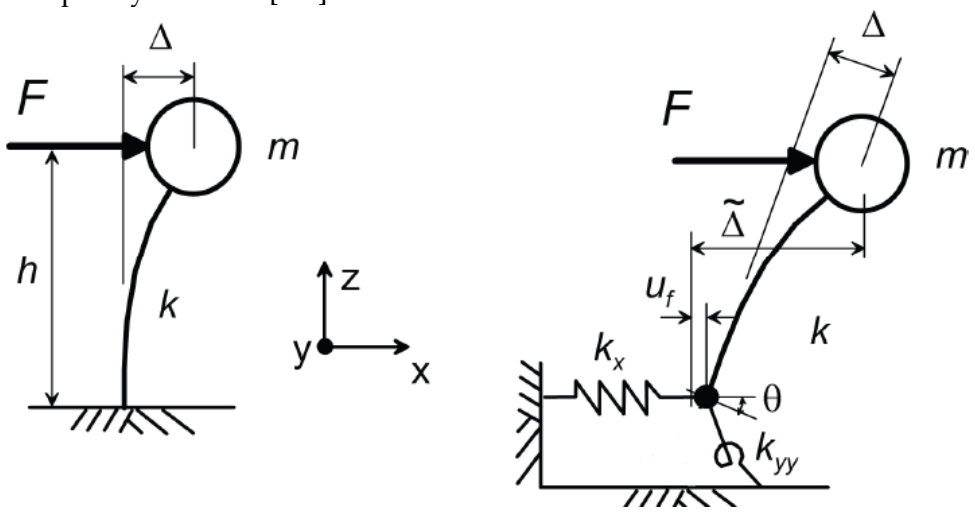

(a) (b)

Figure 3.2 Illustration of the SDOF models and their deformations, (a) structure with fixed base and (b) structure with translational and rotational flexibility at its base. Taken from NIST[9]

This period comparison with the full model is also repeated by comparing it with a model with just the translation spring and a model with just the rotational spring. This results in 2 other period lengthening equations,

$$\frac{\tilde{T}}{T_x} = \sqrt{1 + \frac{k_x}{k} + \frac{k_x \cdot h^2}{k_{yy}}}$$

$$\frac{\tilde{T}}{T_{yy}} = \sqrt{1 + \frac{k_{yy}}{k \cdot h^2} + \frac{k_{yy}}{k_x \cdot h^2}}$$

This methodology uses the results of the period lengthening effects to combining the input of different damping mechanism into a single overall damping ratio, with the formula:

$$\zeta_n = \frac{1}{\left(\tilde{T}/T\right)^2}\zeta_s + \frac{\left(\tilde{T}/T\right)^2 - 1}{\left(\tilde{T}/T\right)^2}\zeta_m + \frac{1}{\left(\tilde{T}/T_x\right)^2}\zeta_x + \frac{1}{\left(\tilde{T}/T_{yy}\right)^2}\zeta_{yy}$$

with,

ζ_s = superstructure structural damping ratio
ζ_m = soil material damping ratio
ζ_x = soil radiation damping ratio from translation
ζ_{yy} = soil radiation damping ratio from rotation

This formula engulfs the damping of the structure, material and radiation damping in both the translation and rocking degree of freedom of the soil in a single "equivalent" damping parameter, that can be used as an estimator for the overall modal damping that includes the influence of SSI.

The superstructure structural damping ratio (ζ_s) is estimated with the empirical damping predictor by Jeary [21], which takes into account the reduction of damping with the increase of flexibility of structures. Due to expected small tip drift ratios, studies by Gomez [6], [7] and Bronkhorst et al. [3] simplified the equation even further to,

$$\zeta_s = f_{n,EC} + 0.15$$

The dynamics stiffness matrix, obtained from the Dynaplile model results, is used to calculate the foundation stiffness and damping parameters.

$$k_x = Re\left[\tilde{K}_{tt}\left(2\pi f_{n,EC}\right)\right]$$

$$k_{yy} = Re\left[\tilde{K}_{yy}\left(2\pi f_{n,EC}\right)\right]$$

$$\zeta_x = \frac{Im\left[\tilde{K}_{tt}\left(2\pi f_{n,EC}\right)\right]}{2\pi f_{n,EC}}$$

$$\zeta_{yy} = \frac{Im\left[\tilde{K}_{yy}\left(2\pi f_{n,EC}\right)\right]}{2\pi f_{n,EC}}$$

Where, $\tilde{K}_{tt}$ and $\tilde{K}_{yy}$ are part of the dynamic stiffness matrix introduced in section 3.3.1, but they are evaluated at the structures natural frequency.

Given that the imaginary part of the stiffness matrix from the results of Dynaplile include both the material and radiation damping of the soil, and cannot be separated. The ζ_m will not be used discretely, and the terms ζ_x and ζ_{yy} will engulf both component of material damping and radiation damping.

3.3 High-Fidelity (HF) model

For the formulation of the HF model three different sub-models are required. First, the foundation model, which provides the influence of SSI through a foundation dynamic stiffness matrix. The model of the wind, which provides the stochastic approximation for the loading. Finally, the tower structure model, which incorporates the results of the foundation dynamic stiffness and the wind loading into its continues beam model to compute the dynamic response of the system. This combination of the models is depicted in Figure 3.3. In the next sections the models are explained further and are assisted by the annexes B.3, C and D where the theoretical derivations and the solution procedures of the models are further explained.

The dynamic response of the system is computed in the frequency domain. Due to the loading being of stochastic nature, the dynamic response of the system is of stochastic nature as well. The procedure used to solve this is presented in the annexes in section D.5. A depiction of this procedure is presented in Figure 3.4.

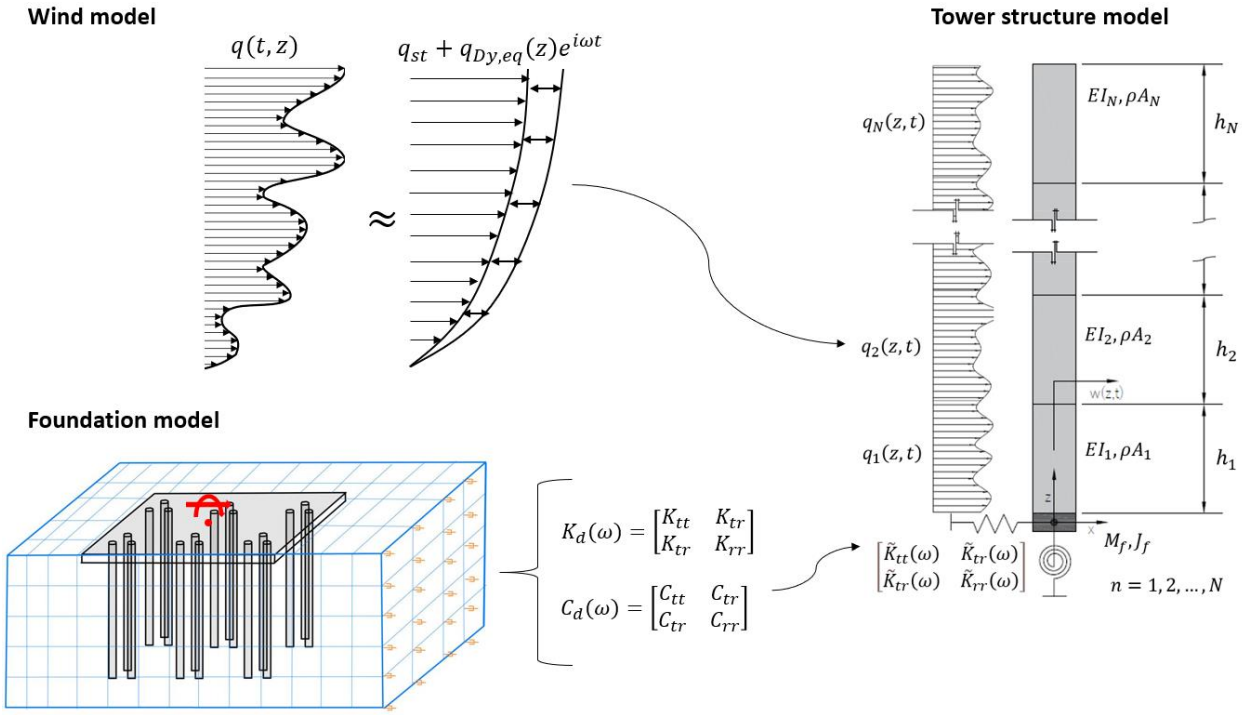

Figure 3.3 Depiction of the assembly of the three-part model (soils, wind and Tower) to produce the HF model.

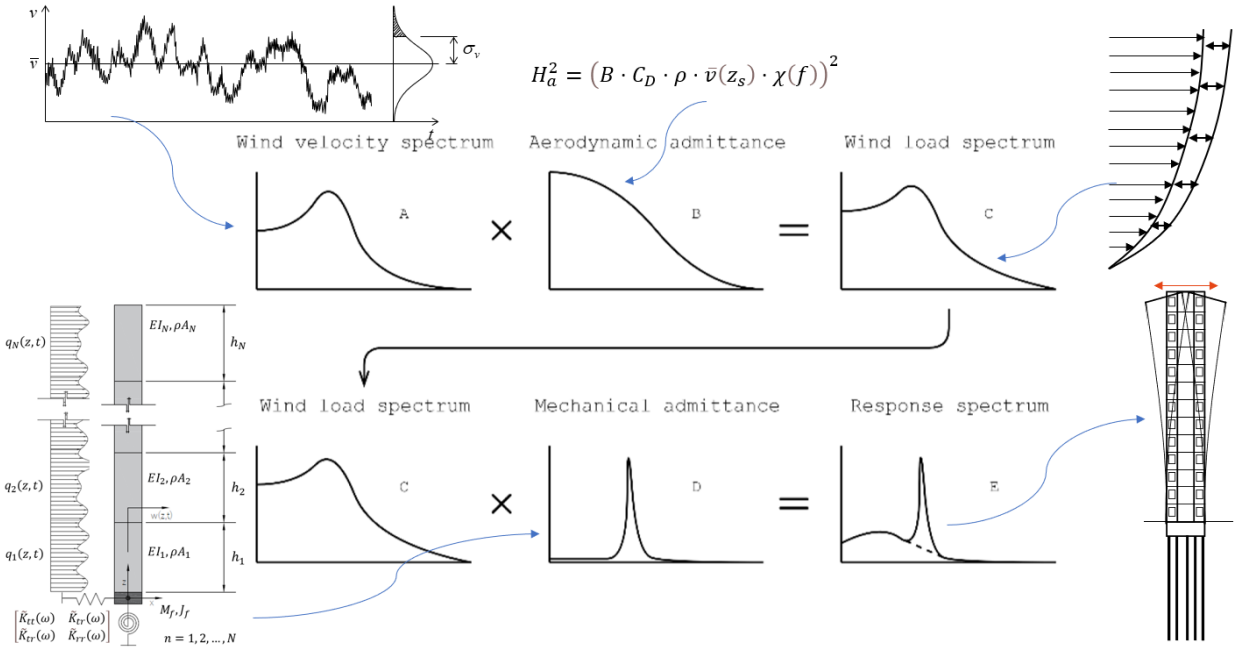

Figure 3.4 Stochastic frequency domain approach to solve for the acceleration power density response function. Some images from Y. Paauwe[11] were used in this figure.

3.3.1 Foundation model

SSI can be modelled in different ways, but most of them can be grouped in one of two categories, the direct approach and the substructure approach and for each approach either a linear or nonlinear model can be used. In the direct approach, the structure, foundation, and soil are all introduced in a single model and the analysis is done on this sole model. This approach is most commonly performed in FEA models. In the substructure approach, the analysis is divided into different parts, first the soil is analysed by itself, where an equivalent foundation system is calculated and separately this equivalent foundation system is applied to the model of the structure. This approach can be used both with analytical and FEA methods. Both approaches are explained in more detail in annexe B.

As mentioned in the previous section, for this study, the substructure approach was used to include the effects of SSI. This was done by creating a separate 3D foundation model that includes the geometrical and linear material properties of both the soil and the foundation structure and use this to compute the foundation dynamic stiffness matrix, which is included in the tower structure model. The aim when including SSI in the model of a structure is to link the interactions between the soil, the foundation, and the structure. This linking of the different systems induces a collective response of the complete system as one. The inclusion of the soil and foundation into the system brings into consideration the inertia, stiffness, nonlinearities and damping of the moving soil, which depending on the properties of structure, foundation and soil, may play an important or insignificant part in the total dynamic response of the system.

In this study, the software Dynaplile is used to model the foundations. Dynaplile uses FEM and CBEM to model the dynamic behaviour of semi-infinite multi-layer soil with embedded piles, assuming a rigid slab tying the piles. Dynaplile can compute the dynamic stiffness of pile foundations, which is the input needed in the substructure approach to analyse the structure. In contrast to other equivalent foundation models, both theoretical and empirical,

Dynaplile and other software with similar capabilities present the advantage that through FEM, the geometric complexity of the pile distribution can be included.

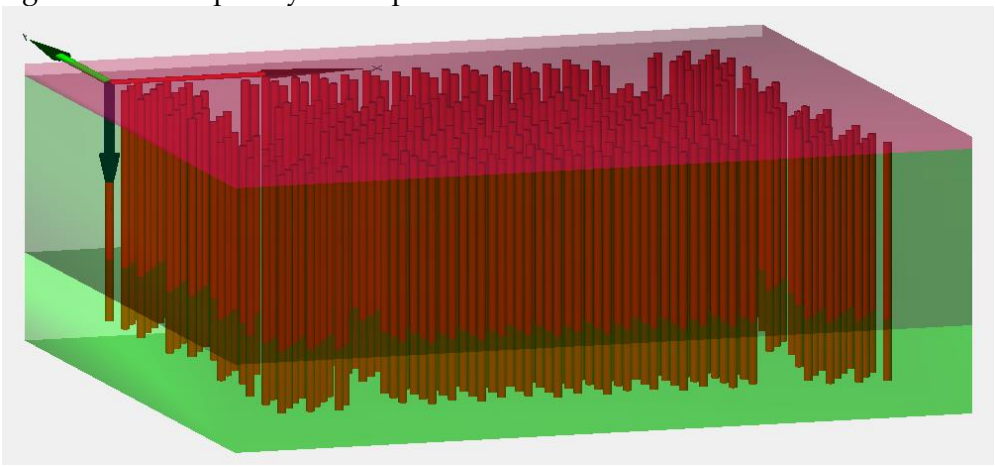

Figure 3.5 Image of a Dynaplile model, depicting piles and 2 soil layers.

Dynaplile has the capabilities for different types of models, but for this study a linear, a complex strain approach was used. Since the deformation induced by the wind in the soil is expected to be low, a linear approach is appropriate. The complex strain approach was used to model the material damping of the soil, where the minimum material damping, observed at low strains was used. On annex section B.2.1.3, the theory on this subject is explained in greater detail.

Dynaplile also allows the modelling of foundation piles. The foundation piles are defined as 1D Euler-Bernoulli beam elements. Separately, the piles can also deform in the axial direction as extension and compression rod elements. To introduce material damping, they are defined with a complex elasticity modulus, a similar formulation of material damping as the soil. This 1D element can undergo deformations in both orthogonal directions in bending, perpendicular to its main beam axis as well as axial deformation.

Since the model is linear and the pile and soil are assumed to have deformed together, a rigid interface element is used. This interface element only takes care that the node of the pile element and the corresponding nodes from the soil have the same deformation, these are needed because the nodes are not in the same position since the node of the element is at the centre of the pile and soil is at the edge of the pile.

As a default, the software already assumes a rigid massless foundation slab connecting all the piles. The 3 translational and 3 rotational degrees of freedom of the foundation system are located at a node in the centroid of this slab. To calculate the dynamic stiffness, a harmonic loading at different frequencies is applied for each different degree of freedom of the slab individually while the other degrees of freedom remain fixed. This is done in the frequency domain through the means of a transfer function, which describes how the displacement in a degree of freedom results in reaction forces and moments in all other degrees of freedom. Using Hooks law, since a linear behaviour of the system is expected, it can be assumed that this relationship between the displacement and the reaction force can be taken as a linear stiffness. This stiffness that takes the inertial, dissipative and elastic behaviour of the dynamic system is a dynamic stiffness of the foundation, which contains a real component (elastic and inertial) and an imaginary component (material and radiation dissipation).The setup of Dynaplile and the results that it provides for the dynamic stiffness matrix are explained in section 4.3.2.

3.3.2 Wind load model

Ultimately the required results from the wind model is the Power Spectral Density function (PSD) of the wind force at a reference height. This will also be referenced as the load spectrum of the distributed drag force. The distribution and magnitude of this load is described by two main factors: the wind and the geometrical properties of the structure. This section concisely describes the general procedure for modelling the wind. The detailed description of the procedure can be found in the annexes on section C.1.

Wind is normally separated into separate events, as depicted in Figure 3.6. The first part of the wind load model comes from modelling the wind event itself, more precisely the wind speeds is of interest. The wind model can be simplified to only the mean wind speed and parallel component or the fluctuations, ad can be expressed as,

$$\underline{v}(z,t) = \bar{v}(z) + \tilde{v}_{\parallel}(z,t)$$

with:

$\bar{v}(z)$ = mean wind speed [m/s]

$\tilde{v}_{\parallel}(z,t)$ = wind speed fluctuations parallal to the mean wind speed [m/s]

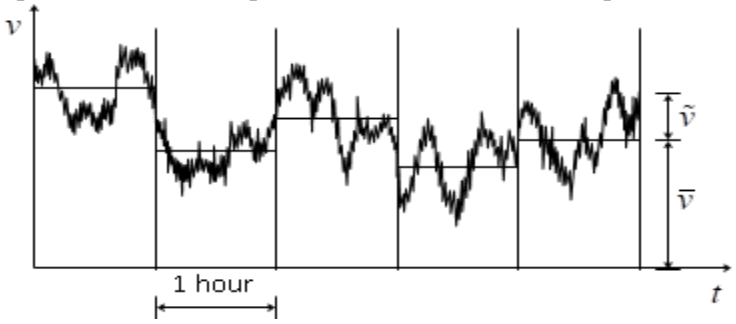

Figure 3.6 Wind speed vitiation. [10]

Both the mean wind speed and the turbulence (fluctuations) are necessary to describe the wind loading. For this study, the logarithmic profile for the mean wind velocity was adopted. The fluctuations, happening in the short term, are described in stochastic terms by probability distribution and Power Spectral Density (PSD) function. For the probability distribution a Gaussian distribution with a mean of zero and a constant standard deviation through the height was adopted. For the PSD the modified Kaimal spectrum recommended in the Eurocode EN 1991-1-4 [2] was used. The mean wind speed distribution, standard deviation of turbulence and its frequency spectrum are depicted in Figure 3.7. The procedure used to calculate these 3 properties of the wind speed can be found in the annexes in section C.1.

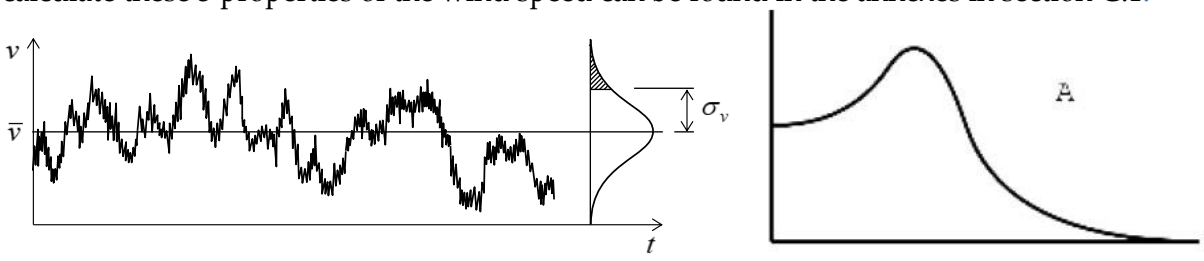

(a) (b)

Figure 3.7 Depiction of: (a) standard deviation probability distribution for wind fluctuations, and (b) Power Spectral Density of the wind [10]

The drag force of the wind can be derived, from the wind speed, the structure's geometry, air density and air drag coefficients. The procedure of deriving these loads is presented in the

annexes in section C.2. As it is explained in further detail on the procedure of finding the dynamic response of the building in the annexes, only the dynamic loading is of relevance to calculate the acceleration. The result of this derivation is the following,

$$q_{Dy}(z,t) = B \cdot C_D \cdot \rho_a \cdot \bar{v}(z) \cdot \tilde{v}_{\parallel}(z,t)$$

With:

$\rho_a =$ 1.25 kg/m^3 = air density
$C_D =$ Drag coefficient
$B =$ Width of the Strucutre [m]

The equation for the dynamic load in the frequency domain can be expressed through the auto-variance spectra (S_{qq}) of the distributed wind drag force.

$$S_{qq}(z,f) = \left(B \cdot C_D \cdot \rho_a \cdot \bar{v}(z)\right)^2 \cdot S_{vv}(z,f)$$

This formula holds true for a single point, but since is needed for a large surface, the fact that wind fluctuation peaks do not always happen simultaneously, needs to be considered. So, the cross-variance spectrum ($S_{v1,v2}$) should be introduced when calculating the force over a large area. The is explored further on the annexes on section C.2, showing the procedure for calculating the aerodynamic admittance, which ensures the procedure to consider the collective wind load acting on the entire building.

Multiplying the aerodynamic admittance and the auto-variance spectrum of the distributed wind drag force at the reference height, yields its cross-spectra or equivalent spectrum.

$$H_a^2 = \left(B \cdot C_D \cdot \rho_a \cdot \bar{v}(z_s) \cdot \chi(f)\right)^2$$
$$S_{q_e q_e}(f) = S_{vv}(z_s, f) \cdot H_a^2$$

3.3.3 Tower Structure model

The tower structure is characterised by a 1D continuous representation of the main load bearing structure as a cantilever beam, supported by the foundation. Also, because of the high slenderness of high-rise buildings, deformation due to bending is predominant, while shear deformation is negligible [22]. Another characteristic to consider is that high-rise buildings do not have the same properties through all their height since the floor plan or the use of the floors can vary, which would impact the stiffness and mass. Finally, the building structure must also have energy dissipation. Considering that the model should fulfil all these characteristics of the building, the model is assembled from a baseline segmented but continuous Euler-Bernoulli beam, with the addition of material damping of the beam as well as fully populated, frequency dependant, complex valued dynamics stiffness matrix as the support of the beam. A depiction of this model can be observed in Figure 3.8.

The previously presented tower structure model is displayed with an arbitrary distributed force, to present the general case, but this load was substituted with the load from the wind model to solve for the dynamic response.

The complete formulation and assembly of the system through the equations of motion, loading, boundary conditions and interface conditions, are thoroughly described in the annexes on section D.1, D.2 and D.3. Likewise, the procedures for finding the solutions for the modal properties of the system as well as the dynamics response of the structure in the frequency domain can be found in the annexes in section D.4 and D.5.

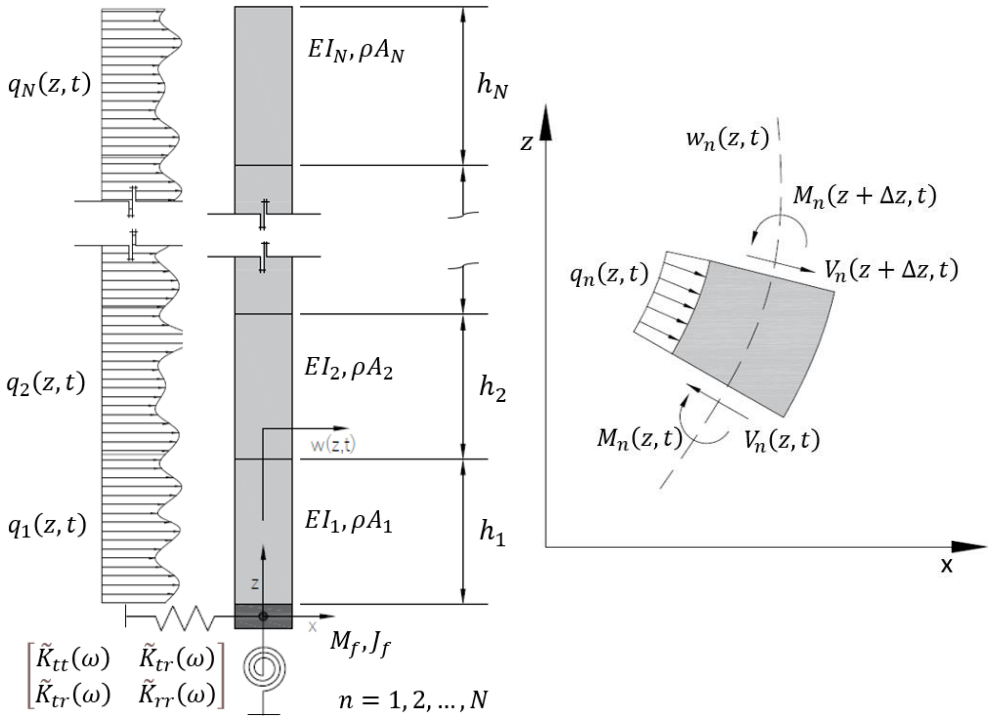

Figure 3.8 Diagram of HF Tower structure model, showcasing the reference and coordinate systems.

Hysteretic damping is also included in the beam model as rate-dependent term in the elasticity modulus (E^*). The final equation of motion that is formulated in the annexes is,

$$\rho A_n \frac{\partial^2 w_n(z,t)}{\partial t^2} + EI_n \left(\frac{\partial^4 w_n(z,t)}{\partial z^4} + \eta_n \frac{\partial^5 w_n(z,t)}{\partial t \partial z^4} \right) = q_n(z,t)$$

with,

$\rho A =$ density area of the cross section

$EI =$ bending stiffness of the section

$\eta = \frac{E^*}{E}$; damping coefficient

$n = 1, 2, \dots, N$; section number

One of the biggest limitations of this model is that it is only suitable for slender structures since the model is constructed under the assumption that bending is the predominant source of deformation. It is reasonable to assume that for most high-rise buildings this is the case, but since this model is used for the parametric study, it is important to mention that there are limits when sweeping for parameters such as height or stiffness of the building since the structure might not be considered slender at certain combinations of parameters.

4

Case Study: New Orleans Tower

4.1 Introduction

An important aspect in the design phase of high-rise buildings is the accurate prediction of the wind-induced dynamic response. This dynamic response is sensitive and heavily influenced by the damping and natural frequency of the system. Bronkhorst et al. [3] showed that the damping and natural frequencies estimated used in designed phase can deviate significantly from the measured damping in Dutch high-rise buildings. Additionally, studies form Bronkhorst et al. [3], Gomez [6], [7] and Cruz and Miranda [8] showed that the presence of soft soils, SSI can play an important role in the energy dissipation and in the natural frequency of the system. So SSI should not be disregarded from the impact it may have on the dynamic response of the system. These studies have investigated the influence of SSI on the overall damping, but do not address the effect on the dynamic response, such as the peak acceleration. The goal of the study presented in this chapter is the assessment of the significance of Soil-Structure Interaction on the wind-induced dynamic response of a high-rise building on soft soil.

To achieve this goal a case study of the 158 m high residential tower "New Orleans" in the city of Rotterdam, was realized. Three models are compared to the acceleration measurements on this tower: the EC model, the NIST model and the HF model. The Eurocode (EC) model computes the wind load and resulting peak acceleration according to the guidelines provided in the Eurocode EN 1991-1-4 [2] . This model does not explicitly account for SSI. The NIST model is the same as the EC model, but it includes the effects of SSI with a simplified approach based on the period lengthening by modifying the natural frequency and modal damping. The period lengthening effect requires equivalent foundation spring stiffnesses which were obtain based on the Dynaplile values at the first natural frequency of the fixed base building. The High-Fidelity (HF) model applies an accurate description of the wind load, tower structure and foundations. The wind load is obtained from the measured wind loads. The building is modelled with a segmented Euler-Bernoulli beam model, with structural properties based on a FEM model. The foundation is described with frequency dependent (dynamic) translation and rotation springs, which are computed from a detailed model of the piles and soil in Dynaplile. The complete model is solved in the frequency domain. More detail explanation on the models are presented in chapter 3.

The HF model provides the most accurate description of the important components in the modelling of the along-wind dynamic response. With this model it is possible to accurately quantify the influence of SSI on the dynamic response.

The EC model is the current approach applied in engineering practice for the design for high-rise buildings. With this model can be determined how the current procedure in design compares to the in-situ measurements and the HF model.

The NIST model is a simplified approach also applied by Bronkhorst et al. [3], and Cruz and Miranda [8]. This model is a relatively simple way to include SSI in the calculation of the wind-induced dynamic response. Nevertheless, these methodologies have been developed for seismic conditions, and have not been validated for high-rise buildings under wind loading. Through the comparison of the NIST model results with the measurement results and the results of the other models can be established whether this simplified approach is appropriate to take into account SSI for high-rise buildings under wind loading.

4.2 New Orleans Tower

Given there are synchronous measurements of both wind loading and accelerations of the New Orleans Tower, it provides an opportunity to verify the HF model. This verification is of great importance since the HF model combines several different physical phenomena and modelling approaches, that by themselves have been vastly studied and validated in literature but have not been studied in combination.

The New Orleans Tower is currently (as for 2022) the third tallest building in the Netherlands, with 44 stories and 154m in height to its roof and 158m in height to the spire. It is a residential building, located in Rotterdam since 2010. In Figure 4.1, the general distribution of the building is depicted. It is a concrete building cemented on concrete piles, with a two-storey basement. The building is composed of two sections, section A being the tower and section B a 3-storey low rise. For this case study, the focus is only on the tower (A).

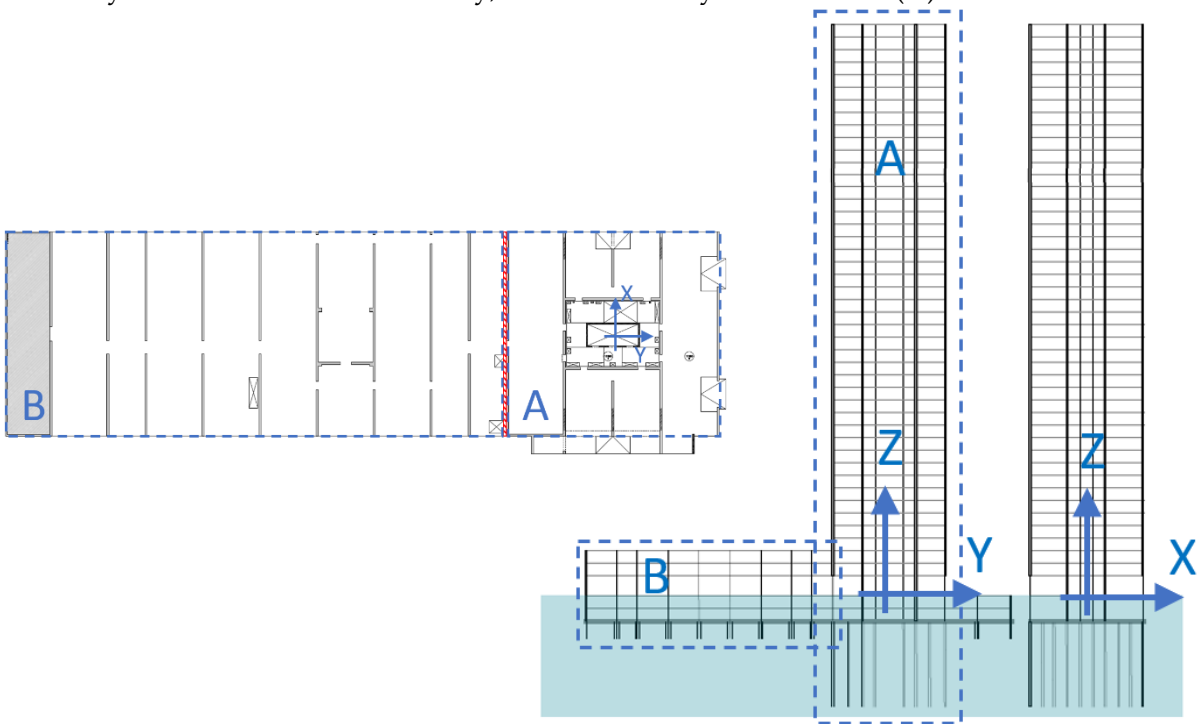

Figure 4.1 Cross-section and plan view of the New Orleans Tower, showing the tower sections and reference frame.

The New Orleans Tower is instrumented with equipment to continuously monitor wind pressure, wind velocity, and the structure's acceleration. The wind velocity was measured by a sonic anemometer (Gill, type 1561-PK-020) that is located on top of a mast at a height of 160 m. This device is 2 m above the roof of the building near the South corner of the top floor, which means that the structure is close enough to influence the wind measurements. The wind pressure was measured by pressure sensors (Sensortechnics, type HCLA12X5DB) which are installed on the façade of the 34th storey at a height of 114 m. In the same storey, there are also four acceleration sensors (Sundstrand, type QA-700). The location both in height and plan distribution of the sensor positions can be seen on Figure 4.2

More information about the monitoring arrangement and the data acquisition can be found in van Bentum, Geurts, Kalkman and Bronkhorst [23],[24], [25]

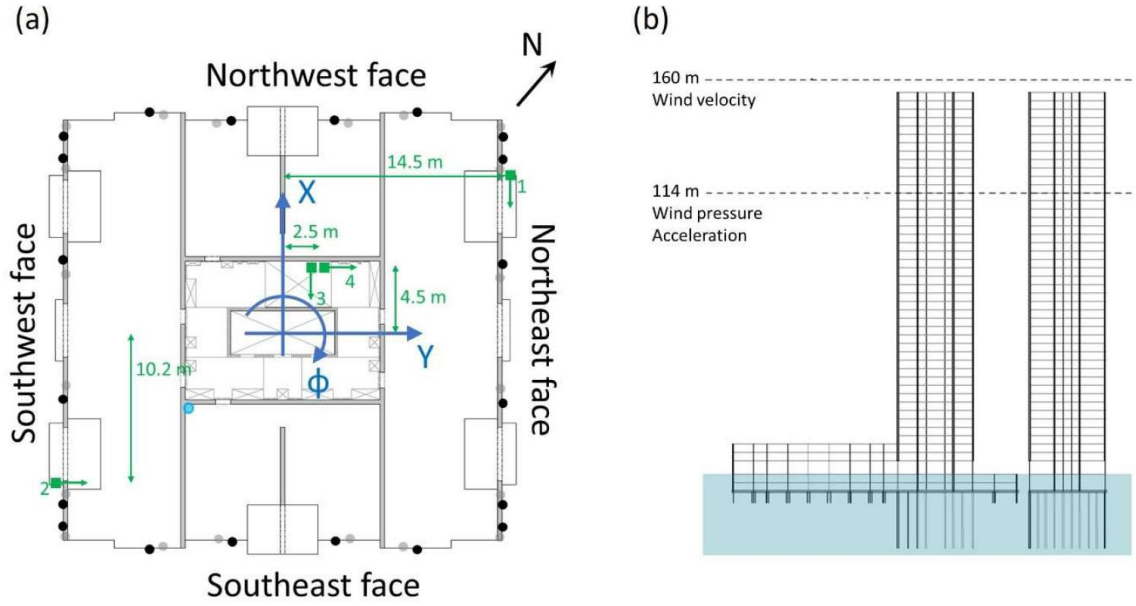

Figure 4.2 (a) Floor plan of New Orleans the location of the acceleration sensors (green), wind velocity (blue) and pressure sensors (grey and black).

The data was recorded synchronously for all sensors over 10 minute periods with a sampling rate of 20 Hz from 2012 to 2016. Each 10 minute period of recoding corresponds to a single event. For this study the drag force of the wind, parallel to the defamation of the structure, is of interest. This wind direction corresponds to 145°±5° with respect to North. Also, to find the expected stochastic values of the response of the structure, it is important to look at events with similar ergodic loading, in this case wind events with the same mean and standard deviation of wind speed are ergodic process and subsequently, the loading will be as well. For this reason, from the 10 min events, the mean wind speed and wind direction from the sonic anemometer is calculated and then used to characterise, filter and group the different events. In the case of the wind speed, they were grouped in 2m/s intervals from 10m/s to 16m/s. For each group the average values for the maximum acceleration, standard deviation and Power spectral Density function (PSD) were calculated. The total set of measurements contains 32 769 events, but only the highest wind speeds events where chosen wind events. There was 495, 220 and 47 events in each group, for 10-12 m/s, 12-14 m/s and 14-16 m/s, respectively. From the PSD functions of the measurements in Figure 4.3 and Figure 4.4. it can be observed that the grouping with a lower number of events shows noisier results, since it has a smaller

sample set. This should not be much of a problem, since the ergodic nature of the wind means that events within their group should al have similar properties.

For each group, mean values, standard deviation and autocorrelation are calculated based on the post-processed experimental data. Additionally used the Fourier Transform of the autocorrelation performed used to compute the PSD. The results of the PSD functions for the acceleration are displayed in Figure 4.3 and for the wind force are displayed in Figure 4.4. Furthermore, these post-processed data need to be extrapolated to other heights since they only describe the stochastic events at the measured heigh, 160 m and 114m for the wind speed and pressures, respectively. For this, the theoretical formulation, and model presented in previous chapters were used. Other information that was calculated from the measurements, was the mean force acting the building, for each group. This force is later used to back calculate the mean wind speed and compare it form the mean wind speed measurements.

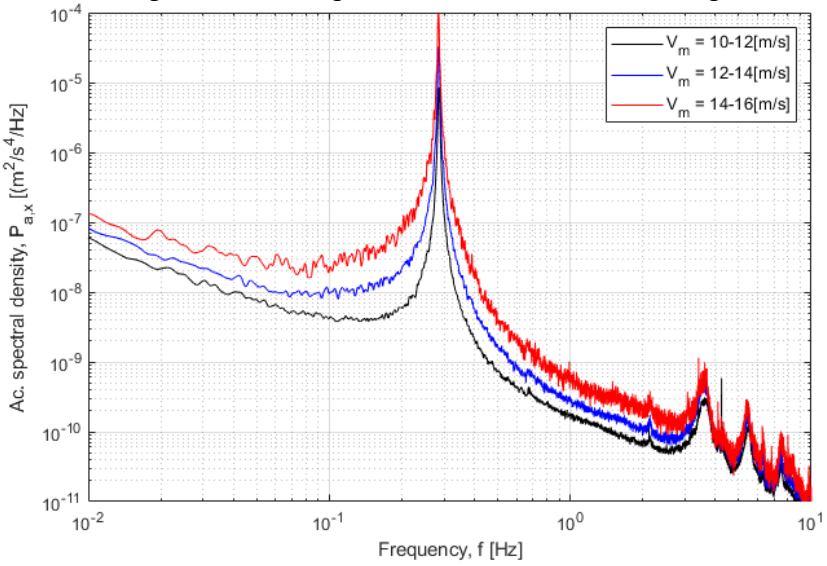

Figure 4.3 Power Spectral Density function of the acceleration measurements divided into the wind speed groups.

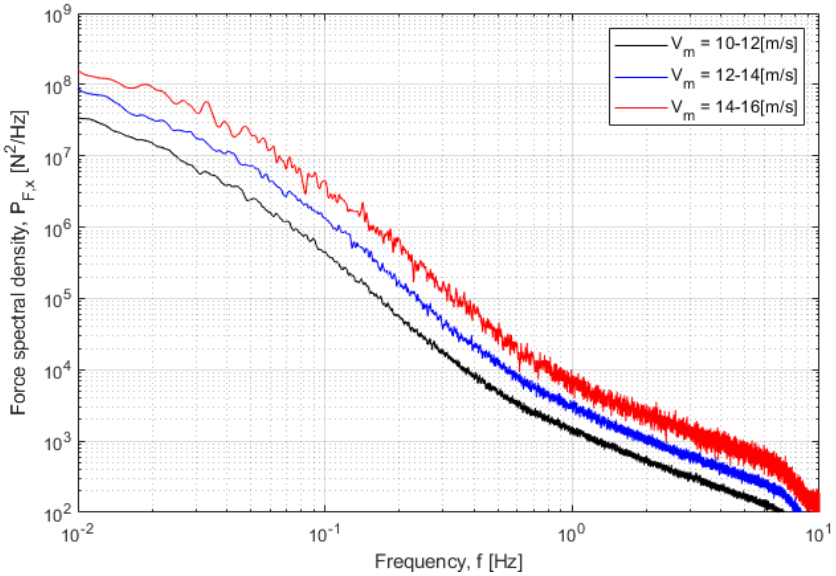

Figure 4.4 Power Spectral Density function of the wind force measurements divided into the wind speed groups.

4.3 System parameters HF model

To accurately predict the behaviour of the New Orleans tower, it is imperative to introduce accurate system parameters. This section focuses on describing the relevant system parameters that were introduced in the model.

4.3.1 Soil

The soil properties were be calculated from the CPT test done close to the building. The CPT information was taken from DINO, a digital archive of the Geological Survey of the Netherlands [26]. In Figure 4.5 a map of the DINO platform can be observed, showing a 100 m radius circle centred on the tower, inside this radius there are 9 locations (marked in brown triangles) with total 27 CPR test results.

From these results, the average properties of the soil were calculated. The ones we are most interested in are shear wave velocity and the density, these results can be seen in Figure 4.6 and Table 4.1. It is important to mention that since there is a grate level of fluctuations in the soil with its depth, but there is a clear soil layer distinction, so the soil layers have been simplified to constant average properties in each layer.

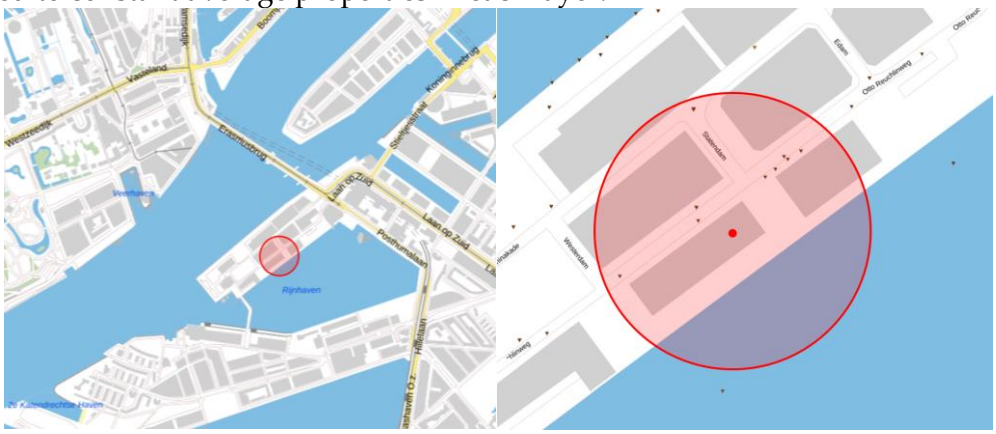

Figure 4.5 Map of the DINO platform showing a 100 m radius circle centred on the tower and the locations (marked in brown triangles) of the test site. Taken from [26]

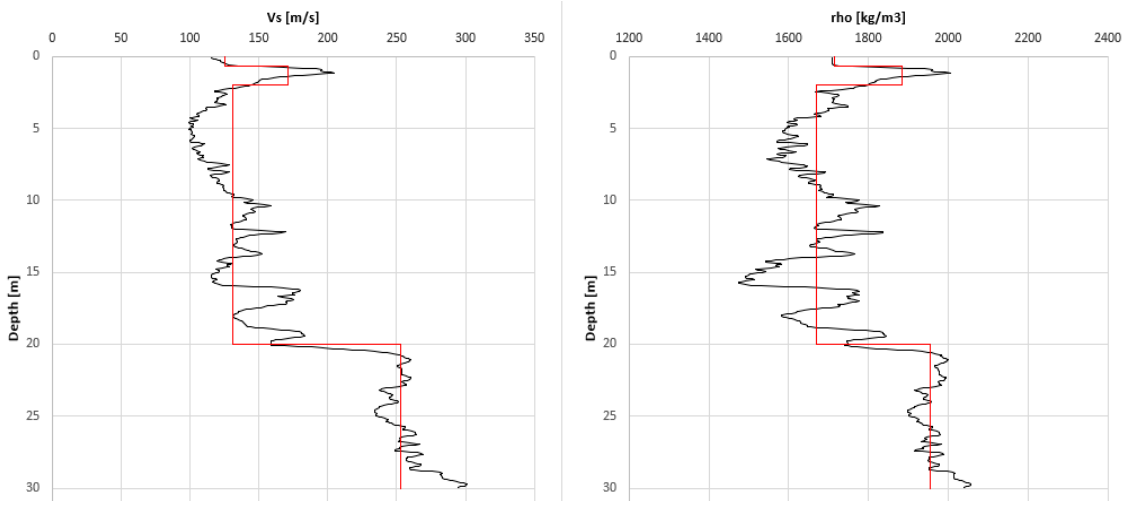

Figure 4.6 Average soil profile in terms of depth of the (a) shear wave velocity, and (b) soil density, for the surrounding area of the New Orleans Tower.

Another property of importance is the material damping of the soil. This property is generally found through dynamic soil testing like the Resonant Column Test. From the information gathered, there are no dynamic soil test results available on the soil on the surrounding of the building. Moreover, there are some empirical formulas like the one proposed by Darendeli [27] that use the properties of the soil to calculate the material damping. This formulation requires, the following information: oscillation frequency, strain amplitude, soil composition, granulometry, plasticity index, over consolidation ratio and mean effective confinement pressure. Furthermore, the empirical formula has some parameters that seem to vary with different geological locations, which means that they should be obtained by fitting the curves with existing soil dynamic test results. Given these complications and the simplifications of the soil already taken, it was decided that approximate values for the damping were accurate enough. From the data in Darendeli [27], for this case study the sands would have a damping ratio between 0.015-0.025 and the clays would have a damping ratio between 0.025-0.035. Average values of 0.02 and 0.03 respectively, were used.

Table 4.1 Soil layer properties

Parameter		1st soil layer	2nd soil layer	3rd soil layer	4th soil layer
Description		Top sand	Clay	Sand	Clay
Depth		0.0 m to 0.7 m	0.7 m to 2.0 m	2.0 m to 20.0 m	20.0 m to 30.0 m
Thickness		0.7 m	1.3 m	18 m	10 m
Share wave velocity	V_s	125 m/s	171 m/s	131 m/s	253 m/s
Density	ρ	1714 kg/m^3	1885 kg/m^3	1670 kg/m^3	1955 kg/m^3
Damping coefficient	η	0.02	0.03	0.02	0.03
Poisson's Ratio	υ	0.3	0.3	0.3	0.3

4.3.2 Foundations

The tower is cemented over 308, reinforced concrete piles of 45 cm in diameter and 27 m in length. The 308 piles are distributed, as presented in Figure 4.7. It is important to notice that some distinct sections have been color-coded. In the centre, in red, the elevator shaft has a 0.5 m thick foundation slab with a 0.3 m wall connecting it to the rest of the foundation. Next in blue there is a ring of a 2.5 m tick concrete slab working as a header for the piles in the core. In yellow, a thick outer ring slab of 2.5 m connects all perimeter piles. In green, a thinner concrete slab of 0.3 m connects the outer and inner ring. To prevent stress on the foundation due to differential settlement during the construction, the connection between the rings is done after the structure has been built. This should not have any effect on the dynamic behaviour during the operational phase, which was investigated at very short time scales. From this geometry, the foundation can be simplified to a rigid foundation slab with the same pile distribution. The properties of the piles are presented in the Table 4.2.

Dynaplile does not have the capability to model basement opening so the rigid slab will be modelled at the ground level. To set up the Dynaplile model you need: the 4 material properties of the soil layers $(\rho, G, \beta, \upsilon)$, the geometric distribution (depth) of the soil layers, the 4 material properties of the piles $(\rho, E, \beta, \upsilon)$, the cross-sectional properties of the pile (ϕ) and the geometrical distribution of the piles. With all these properties the model can be set up, which can be observed in Figure 4.8. Also, the frequencies of interest was from 0 Hz to 6 Hz. It was considered the expected frequencies of relevance with respect to both the force and the

mechanical admittance of the structure ± one order of magnitude, to be able to see effects of at least the third mode. With this range of frequencies the mesh size also can be defined taking into account the smallest expected wavelength. The most critical combination is the lowest soil stiffness and the highest frequency. The smallest wavelength would be of 20 m so a mesh size of 1 m sufficient resolution to be able to convey it.

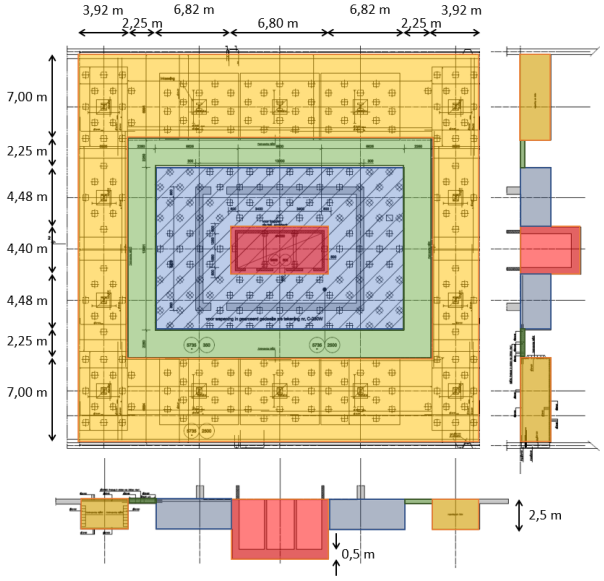

Figure 4.7 Pile plan and foundation slab drawing showing the location of the piles and the varying thicknesses of the slab.

Table 4.2 Concrete pile properties

Parameter		Concrete pile
Amount		308
Depth		8.2 m to 25 m
Diameter	$\emptyset$	0.45 m
Elastic Modulus	E_p	30 GPa
Density	ρ	2300 kg/m^3
Damping coefficient	η	0.005
Poisson's Ratio	υ	0.2

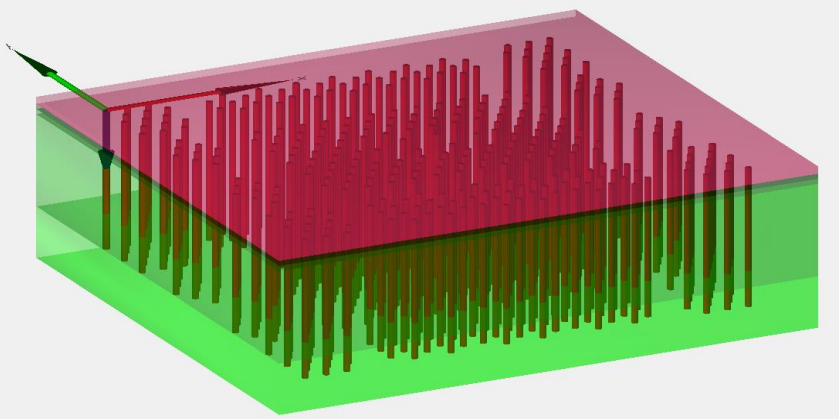

Figure 4.8 Image from Dynaplile of the foundation model for the New Orleans Tower.

The results from the Dynaplile software, provide the complex valued frequency dependant stiffness. In the figure below from the Dynaplile manual, shows clearly that the software does not calculate the full dynamic stiffness matrix, it calculates 11 out of the 21 unique stiffness.

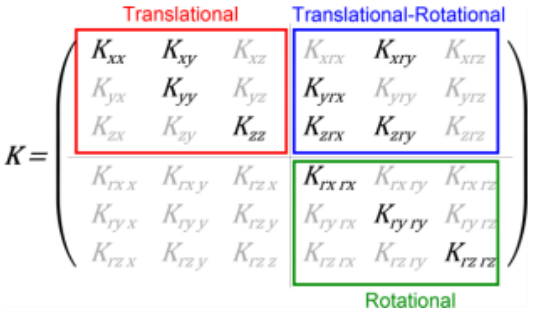

Figure 4.9 3D dynamic stiffness matrix. Taken from Dynaplile Technical Manual [28]

For this study this is not a limitation, since only the translational and rotational stiffnesses in one plain are relevant not the full 3D dynamic stiffness matrix. This means that the stiffness matrix reduced to 4 terms, one translational, one rotational and their coupling terms. In this document is represented by,

$$\bar{\bar{K}}_d(\omega) = \begin{bmatrix} \tilde{K}_{tt}(\omega) & \tilde{K}_{tr}(\omega) \\ \tilde{K}_{tr}(\omega) & \tilde{K}_{rr}(\omega) \end{bmatrix}$$

this dynamic stiffness matrix is complexed valued.

The dynamic stiffness matrix used in the case study, was computed using the system properties of the soil and the foundation presented in this section and the previous one. Figure 4.10 displays the results of the dynamic stiffness matrix. The different components of the dynamic stiffens are presented in a 2x2 grid, mirroring the 2x2 matrix form distribution.

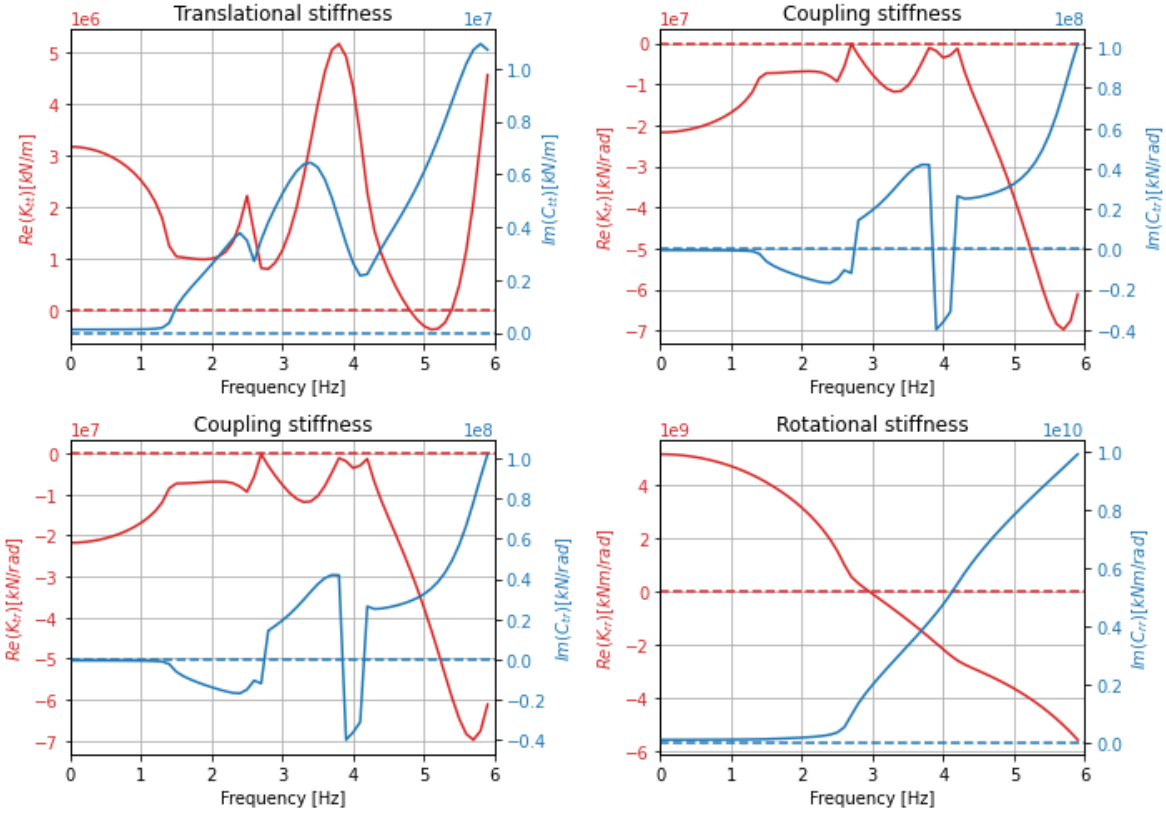

Figure 4.10 Dynamic stiffness matrix in graphical form.

4.3.3 Wind

This section explains how the data acquired from wind measurements, was used to construct a model of wind pressure on the reference height of the building. First, the PSD of the wind force at 114 m shown in Figure 4.4, were converted to a distributed drag force by dividing it by the tributary height of the force. This PSD of the drag force at 114 m was then used to calculate the PSD of the drag force at the reference height.

From the wind model provided by the Eurocode EN 1991-1-4 [2], the standard deviation of the wind speed does not vary with height, and in fact, for events with the same mean velocity and roughness factor, it is a constant, which means that standard deviation of the wind speed does need to be recalculated. The PSD of the wind velocity ($S_{vv}(f)$) as presented in previous chapters, is computed from the constant standard deviation of the wind speed and components computed from the frequency, which means that it is also height independent.

The calculations for the equivalent wind pressure power density spectrum require the aerodynamic admittance and the PSD of the drag force at the reference height, to solve,

$$S_{q_e q_e}(f) = S_{qq}(z_s, f) \cdot \chi(f, \bar{v}(z), z_s)^2$$

The aerodynamic admittance was calculated with the procedure stated in section 0 using the values of height and width of the building (H, B) as defined in the geometrical description of the building in this chapter. This procedure also requires the mean wind speed distribution and at the reference height. This reference hight comes from the hight of the wind stagnation point which is an appropriate reference point for the overall admittance.

For the mean wind speed, flowing the Eurocode EN 1991-1-4 [2] the measurements were made at 160 m and need to be calculated at a reference height of 60% of the total height of the building (96 m). The formulation of the Eurocode EN 1991-1-4 [2] as presented in previous chapters is the following:

$$\bar{v}(z) = v_b \cdot k_r \cdot \ln\left(\frac{z}{z_0}\right)$$

Which can be manipulated to find the value at 96 m, $\frac{\bar{v}(z_s)}{\bar{v}(H)}$,

$$\bar{v}_1(z_s) = \bar{v}(H) \cdot \frac{\ln\left(\frac{z_s}{z_0}\right)}{\ln\left(\frac{H}{z_0}\right)}$$

with,

z_s = Reference height of the structure ($z_s = 0.6H = 96\text{m}$)
z_0 = terrain roughness length

The terrain roughness length (z_0) can be calculated using the Dutch national annex NEN-NE 1991-1-1-4+A1+C2 [20].

As it was mentioned before the measurements of wind speed are taken only 2 m away from the building rooftop, so this mean wind speed measurements potentially have been influenced by the wind flow around the building. So, a second set of mean wind speed at reference height are calculated from the average static pressures.

$$F = {\bar{v}_2}^2 \cdot C_D \cdot \rho \cdot A$$

$$\bar{v}_2(z_s) = \sqrt{\frac{F}{C_D \cdot \rho \cdot A}}$$

The second set of results of wind speed are indirect measurement, which comes its own set of assumptions. For this reason it was decided that the average of both measurements will be used. The results of this wind speed calculations and their average are presented on Table 4.3.

The PSD of the drag force was measured at 114 m and it is required at the reference height (96m). A similar procedure than for the mean wind speed is used to make the height transfer.

Table 4.3 Mean wind speed at reference height results, for each group.

Groups $\boldsymbol{v_m}[m/s]$	$\bar{v}_1(z_s)$ $[mm/s]$	$\bar{v}_2(z_s)$ $[mm/s]$	$\bar{v}_{av}(z_s)$ $[mm/s]$
10-12	9.86	6.23	8.05
12-14	11.05	7.20	9.13
14-16	12.86	8.81	10.84

The formulation of the S_{qq} as presented in previous chapters is the following:

$$S_{qq}(z,f) = \left(B \cdot C_D \cdot \rho \cdot \bar{v}(z)\right)^2 \cdot S_{vv}(f)$$

This formulation can be manipulated to find the value at 96m through ,

$$\frac{S_{qq}(z_s,f)}{S_{qq}(z=114,f)} = \frac{\left(B \cdot C_D \cdot \rho \cdot \bar{v}(z_s)\right)^2 \cdot S_{vv}(f)}{\left(B \cdot C_D \cdot \rho \cdot \bar{v}(114)\right)^2 \cdot S_{vv}(f)}$$

$$S_{qq}(z_s,f) = S_{qq}(z=114,f) \cdot \frac{\ln\left(\frac{z_s}{z_0}\right)^2}{\ln\left(\frac{114}{z_0}\right)^2}$$

From this, the equivalent wind pressure power density spectrum can be calculated as:

$$S_{q_e q_e}(f) = S_{qq}(z=114,f) \cdot \frac{\ln\left(\frac{z_s}{z_0}\right)^2}{\ln\left(\frac{114}{z_0}\right)^2} \cdot \chi\left(f, \bar{v}(z)\right)^2$$

The results of the equivalent wind pressure PSD are presented in Figure 4.11

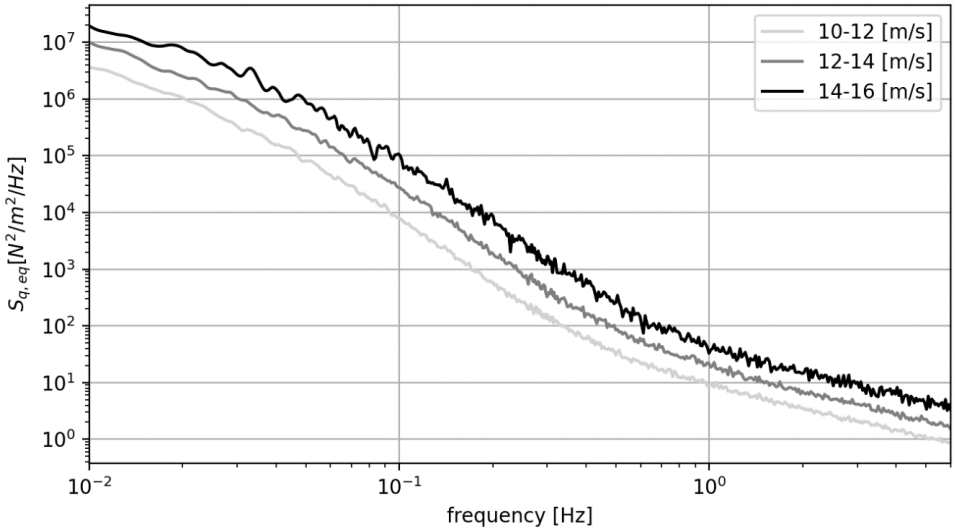

Figure 4.11 Equivalent wind pressure power density spectrum for the 3 wind speed groups.

4.3.4 Tower structure

The tower has a reinforced concrete shear wall system with prefabricated concrete slabs. The properties of interest of the building, for the model are: the bending stiffness (EI), density (ρ), cross section geometry, material damping coefficient (η). Since the building is not completely homogeneous all through its height, it is important to divide the building into segments which do have the same properties. A depiction of this division is depicted on Figure 4.12.

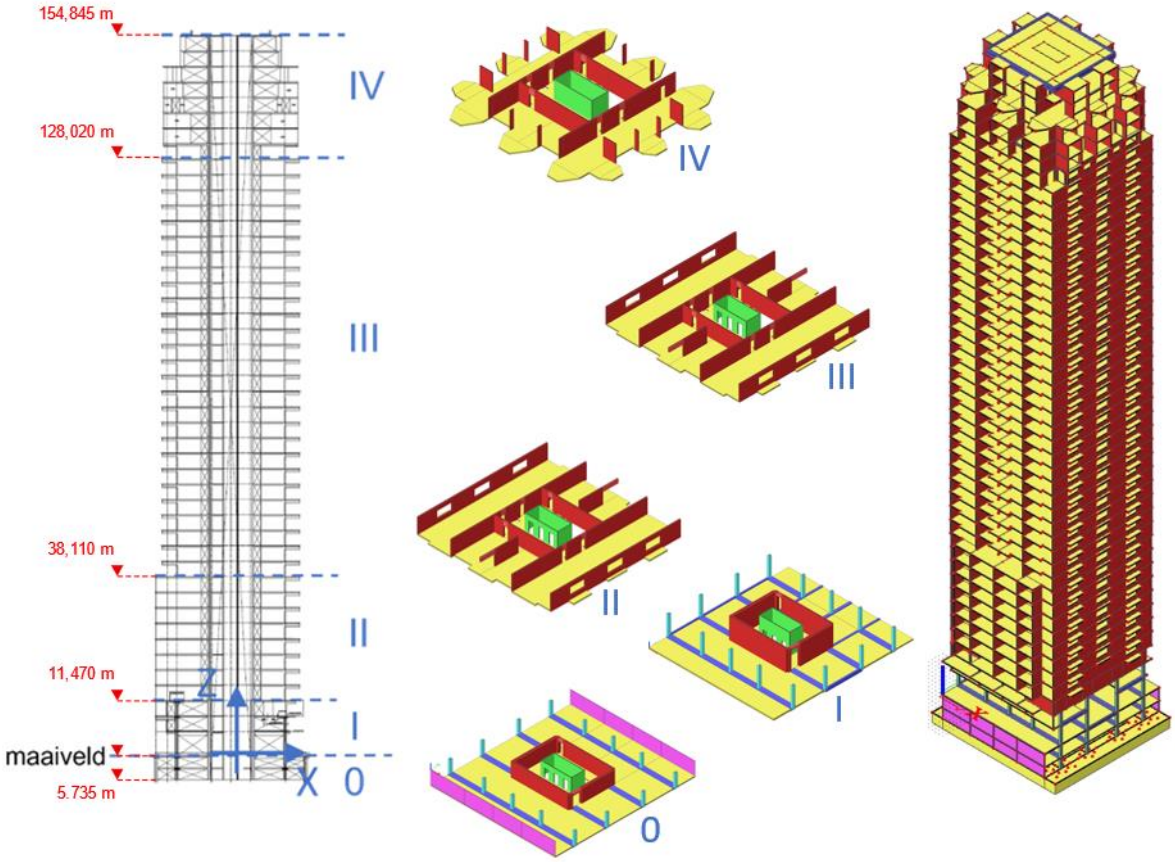

a) b) c)

Figure 4.12 (a) Vertical section of Tower from the structural plans, (b) Representative stories from this sections modelled in SCIA Engineer , and (c) Complete model of the tower in SCIA Engineer.

From the properties previously listed, the bending stiffness is one of the hardest properties to define accurately due to the irregular geometries, connections between members and considering partially cracked concrete members. To account for this, a 3D FEM model in SCIA Engineer, of the complete tower structure, was used to calculate the bending stiffness. As mentioned in section 4.3.2, the Dynaplile software does not provide the capability to model the basement so Section 0 is not included in the mode.

The damping coefficient for a reinforced concrete structure is between 1% and 0.5% as presented by S. Chowdjury [29]. For this study it the mid value of 0.75% was used. This damping value was introduced as a constant value.

This model was also used to calculate the mass density of the sections. This model included not only the permanent load of the structure also a partial contribution of the variable load. A summary of all properties of the tower, provided by BESIX, is listed in Table 4.4.

Table 4.4 Tower structure properties

Parameter		Section I	Section II	Section III	Section IV
# of stories		3	8	27	8
Heights		0.0 m to 11.5 m	11.5 m to 38.1 m	38.1 m to 128.0 m	128 m to 154.8 m
Length		11.5 m	26.6 m	89.9 m	26.8 m
Cross section	BxL	28 m x 30 m	28 m x 30 m	28 m x 28 m	25 m x 25 m
Cross section area	A	840 m²	840 m²	784 m²	625 m²
Bending Stiffness	EI	36.2 x10¹² Nm²	104.2 x10¹² Nm²	89.2 x10¹² Nm²	29.7 x10¹² Nm²
Density	ρ	444 kg/m³	436 kg/m³	423 kg/m³	463 kg/m³
Damping coefitient	η	0.0075	0.0075	0.0075	0.0075

The EC and NIST models, introduced in chapter 3 used the same system parameters as the HF model, with the simplifications and procedures explained in sections 3.1 and 3.2. A noteworthy property is that the wind power spectra density function ($S_L(z_s, f_n)$) is obtained using the mean wind speeds calculated in section 4.3.3.

4.4 Results and discussion

4.4.1 Effect of tilt on the dynamic response

This section presents the results of the dynamic analysis of the HF model with and without tilt compared to the result of the post-processed measurements for the New Orleans Tower Case Study. This was done by calculating the transfer function of the lateral and tilt components of the acceleration separately and comparing those results to the complete HF model and the measurements. The results presented in this section build upon the explanation of the tilt and lateral component of the acceleration as presented in annexe D.5.2, and reference to the nomenclature and figures from this section. Figure 4.13 shows the acceleration response density function of tilt and lateral acceleration separately, the combined results and the measurements, for the 10-12 m/s event group. The other 2 groups displayed similar results and the same tendencies.

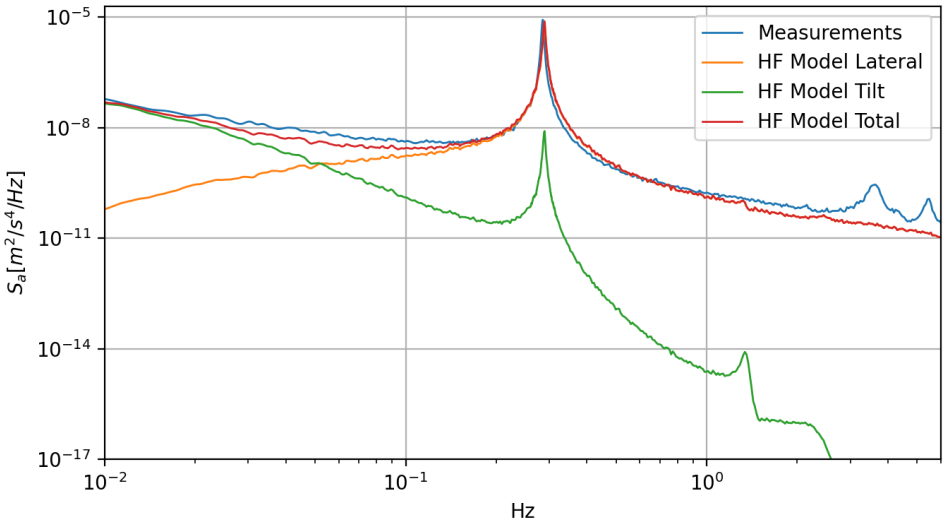

Figure 4.13 Acceleration response density function of the HF model (tilt, lateral and complete) and acceleration measurements at a height of 114 m, for the 10-12m/s event group

From this figure, it can be observed that the lateral component of the acceleration has a close fit to the measurement for frequencies higher than 0.1 Hz, but does not present the same behaviour as the measurements for low frequencies, especially in the 0.01 Hz range. From a physical stand point, this is to be expected since static equilibrium as expected lateral acceleration of the building should be zero, therefore, at low frequencies, there should be a tendency to zero acceleration. The lateral acceleration transfer function can be written as the transfer function of the lateral deformation multiplied by the frequency squared.

$$H_{\ddot{w}}(z,\Omega) = -\Omega^2 \cdot H_w(z,\Omega)$$

So it is expected that the tendency of the lateral acceleration for decreasing frequencies is decreasing and eventually tends to zero acceleration on the statical case. Which is the case when only looking at the lateral component. But in the measurements there seems to be an opposite tendency were at very low frequencies, that could be consider almost static have a significant acceleration magnitude.

Given this large discrepancies at low frequencies the effect of the tilt of the structure was studied. The frame of reference of the accelerometer making measurements changes with the tilt of the floor of the structure, which means that total acceleration experienced by the acceleration sensor has a gravitational component due to the change in frame of reference.

In the case of the tilt component of the acceleration it can be observed that it has a high influence in the acceleration for low frequencies. From a physical stand point this is to be expected since this component is related to the rotation of the structure and the small component of the gravitational acceleration that is now is parallel to the floor of the building. This rotation of the structure will be present any frequencies including under static conditions. Figure D.2 helps illustrate this concept. Mathematically it can be noted that the tilt is computed from the transfer function of the rotation angle multiplied by acceleration of gravity.

$$H_{tilt}(z,\Omega) = g \cdot \sin\left(H_{\phi}(z,\Omega)\right)$$

The HF model that includes the influence of both components is a much better match with the measurements. Note that the tilt component only has a significant impact on the low frequencies since above 0.1 Hz it has more than 2 orders of magnitude difference than the lateral component. The same can be said of the lateral component for low frequencies.

Table 4.5 shows that around 96% of the overall acceleration can be explained from the lateral component of the acceleration and only around 6% comes from the tilt. The sum is not expected to add up to 100% since the combination of the transfer functions to compute the acceleration is not a linear summation of the components. The results form Table 4.5 and Figure 4.13 concur, since it is clear that at the natural frequency, where most of the frequency content of the response is located the impact on the acceleration of the building will be small.

Table 4.5 Peak acceleration of each component of the HF model compared to the total

	$\boldsymbol{a_P}$ $[mm/s^2]$	
HF Model Total	0.846	-
HF Model Lateral	0.814	96%
HF Model Tilt	0.053	6%

This extra step of adding the tilt does not increase significantly the computational time since it uses information already necessary for the lateral acceleration transfer function. From this,

it can be concluded that even though the component of the tilt has a small impact on the global acceleration, it can provide an extra level of detail if the predictions need to be accurate at a low set up and computational cost. For this study, it has been decided to use the complete HF model, given that a wide range of parameters will be studied and for some of them, the tilt could become of greater importance.

4.4.2 Comparison between models

This section presents the results of the dynamic analysis of the HF, NIST and EC models and the result of the post-processed measurements for the New Orleans Tower Case Study. The models are assembled using the system parameters described in the previous sections and following the procedures in chapter 3. Given that the measurement of the acceleration was performed at the 34th floor (114 m), this is the height where the dynamic response is compared.

In Figure 4.14, the acceleration PSD of the HF model is plotted with the acceleration PSD extracted from the measurements, for each explored wind speed range. From this figure, for all wind speed groups, there is a good match between the acceleration density functions of the HF model and the measurements. Especially, that the peak responses share a similar frequency, magnitude and shape. This location of the peak corresponds to the natural frequency, for the three HF models and for the measurement groups are at 0.29 and 0.28 Hz, respectively. This natural frequency values are in accordance with the 0.28 Hz measured in the TNO report [23], [30]where a broader set of measurements was used.

From these results, it is important to point out that the structure's second resonance frequency of 1.36 Hz, does not display a peak in neither the HF model nor measurements spectra density function in Figure 4.14. This is an expected result since at the observed high of 114 m, the mode shape has almost zero amplitude. This can be seen from in Figure 4.16, where the mode shapes of the first three modes are shown. In the study by Bronkhorst et al. [30] temporary sensors were added at different locations and heights of the building, with which they could find mode shapes and the higher natural frequencies. In this study the second resonance frequency in the relevant direction was measured at 1.53 Hz, which is an 11% difference from the second natural frequency from the HF model. Also, the second mode shape obtained in the study from Bronkhorst et al. [30] also finds insignificant magnitude at 114 m.

From the mode shapes in Figure 4.16, it can be observed that for the first model it looks like a regular cantilever with very little to no translation or rotation at the base, while modes 2 and 3 do show doses show translation or rotation at the base. This means that the structure has a stiffer base on the 1st mode than on the 2nd and 3rd. This coincides with the stiffness magnitudes present on the foundation dynamic stiffness matrix for each of the mode's natural frequency, where in translation and rotation, the stiffness of the first mode would be between 3 and 5 times greater than the 2 other modes. This is demonstrated in Figure 4.15, where the translational and rotational stiffness are presented, paired with markers at the natural periods of the system.

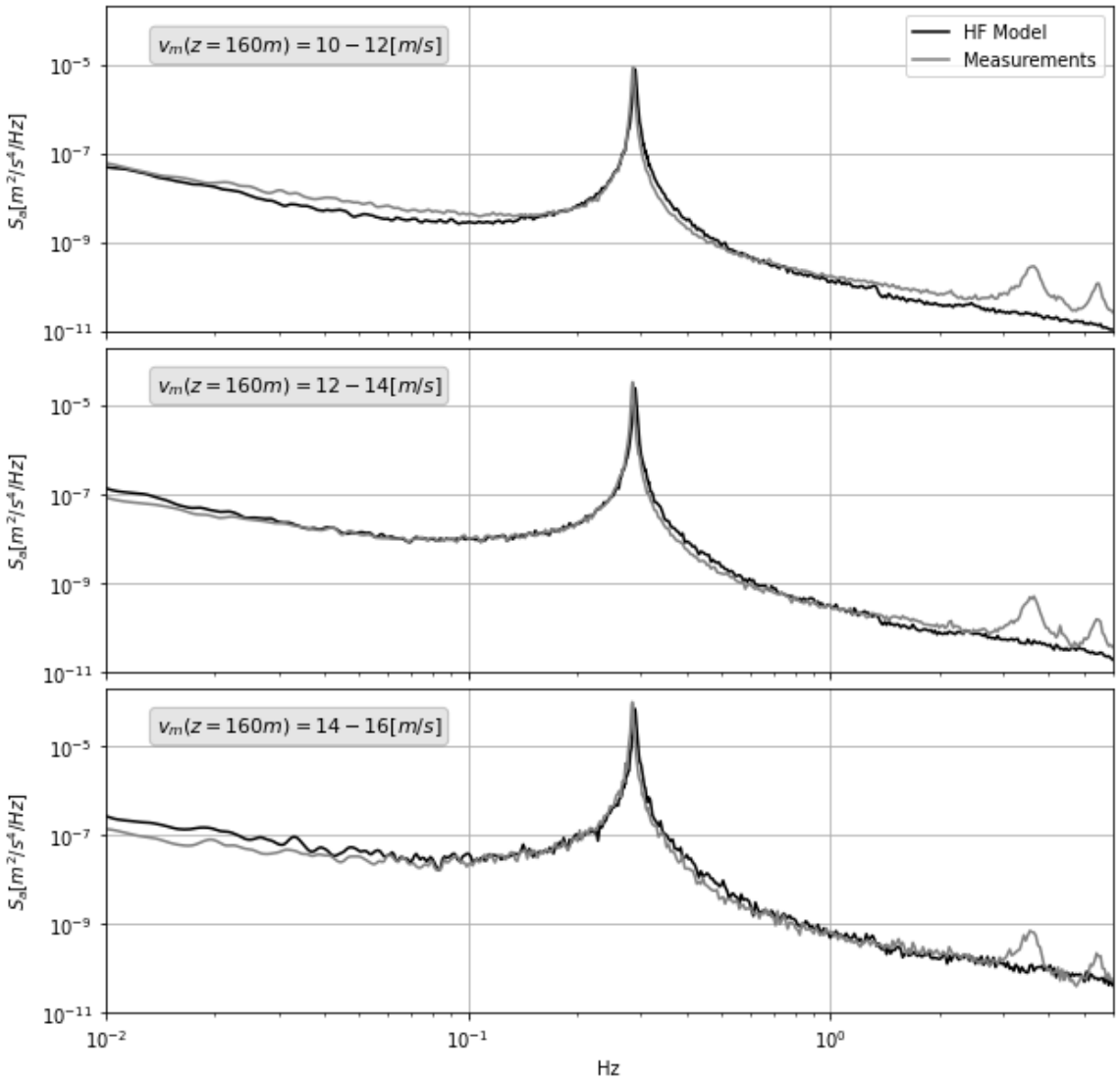

Figure 4.14 Acceleration response density function of the HF model and acceleration measurements at a height of 114 m.

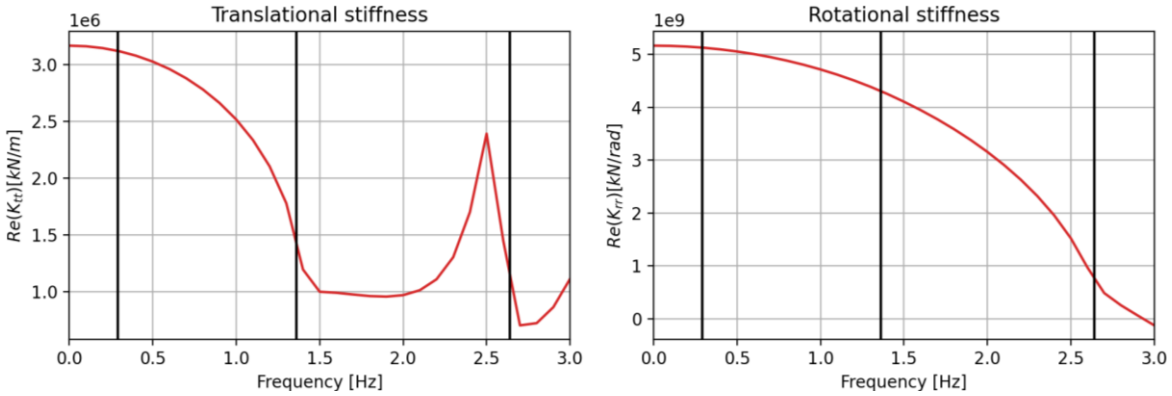

Figure 4.15 Translational and rotational dynamic stiffness with markers for the first eigen frequencies.

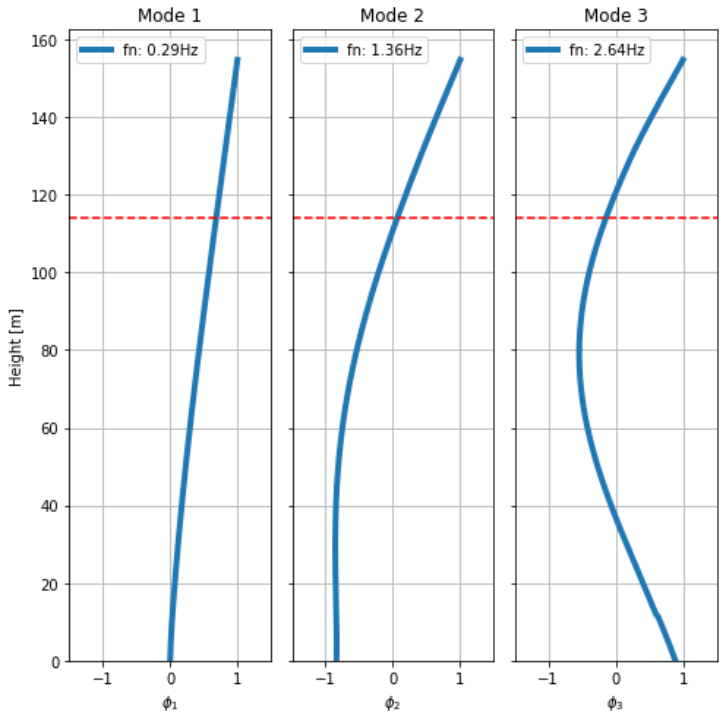

Figure 4.16 First three mode shapes from the HF model of the New Orleans Tower.

The dynamic properties of the HF, NIST and EC models are compared to the measurements in Table 4.6. Hear the standard deviation of the acceleration (σ_a), expected peak value of the acceleration (a_P), the global damping ratio (ζ) and the first natural frequencies are compared. For the HF, the acceleration results are calculated using the procedure shown in annex D.5. The acceleration results for the NIST and EC models were calculated using the procedure shown in sections 3.2 and 3.1, respectively. An extra EC model has been included which follows the same procedures but uses the natural frequency used during design ($f_n^* = 0.19\ Hz$) instead of the natural frequency proposed by the Eurocode. For the HF model and the measurements, the damping ratio was calculated through the Half Power Band Width method (HPBW) on the acceleration spectral density functions. The EC model has a constant 1.6% damping, while the NIST model method for recalculating this damping ratio is presented in annexes 3.2.

Table 4.6 Dynamic properties of the all model compared to measurements

	v_m $[m/s]$	a_P $[mm/s^2]$	$\%E$	ζ	$\%E$	f_n $[Hz]$	$\%E$
Measurements		0.830	-	0.842	-	0.285	-
HF Model		0.846	2%	0.802	-5%	0.289	1%
NIST Model	10-12	0.730	-12%	0.910	8%	0.250	-12%
EC Model		0.551	-34%	1.600	90%	0.297	4%
EC Model*		1.250	51%	1.600	90%	0.190	-33%
Measurements		1.562	-	0.804	-	0.284	-
HF Model		1.455	-7%	0.833	4%	0.289	2%
NIST Model	12-14	1.272	-19%	0.910	13%	0.250	-12%
EC Model		1.040	-33%	1.600	99%	0.297	5%

EC Model*		2.325	49%	1.600	99%	0.190	-33%
Measurements		2.673	-	0.759	-	0.284	-
HF Model		2.610	-2%	0.769	1%	0.289	2%
NIST Model	14-16	2.207	-17%	0.910	20%	0.250	-12%
EC Model		1.853	-31%	1.600	111%	0.297	5%
EC Model*		3.885	45%	1.600	111%	0.190	-33%

The peak acceleration values are displayed in graphical form in Figure 4.17. From this figure, the difference in magnitude between the different prediction methods is clear. This figure also illustrates the difference in magnitudes of the three groups of events, which is difficult to appreciate in the acceleration density function because it is in logarithmic scale. The percent error with respect to the measurements is displayed in graphical form in Figure 4.18.

The acceleration measurements show that the HF model provides an accurate prediction with less than 7% under or over estimation compared to the measurements. This coincides with the match on the spectral density functions as well as very low error in damping and natural frequency estimations. Among all dynamic properties studied in the Case Study, the HF model is an accurate representation of the dynamic response for the New Orleans Tower.

The EC model provides a poor prediction with around a 30%-35% underestimation. Even though this is a worse prediction than the HF model, is important to consider that the HF model uses the load measurements directly, while the EC and NIST models required to calculate the load indirectly through the mean wind speed. Aggravating the situation, the wind load is very sensitive to changes in the wind velocity, that as mentioned in the previous section had a great deal of uncertainty within itself.

However, the NIST results provide a better approximation than the EC model, with a 13%-19% underestimation. The procedure followed by the NIST model only changes the natural frequency and the damping due to the SSI. Both values received a reduction compared with the standard EC model, which, in turn both provided an increase in the peak acceleration. It is important to mention that the NIST procedure, as presented in this study, will always present to a reduction in natural frequency and damping ratio compared to the EC model. This means that this methodology will always leads to higher or equal peak accelerations compared to the EC model.

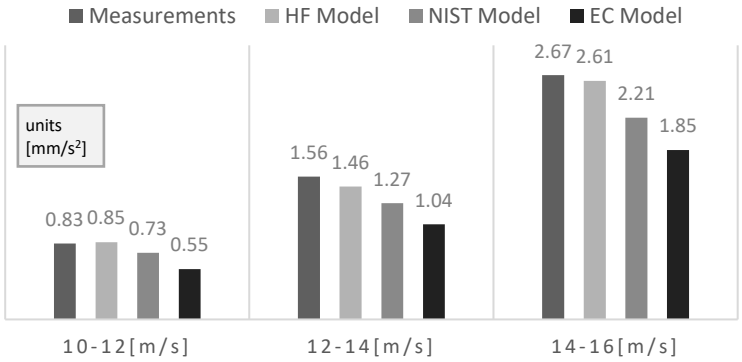

Figure 4.17 Comparison of expected peak acceleration predictions of the models with respective group of measurements.

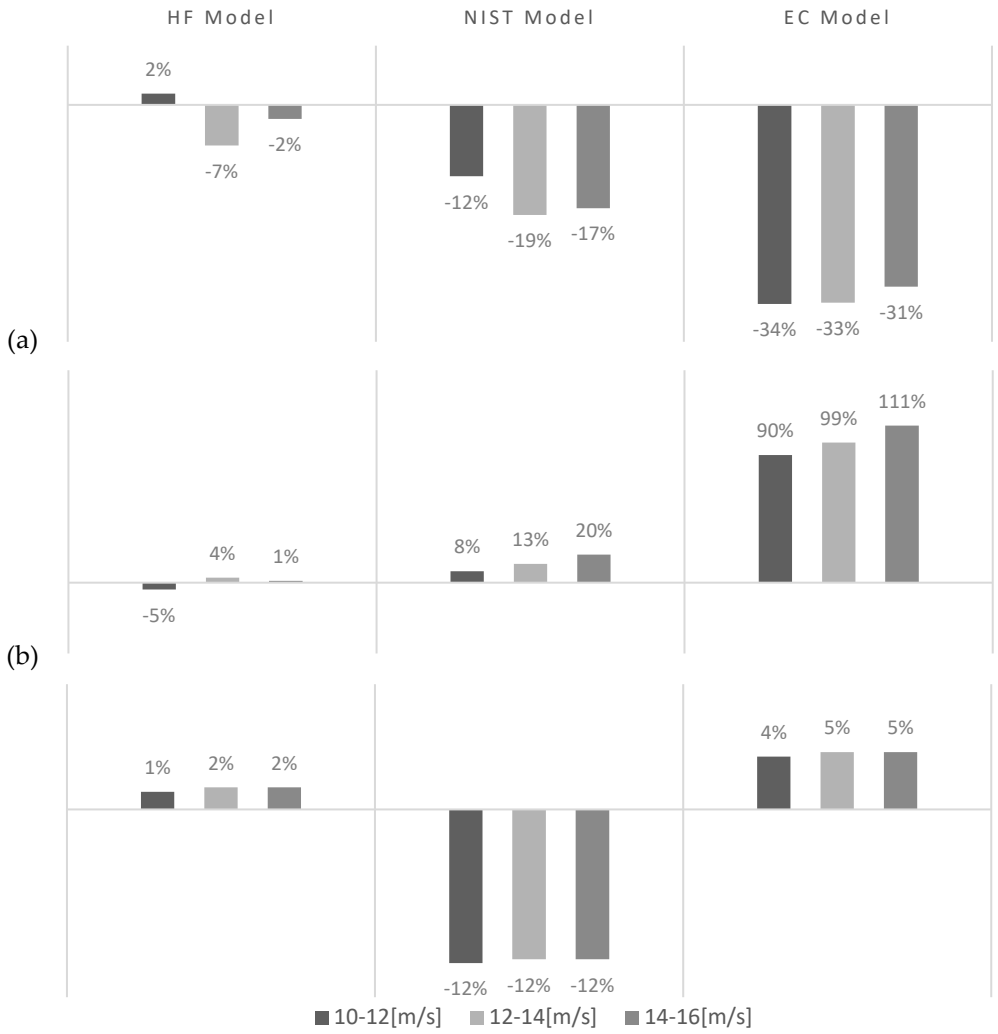

Figure 4.18 Percentage error for the 3 model compared to respective group of measurements. (a) expected peak acceleration, (b) global damping ratio, and (c) first natural frequency.

The NIST approach has a lower peak acceleration prediction than the HF and measurements even though it has a lower natural frequency, which would normally mean that the peak acceleration is higher, but in this case, since the NIST model has higher damping, this is counter balanced. This is reinforced when observing that on the models with the least difference in damping between the NIST models and the measurements it is the acceleration less underestimated.

Additionally, an accurate calculation of the natural frequency also has a significant impact on the peak acceleration. This is exemplified by the EC model*, which uses the design natural frequency of 0.19 Hz instead of the 0.30 Hz from the Eurocode. This difference in natural frequency of 37% had impact of around a 120% increase in the peak acceleration. This is mainly because the wind loading spectra is much higher at lower frequencies, as can be observed in Figure 4.4. When compared the model using the design natural frequency to the measurements there was around a 50% of peak acceleration overestimation.

4.5 Main findings

The acceleration PSD function of the lateral movement in the HF model compared to the measurements showed a mismatch at low frequencies. In the ranges of 10^{-2} to 10^{-1} Hz the acceleration PSD function have opposite tendencies, which leads to a 10^{3} order of magnitude difference in the PSD around 10^{-2} Hz. Given this large discrepancies at low frequencies the effect of the tilt of the structure was studied.

The inclusion of the tilt component to the lateral acceleration increased significantly the match in the acceleration PSD function with respect to the measurements. The tilt had significant impact only on the low frequencies, while the lateral component of the acceleration had the higher impact around the natural frequency and for higher frequencies. With respect to the overall expected peak acceleration around 96% can be predicted only from the lateral component of the acceleration. It was also noted that the tilt component uses information already computed for the lateral acceleration transfer function. From this, it can be concluded that even though the acceleration component of the tilt has a small impact on the global acceleration, it can provide an extra level of detail if the predictions need to be accurate, at a low set up and computational cost.

Among all dynamic properties studied in the Case Study, the HF model provided an accurate representation of the dynamic response for the New Orleans Tower. For all wind events groupings, there was a significant match between the acceleration density functions of the HF model and that from the measurements. Compared to the measurements the error was less than 7% for all evaluated dynamic properties: expected peak acceleration, global damping ratio and first resonance frequency.

The results of Case Study showed that the HF model performed much better than the NIST and EC models. More specifically, the EC model provides a 30%-35% underestimation of the peak acceleration compared to the measurements. The NIST results provide a better approximation than the EC model, with a 13%-19% underestimation of the peak acceleration compared to the measurements. The better performance of the NIST model resides in the influence of the SSI: the reduction of natural frequencies and damping results in a larger peak acceleration.

Nevertheless, it must be considered that the HF Model has more accurate measurement information than EC and NIST models. The HF Model uses the load directly from pressure measurements, while the EC and NIST models require to calculate the load indirectly through the wind speed measurements. This indirect approach adds uncertainty to the loads. Aggravating the situation, the wind load is proportional to the wind velocity squared, and the wind velocity measurements have a great deal of uncertainty because the measurements have been taken close to the building structure. This limits the extent of the comparison between models in the Case Study. Nevertheless, the EC and NIST models share the same loading, which means that the comparison between each other is not affected by any wind speed uncertainties. Which means that the statement that the EC model provides lower predictions for peak acceleration than the NIST model is independent from the wind speed uncertainties. This drawback is overcome in the Parametric Study since the three models use SLS wind speed and the Eurocode spectrum to determine the wind load.

The Case Study also showed that an accurate calculation of the natural frequency has a significant impact on the peak acceleration. From the exercise of calculating the dynamic response using the EC model but with the natural frequency used during the design, a reduction of 37% in natural frequency led to an increase of around 120% in the peak acceleration, due to low frequencies providing higher wind loads.

As mentioned in section 2.1 the underestimation of natural frequency with the current design practices is common. For this tower, this underestimation in design practice of the natural frequency counteracts the Eurocode overestimate of the damping and at the final result is an 50% overestimation of the peak acceleration, which is on the safe side.

Nevertheless, a procedure which has two wrong intermediate steps that counteract each other to find conservative result is not desired. For example, if the designer were to use more precise procedures to predict the natural frequency of the structure but continued using the recommended overestimated damping this would lead to underestimating the peak acceleration and non-conservative design.

5
Parametric study

5.1 Introduction

Previous studies form Bronkhorst et al. [3], [30], Gomez [6], [7] and Cruz and Miranda [8] showed the relevance of the influence SSI on the wind-induced dynamic response of high-rise buildings on soft soils. From the case study in the previous chapter it is clear that the HF model provides an accurate prediction for the wind-induced dynamic response of the New Orleans Towers. In this chapter the HF model is used to study the effect of soil material damping and soil stiffness on the dynamic properties of the system. This is achieved through a parametric study of the influence of building and soil parameters on the dynamic response.

While one use of parametric results of the HF model are to characterise the influence of the selected parameters on the dynamic response, they will also be used to compare the results of predictions of Eurocode (EC) and NIST models. This way investigating if the comparisons between models and conclusions found for the New Orleans Tower case study can be generalised for a wider set of combinations of parameters, and if these comparisons and conclusions change with the parameters, then explore how they evolve.

5.2 System setup

The models in this chapter use system properties from those expected of high-rise buildings in the Netherlands. This section focuses on describing the relevant system parameters that were introduced in the models. First the baseline parameters that all models will share are presented. Subsequently, the parameters that will be varied are introduced.

5.2.1 Baseline

This section introduces the baseline of properties from which the parametric model branches out. This baseline properties resemble those of common high-rise buildings in the Netherlands. Some of these common factors would be:

- A square cross-section is a common distribution that provides a good ratio of structural stiffness to wind load surface area.
- Because of the architectural requirements in the Netherlands, a constant cross-section with the maximum area allowed is a common solution. Combining it with the first criteria would lead to a square plan distribution of sides 30 m.
- Pile foundations over a first soft sand layer and a second medium strength clay layer.

Regarding this criterion, the New Orleans Tower in Rotterdam provides a representative building for high-rise buildings in the Netherlands. So the properties resemble closely to those presented in the Case Study.

Some changes with respect to the properties presented in the Case Study were made. The values were rounded to the nearest order of magnitude of interest. As well as, the parameters such as the segmented bending stiffness were generalised to a single bending stiffness since the configurations are very case dependant.

The foundation pile plan may vary from project to project, but studies by Gomez [6] and Bronkhorst et al. [3] show that the variation in the pile distribution does not change much in the dynamic stiffness matrix if the number of piles and the width and length of the base stay constant. For this reason, the exact pile distribution from the Case Study was be used.

The system parameters used on the base line model are presented in Table 5.1, Table 5.2 and Table 5.3. The properties of **bold letters** are the only parameters that were varied in the parametric study and their ranges of variation are presented in the next sections.

For the wind load a base wind velocity (v_b) of 20.5 m/s is used. This wind speed is the one used in Bronkhorst et al. [3], and it is in the magnitude range for Serviceability Limit State (SLS) base wind velocity form the Eurocode [2], [20], and the NEN 6702 [31] for Dutch cities.

Table 5.1 Baseline Tower Structure properties for parametric study

Parameter		
Height		**150 m**
Cross section	BxL	30 m x 30 m
Cross section area	A	900 m^2
Bending Stiffness	$\boldsymbol{EI}$	**70x10^{12} Nm^2**
Density	ρ	500 kg/m^3
Damping coefficient	η	0.027

Table 5.2 Baseline Soil properties for parametric study

Parameter		1st soil layer	2nd soil layer
Description		Sand	Clay
Depth		0.0 m to 20.0 m	20.0 m to 30.0 m
Thickness		20 m	10 m
Share wave velocity	$\boldsymbol{V_s}$	**125 m/s**	**250 m/s**
Density	ρ	1650 kg/m^3	1950 kg/m^3
Damping coefficient	$\boldsymbol{\eta_s}$	**0.02**	**0.03**
Poisson's Ratio	υ	0.3	0.3

Table 5.3 Baseline Pile properties for parametric study

Parameter		Concrete pile
Amount		308
Depth		25 m
Diameter	$\emptyset$	0.45 m
Elastic Modulus	E_p	30 GPa
Density	ρ	2300 kg/m^3
Damping coefficient	η_P	0.005
Poisson's Ratio	υ	0.2

5.2.2 Slenderness-building height

One of the main descriptive properties of a high-rise building is its slenderness, which is calculated as the width-to-height ratio. This property provides an initial overview of some of the overarching expected behaviour of the structure. The exploration of this parameter provides information on how the other parameters affect a wide range of high-rise buildings.

For the type of building presented in the previous section, where the architectural and structural requirements constrain the base dimensions, the height is the only parameter that influences the slenderness. The structure with the baseline parameters with a height of 150 m and a base of 30 m has a slenderness ratio of 5.

The rages that are covered by this slenderness ratio parameter are between 2 and 8. To define the range of this parameter, the limits of the model need to be considered. The lower bound of the range for this parameter are dictated by the slenderness were shear deformation starts to play an important role, so the Bernoulli bending model is not an accurate representation for the deformation. Using the FEM model in SCIA Engineer on the Case Study cross-section, it was concluded that for this cross-section, shear deformation played an important role in slenderness under 3. The upper bound of the range for this parameter is dictated by when the shear wall structural system used is not considered a viable option anymore. For super-slender structures with a slenderness of above 8, outrigger systems are commonly used. This parameter has a very dense number of samples to ensure a continuous representation.

5.2.3 Bending Stiffness

To have a realistic representation of buildings with different heights, if the height parameter is changed the stiffness of the structure also needs to be changed as well, otherwise this would lead to unrealistic structures. For shorter sutures than the New Orleans Tower, this combination of properties would lead to an over designed structure that is too stiff and, the structural engineer would have reduced the structure's stiffness to optimise the structure. On the other hand, a taller building would lead to much higher deformations than the ones allowed, the structural engineer would have increased the structure's stiffness to comply with regulations.

The proposed solution to this problem is to recalculate the stiffness of the building so that it will maintain a constant drift to that of the New Orleans Tower. By approximating the static part of the wind force as a constant distributed load, the drift can be calculated with,

$$\frac{\Delta}{H} = \frac{q \cdot H^3}{8 \cdot EI}$$

Since the drifts for all the structures are equal, the bending stiffness can be rewritten in terms of the height as,

$$EI_b = EI_a \frac{H_b^3}{H_a^3}$$

In this case the reference height and bending stiffness are from the baseline properties,

$$EI_b = 70 \cdot 10^{12} \left(\frac{H_b}{150}\right)^3$$

Bending stiffness is a parameter is completely dependent to the building height parameter.

5.2.4 Shear wave velocity Study

Shear wave velocity effects directly the amount of energy radiated away from the building. The values of shear wave velocity presented for the base line is already considered a very soft soil. Looking at examples of soil profiles using the TNO Archive DINOloket [26] as well as examples of representative soils from Deltares [32], the relevant soil properties were selected. Un Table 5.4 the groupings of soil stiffness are shown. Only properties from Very soft to Medium-hard are relevant to the Netherlands. The properties named Hard and Very Hard are only used in a single case as a point of comparison. The infinity stiff clamped foundation is added to provide a reference frame for those simplified models that exclude any SSI.

Table 5.4 Shear wave velocity groupings

Groups	Shear wave Velocity V_s [m/s]	
	1st soil layer	2nd soil layer
Very soft	100	200
Soft	125	250
Medium-soft	150	300
Medium	175	350
Medium-hard	200	400
Hard	300	600
Very-hard	400	800
Clamped	∞	∞

5.2.5 Soil material damping Study

From the data presented in Darendeli's [27] study, for soils the range of extreme values for material damping is between 1% to 4% for small strains. The 0% strain value is also studied to provide a reference frame for those simplified models that exclude any material damping. The 6% strain value is also studied to provide a reference frame for material damping that would be present if the displacements were high enough to display nonlinear behaviour. On Table 5.5 the divisions for soil material damping parametric study are presented.

Table 5.5 Soil material damping groupings

Amount of Material damping	
No damping	0%
Average damping	2%
High damping	4%
Non-linear range	6%

5.3 Results

In this section, the results are presented in two parts. First, the results of the Dynaplile models, which are the dynamic stiffness of some of the representative soil property configurations. These are intermediate results that are afterwards used as part of the boundary conditions of the HF model. These intermediate results also provide context that is later needed when studying how the impact of the properties of the soil influence the dynamic properties of the system. Subsequently, the results of the dynamic properties of the building are presented.

5.3.1 Foundation model

As introduced in the Case Study, a translational, rotational and their coupling terms are extracted from the results of the Dynaplile software, to construct the complex valued dynamic stiffness matrix ($\widetilde{K}_d(\omega)$). In the next section, the influence on the dynamic stiffness of shear wave velocity and the soil material damping is explored. The results used for the HL model span from 0 Hz to 6 Hz, but the presented results only from 0 to 1.4 Hz, since the dynamic stiffness of magnitudes close to the natural frequency has the greatest influence on the dynamic response of the system.

5.3.1.1 Influence of material damping in dynamic stiffness

Figure 5.1 shows the real part of the dynamic stiffness of the translational and rotational terms. The real part corresponds to the inertia and stiffness of the soil. From this figure, it can be observed that for both, the translational and rotational stiffness, the real component of the dynamic stiffness matrix are the same for the different soil material damping. Also, there is a slight tendency of the stiffness to decrease for as the frequencies increase, nevertheless, this tendency is quite small, which means that for the expected range of natural frequencies, the real component of the dynamic stiffness matrix remains practically unchanged.

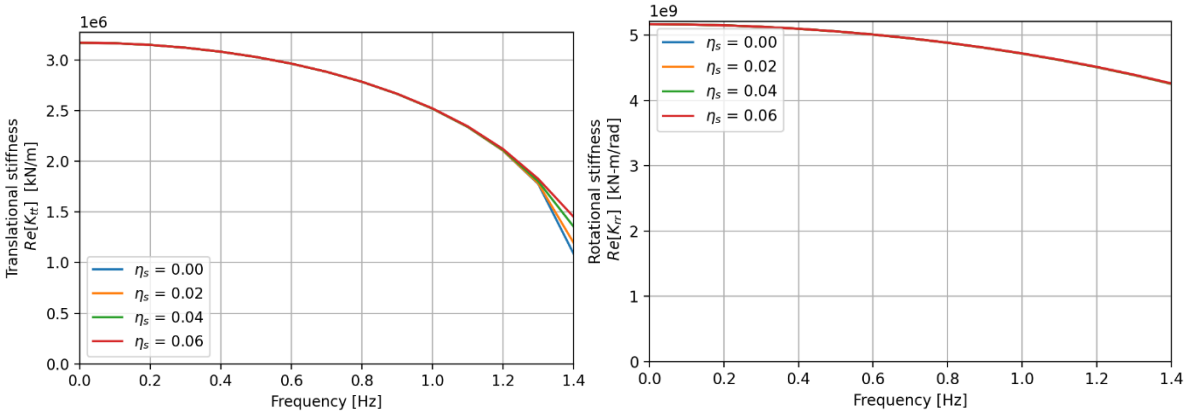

(a) (b)

Figure 5.1 Real part of the dynamic stiffness for all material damping parameters of the (a) translational and (b) rotational terms

Figure 5.2 shows the imaginary part of the dynamic stiffness of the translational and rotational terms. The imaginary part corresponds to the damping of the soil, which come from radiation and material damping. From this figure, it can be observed that for both, the translational and rotational stiffness, there is a slight tendency of the stiffness to increase; nevertheless, this tendency is quite small, which means that for the expected range of natural frequencies and damping component of the dynamic stiffness matrix remains practically unchanged. Conversely, it is quite clear and expected, that the increase in material damping leads to an increase in the imaginary component of the dynamic stiffness matrix, for both rotation and translation.

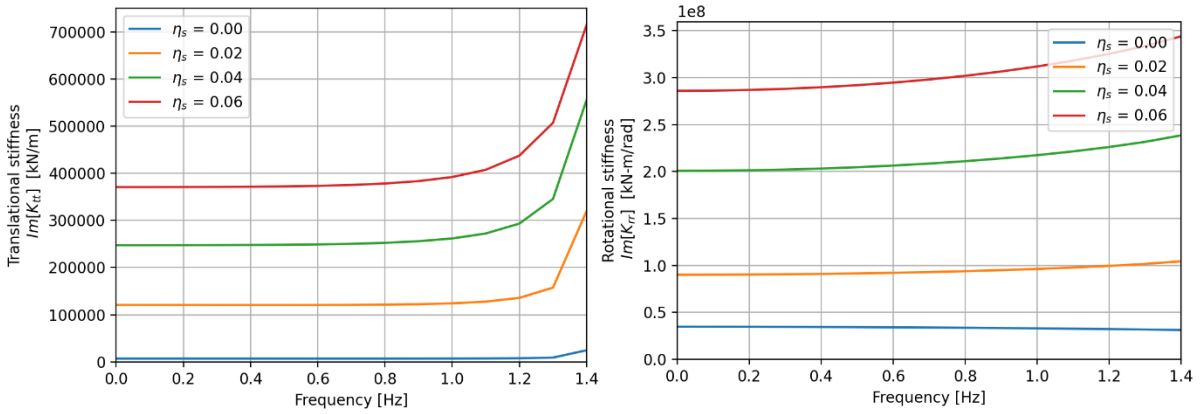

(a) (b)

Figure 5.2 Imaginary part of the dynamic stiffness for all material damping parameters of the (a) translational and (b) rotational terms

5.3.1.2 *Influence of shear wave velocity of the soil in dynamic stiffness*

Figure 5.3 shows the real part of the dynamic stiffness of the translational and rotational terms, energy radiated away from. This real part corresponds to the inertia and stiffness of the soil. From this figure, it can be observed that for both, the translational and rotational stiffness, the real component of the dynamic stiffness values increases with the shear wave velocity. Also, there is the same slight tendency of the stiffness to decrease for as the frequencies increase, that is present in Figure 5.1.

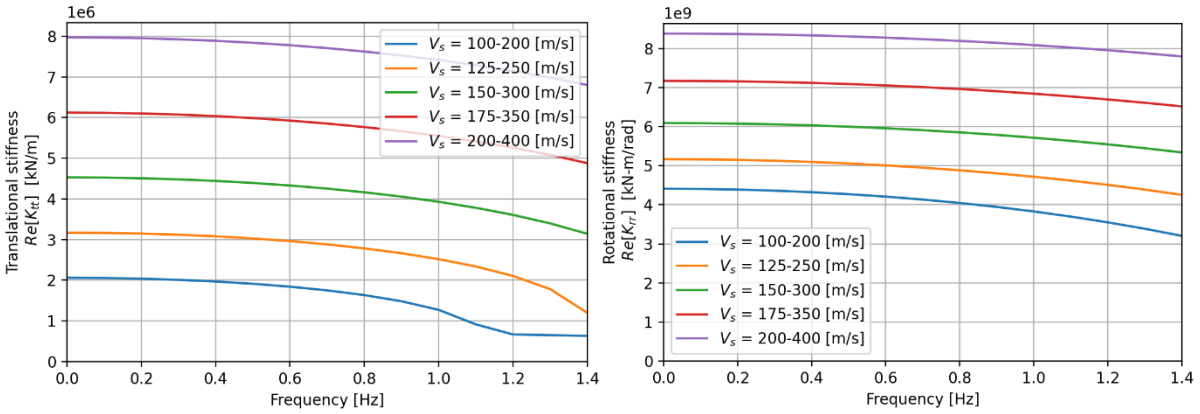

(a) (b)

Figure 5.3 Real part of the dynamic stiffness for all soil stiffness parameters of the (a) translational and (b) rotational terms

Figure 5.4 shows the imaginary part of the dynamic stiffness of the translational and rotational terms, corresponding to the damping of the soil. From this figure it can be observed that the increase in shear wave velocity leads to an increase in an increase in the imaginary component of the dynamic stiffness matrix, for both rotation and translation. This might seem contradictory since stiffer soils should experience less radiation damping, but this is not considering that the change in stiffness will also influence other dynamic properties of the system. Also, there is the same slight tendency of the stiffness to increase as the frequencies increase, that is present in Figure 5.2.

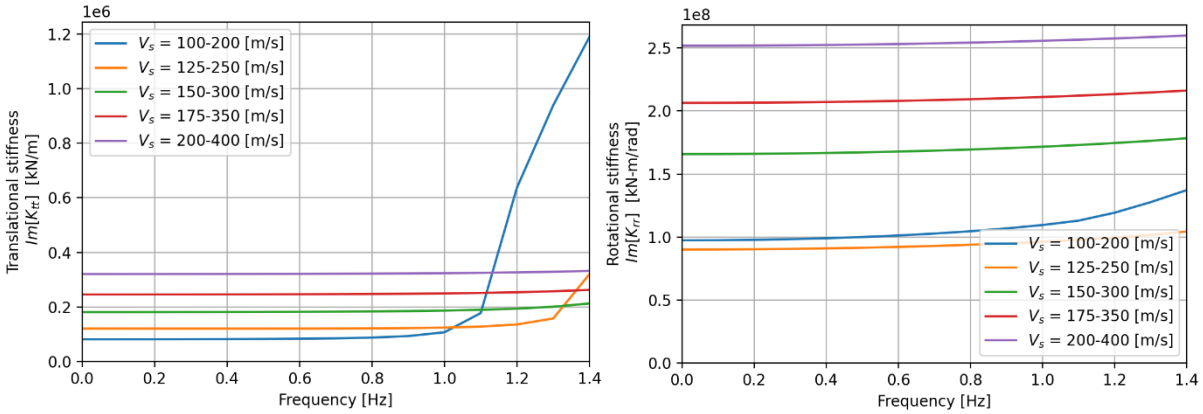

(a) (b)

Figure 5.4 Imaginary part of the dynamic stiffness for all soil stiffness parameters of the (a) translational and (b) rotational terms

5.3.2 Dynamic properties of the building

This section presents the results of the Parametric study the dynamic analysis of the HF, NIST and EC models. These models are assembled using the system parameters of a base model and the parameter vitiations described in the previous sections and following the procedures in chapter 3. The results show the dynamic response of the building predicted by each model at the top of the building. The dynamic properties that will be explored are expected peak acceleration (a_P), overall damping ratio (ζ) and first natural frequency (f_n).

5.3.2.1 Exploration into the impact of slenderness on the predictions of the different models

Figure 5.5(a) shows the effect of the slenderness parameter on the expected peak acceleration, while all other parameters maintain the baseline properties. In this figure, the difference between the predictions of the different models is evident. For all slenderness studied, the HF model predicts the higher accelerations while the EC model predicted the lowest accelerations. In all aspects studied on the previous Case Study, the HF model was an accurate representation for the dynamic response for the New Orleans Tower. Because of this, the HF model is uses as the point of comparison of the performance.

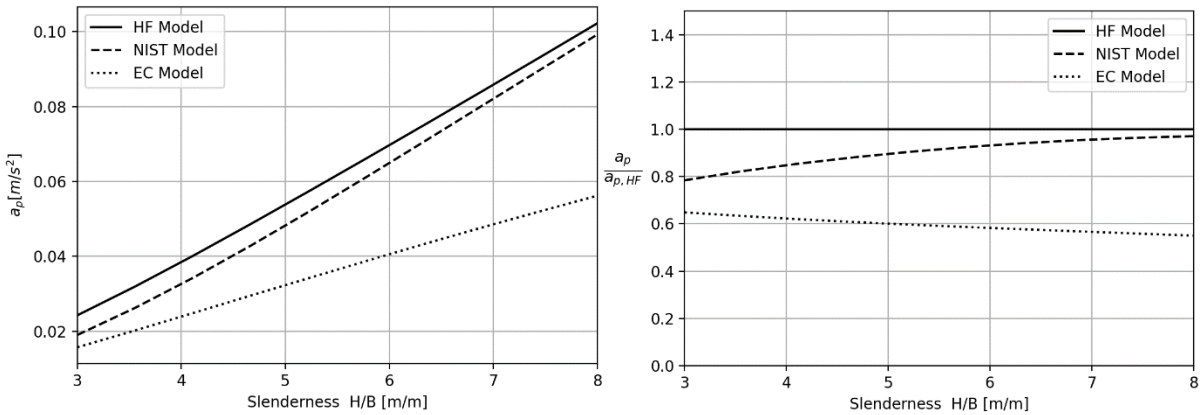

(a) (b)

Figure 5.5 Expected peak accelerations with respect to slenderness for the three models, in absolute terms (a) and relative terms compared to HF model (b).

In Figure 5.5(b) the expected peak acceleration relative to the HF model is displayed, where it is shows that the EC is predicting around 60% of the HF model and that the predictions are

getting slightly worse with the increase in slenderness. Conversely, the NIST is predicting around 80% of the HF model for low slenderness and the predictions become more accurate with the increase in slenderness, displacing 95% compatibility at in slenderness above 6.

Diving into other aspects of the dynamic response Figure 5.6(a) presents the global damping ratio (ζ). Remembering that the EC model has a constant value for the damping ratio, and that the NIST model includes the contribution of SSI to the overall damping, this methodology shifts the unchanging damping ratio of the EC model closer to the HF model results. Nevertheless, from the Figure 5.6(b), it can be observed that at low slenderness, there is still a important deviation with respect to the HF model, even though it gets better at higher slenderness. This tendency of the damping results of the NIST supports the results from the peak acceleration since a higher damping ratio would result in a lower acceleration. This inverse proportionality between damping and acceleration can be seen when comparing Figure 5.5b) and Figure 5.6(b).

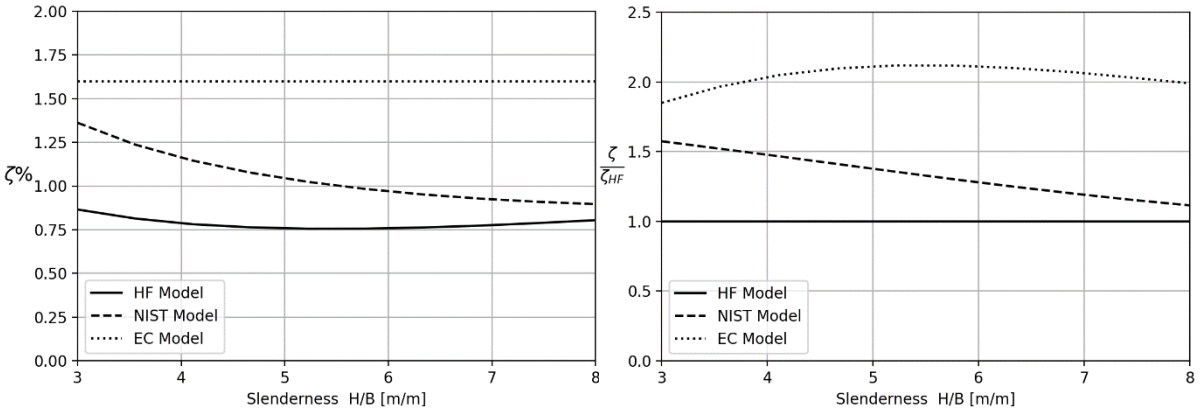

(a) (b)

Figure 5.6 Global damping ratio with respect to slenderness for the three models, in absolute terms (a) and relative terms compared to HF model (b).

The tendency of the natural period of the first mode with respect to slenderness is presented in Figure 5.7(a). For all studied slenderness ratios, the EC model predicts higher natural frequencies, which provides another reason why the peak acceleration is lower than the other models. In the case of the NIST model the period lengthening effect reduces the natural frequencies from those obtained using the EC model, this reduction serves to approximate the natural frequencies by considering the contribution of SSI. Compared to the HF model, this period lengthening slightly improves the resulting natural frequency, but to match the HF model, the reductions should be larger for low slenderness ratios and lower for high slenderness ratios. This is also presented in Figure 5.7(b), where the natural frequencies are compared to the EC model. In this plot, the comparison is against the EC model to show the period lengthening effect. These results demonstrate that the tendency of the current Period lengthening effect method is quite different from the one that would be needed to match the HF model.

From these results it is clear that, for the slenderness range under study, the EC model provides a poor approximation to the dynamic properties with respect to the HF model: underestimating the expected peak acceleration and overestimating the global damping ratio and the first natural frequency. The modification to the EC model included in the NIST formulations provides a much closer approximation of the dynamic properties of the building.

Nevertheless, the model present important inaccuracies in damping at low slenderness ratios and the period lengthening effect tendency is not the expected compared to the HF model.

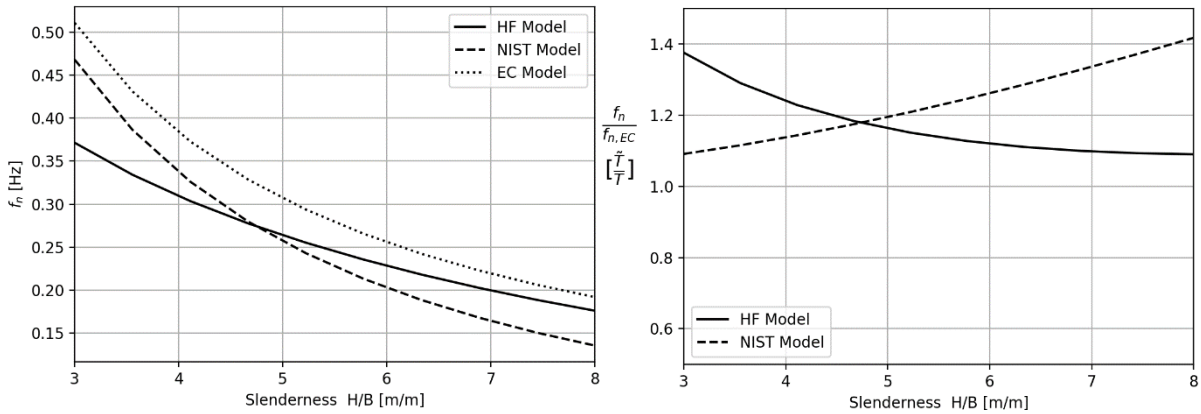

(a) (b)

Figure 5.7 First natural frequency with respect to slenderness for the three models, in absolute terms (a) and relative terms compared to EC model (b).

As mentioned in the system parameters chapter, the wind loads used for this study are in the range for SLS. Figure 5.8 compares the peak acceleration and their respective natural frequencies to the limitation requirements for acceleration by wind for occupied spaces in buildings from the Dutch national code, NEN 6702 [31]. This shows that the magnitude of the studied accelerations are quite lower than the maximum allowed but they are still in the same order of magnitude. These results are expected since the baseline properties were obtained from the New Orleans Tower, and Bronkhorst et al. [3] in a study of the complete set of measurements of the New Orleans Tower of 5 years it was determined that from the fit of the measurement data, the expected peak acceleration would be 0.033 m/s^2. Considering that the natural frequency measured in that study was 0.28 Hz, it can be observed that the results are of the same magnitude. This can be further evidenced when plotting the measurement results in Figure 5.8.

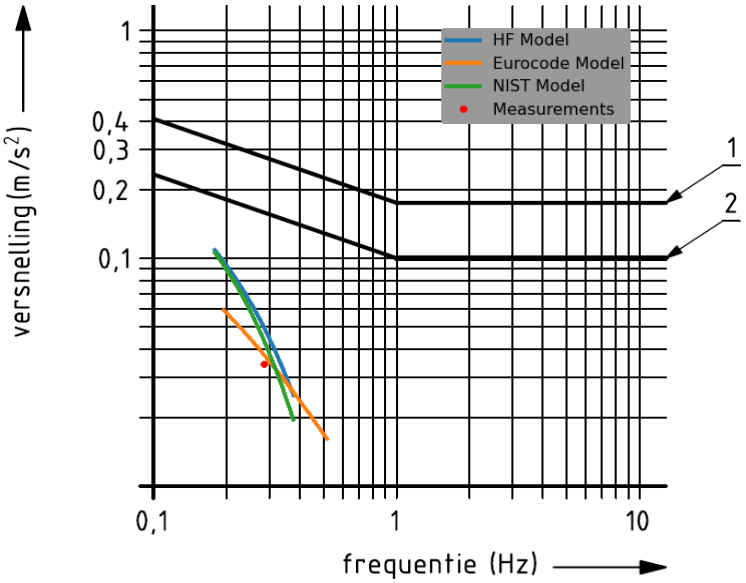

Figure 5.8 Results of the three models and the measurements date for SLS condition compared to the limitation requirements for acceleration by wind for occupied spaces in buildings from the Dutch national code, NEN 6702 [31].

Figure 5.9 presents the same comparison between the prediction of the dynamic properties of the three models presented in Figure 5.5(a) and Figure 5.6(a), but adding the parametrization of the shear wave velocities in the ranges relevant to the Netherlands. This section is building up from the previous results, where only the slenderness ratio was parameterized, and all the other system parameters remained with the baseline. From these results, it is evident that, the tendencies between the models observed in the previous section are essentially the same for the soil stiffnesses under study.

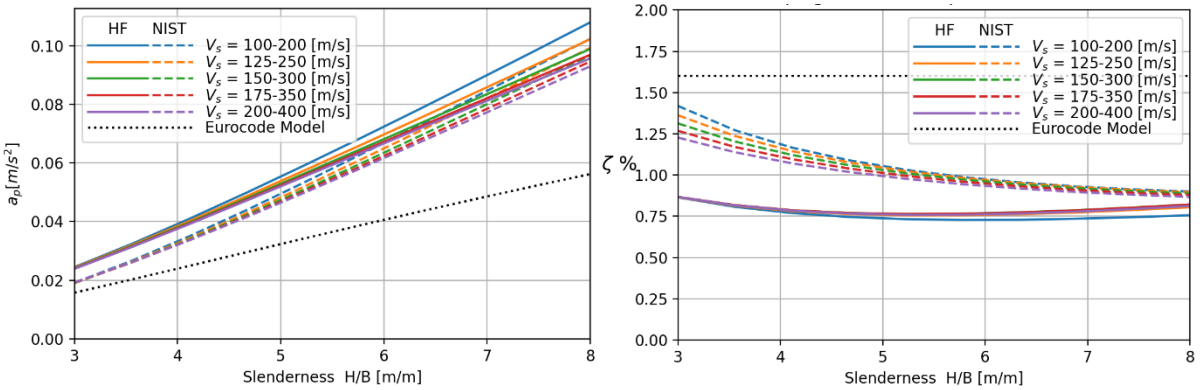

(a) (b)

Figure 5.9 (a) Expected peak accelerations and (b) global damping ratio with respect to slenderness and soil stiffness, for the three models.

Figure 5.10 presents the same comparison between the prediction of the dynamic properties of the three models presented in Figure 5.5(b) and Figure 5.6(b), but adding the parametrization of the soil material damping (η_s). Comparing the results in Figure 5.5(b) , where only the slenderness ratio was parameterised and all the other system parameters remained with the baseline, with the results in Figure 5.10(a) for the changing soil material damping, there is little variation in the tendencies of the acceleration between models observed in the previous section, even though there is a large spread of magnitudes for different amounts of soil material damping.

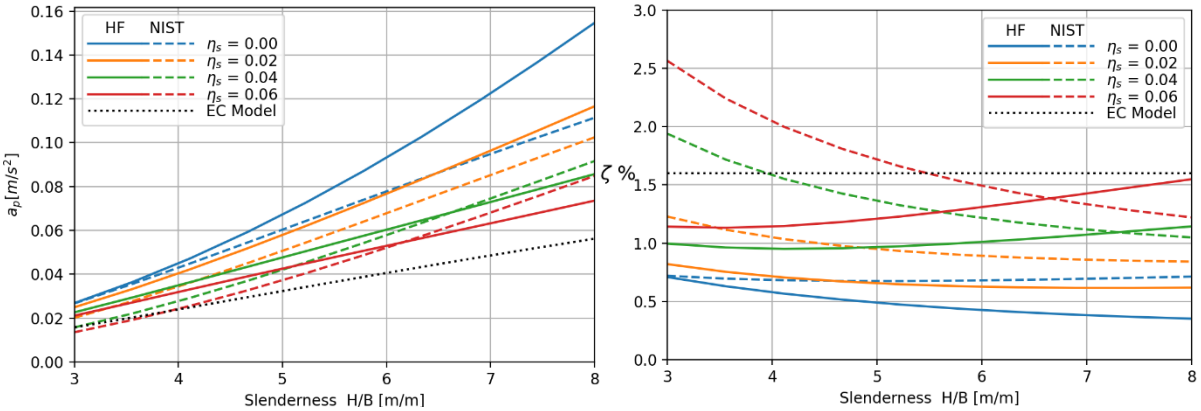

(a) (b)

Figure 5.10 (a) Expected peak accelerations and (b) global damping ratio with respect to slenderness and soil material damping, for the three models.

From Figure 5.10 where the magnitudes of the acceleration and damping ratios are presented, the variation between the predictions in each model for different amounts of material damping can be difficult to discern. For this reason, Figure 5.11 offers a perspective in relative terms, where the results for each NIST and EC models are compared to their respective HF

model counterpart's results. This provides a view of how the NIST and EC models deviate from the HF model. From the relative peak acceleration, it can be evidenced that at low soil material damping, the EC model predicts significantly lower acceleration compared to the HF model, and that the NIST model much closer resembles the HF model acceleration results. However, for high soil material damping the HF model and the EC model acceleration results are much closer, with around 25% difference. For these higher soil material damping parameters, the NIST model only provides significant improvement over the EC model for a window of slenderness ratio. Looking at the results for $\eta_s = 0.06$ only around the 5 to 7 slenderness ratio, the NIST model provides significant improvement over the EC model, but outside this range having similar percentage deviation over the HF model.

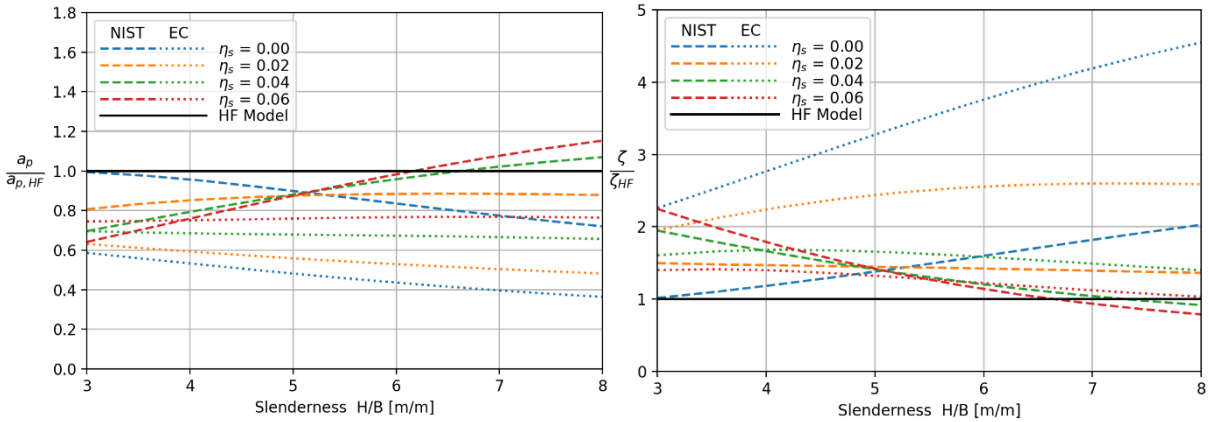

Figure 5.11 (a) Expected peak accelerations and (b) global damping ratio, with respect to slenderness and soil material damping, for the three models, relative to their HF model counterpart.

From the relative overall damping results, there is no uniform tendency on which model has the closer prediction. The results show that for low soil material damping conditions the NIST model is much closer to the HF model, while for high soil material damping conditions the EC model is slightly closer to the HF model. These results reinforce the results noticed on the acceleration, that at higher material damping the EC model resembles closer the HF model. From these results, there is a clear tendency for the EC and HF models to have closer predictions for high soil material damping.

5.3.2.2 *Exploration into the impact material damping on dynamic properties using the HF model*

Figure 5.12 shows the results of the of the dynamic properties calculate with the HF with the baseline system parameters with only varying the soil material damping. The results on the peak acceleration show an overall trend of an increase in peak acceleration for higher slenderness ratios. Which is the same trend found on the other results. Furthermore, there is an increase in the predicted peak acceleration of the system as the material damping decreases. As well as an increase in the predicted overall damping of the system as the material damping increases. Also, since the modal properties, ergo the natural frequencies, are obtained from the undamped system, the natural frequencies are not affected by the change in soil material damping properties. Given that the others structure and soil properties such as the soils stiffness are constant, the increase in the predicted peak acceleration of due to the soil material damping reduction can be linked completely to observed increase in overall damping of the system. This is the intuitive and expected result.

Furthermore, the results for high soil material damping (0.06) show a tendency to increase with the increase in slenderness. This does not align with the general tendency of the measurements presented in section 2.5.2, where the taller the building the damping has a tendency to decrease. This could be explain by that the soil of the buildings measured do not display high soil material damping which are only achieved when soil deforms in the non-linear range.

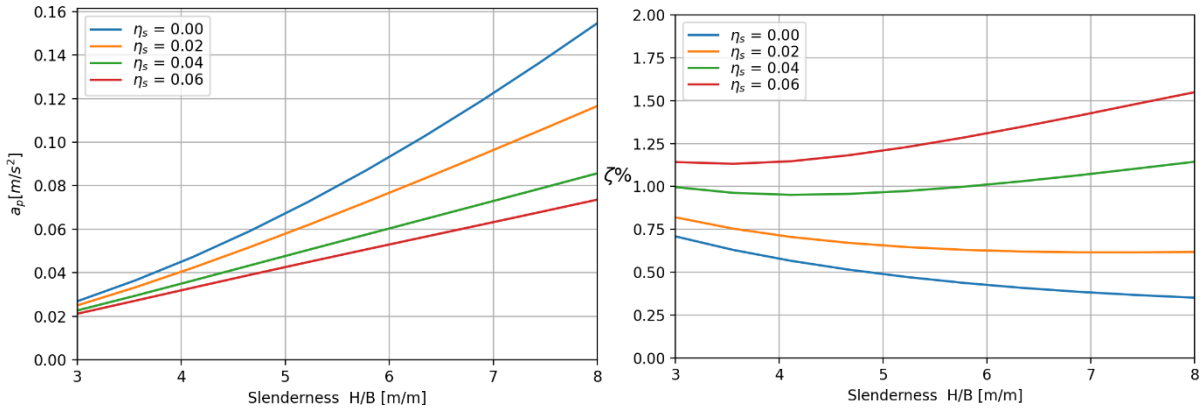

Figure 5.12 (a) Expected peak accelerations and (b) global damping ratio with respect to slenderness and soil material damping, for the HF model, relative to their respective HF model counterpart.

In Figure 5.13 the results are presented in relative form where the results are compared to the results of the HF model with 0 material damping, which would be the case of not considering the effect of soil material damping. From both Figure 5.13 (a) and (b), notably, as the slenderness ratio increases, there is an increase in the disagreement of the models with different amounts of soil material damping. It can be observed that not considering the effect of soil material damping can lead to 10%-50% overestimation of peak acceleration and a 15%-80% underestimation of the overall damping ratio, depending on the slenderness ratio and soil material damping combination.

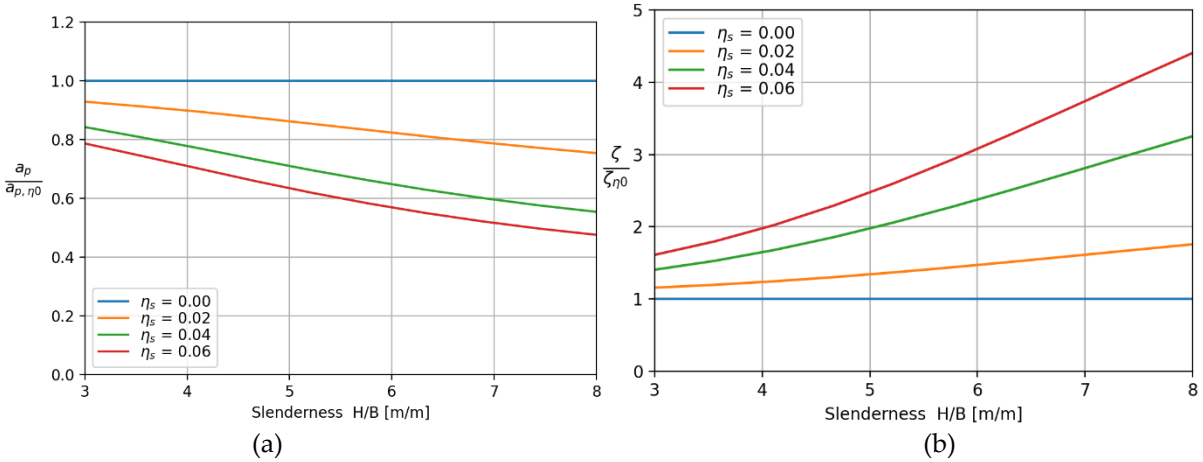

Figure 5.13 (a) Expected peak accelerations and (b) global damping ratio with respect to slenderness and soil material damping, for the HF model, relative to the results of the model with 0 soil material damping.

5.3.2.3 *Exploration into the impact shear wave velocity on dynamic properties using the HF model*

Similar to Figure 5.9, the Figure 5.14, Figure 5.15 and Figure 5.16 present the results with the baseline system parameters with only varying shear wave velocities on the ranges relevant to the Netherlands but for only the HF model. All these results are compared to the results of a model with a fixed foundation since this would be the case of not taking into consideration SSI. On the rest of the figures in this section, the results on the left show the magnitude of the dynamic property and on the right the ratio compared to the results of the fixed foundation models.

From Figure 5.14, the same trend shown in previous sections is present, where for the relevant shear wave velocities in the Netherlands, the overall damping is quite similar between each other, at each slenderness ratio. Also, for all shear wave velocities under study the damping ratios are much higher than the fixed base model. From the comparison relative to the fixed base, it is also evident that there is an increase in discrepancy between the models with or without SSI with the increase of slenderness. By itself, this damping ratio tendency would result in higher acceleration on the fixed base results.

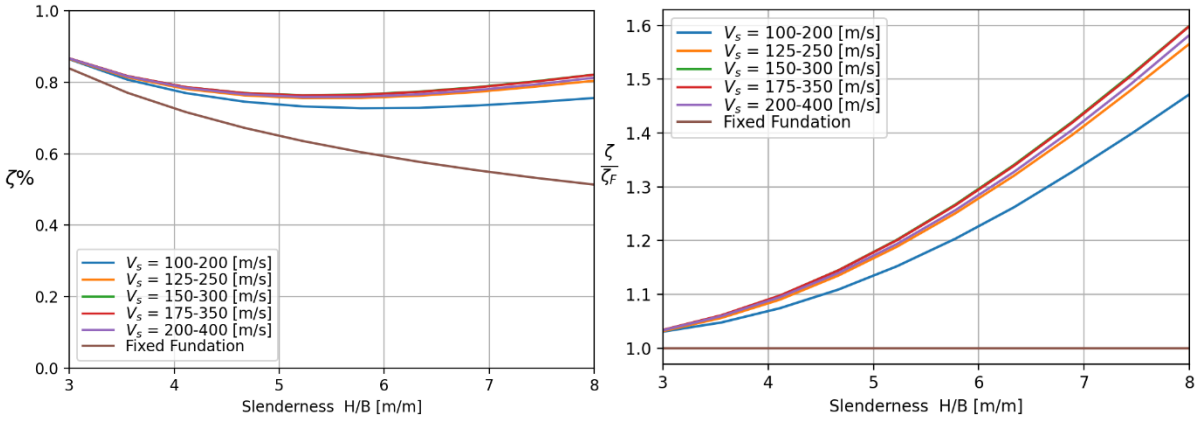

(a) (b)

Figure 5.14 Global damping ratio with respect to slenderness for the HF model, in absolute terms (a) and relative terms compared to fixed foundation model (b).

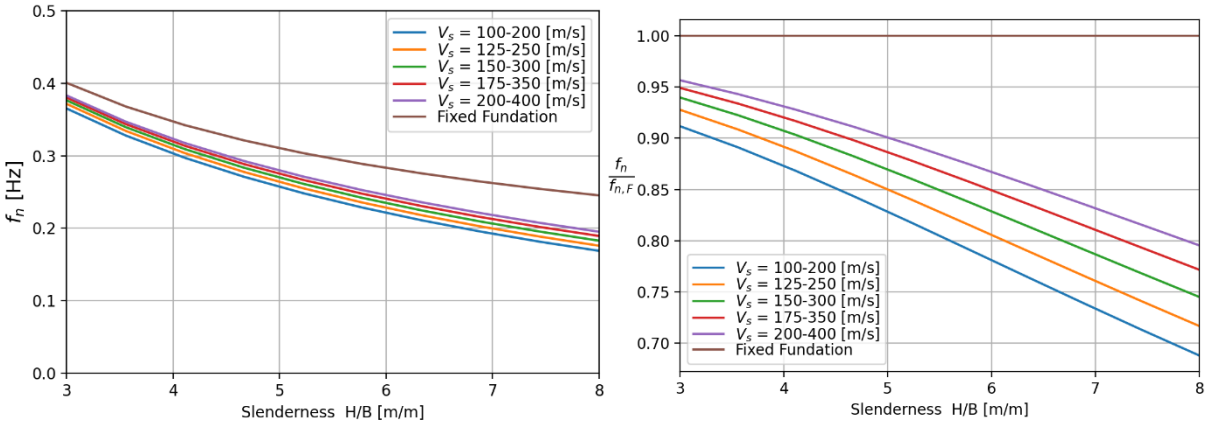

(a) (b)

Figure 5.15 First natural frequency with respect to slenderness for the HF model, in absolute terms (a) and relative terms compared to fixed foundation model (b).

Contrary, in Figure 5.15, for all shear wave velocities under study the natural frequencies are lower than the fixed base model. But from the comparison relative to the fixed base, it is also

evident that the discrepancy between the models with or without SSI increases with the increase of slenderness. By itself, this natural frequency tendency would result in lower acceleration on the fixed base results. Since a higher natural frequency means that the wind loading spectra is lower.

From Figure 5.16, in terms of the magnitude of the acceleration, the HF model predicts that the acceleration with varying shear wave velocity does not have a great impact on the predicted peak acceleration. This is reinforced by the results relative to the fixed foundations where for the most part the difference between models is less than 5%. On itself these results could lead to the conclusion that the shear wave velocity does not impact the dynamic response of the system. However, looking at the results of the damping ratio and natural frequency, where the difference in the damping ratio would prompt an increase in the acceleration and in the natural frequency would prompt a decrease in the acceleration, where both effects counteract each other and for this specific set of structure and soil properties, they cancel out each other's effects. This means that even though for this specific set of soil and structure properties the varying shear wave velocity does not have a significant impact on the predicted peak acceleration, it cannot be assumed that the other dynamic properties of the system are the same for different shear wave velocities.

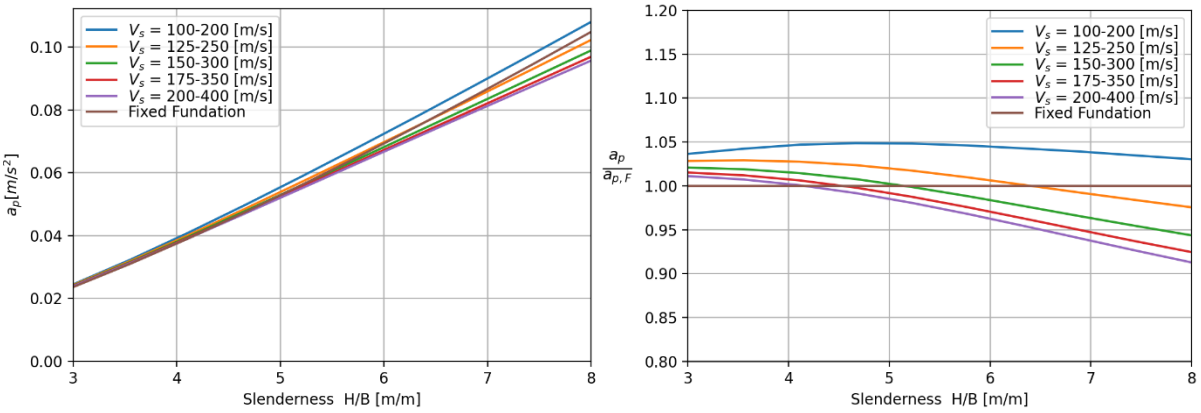

(a) (b)

Figure 5.16 Expected peak acceleration with respect to slenderness for the HF model, in absolute terms (a) and relative terms compared to fixed foundation model (b).

To further investigate the influence of soil stiffness, and consequently the influence of the radiation damping on the HF model is studied, using the results of Dynaplile of models with no soil material damping ($\eta_s = 0$) and varying shear wave velocities. All these results are compared to the results of a model with a fixed foundation since this would be the case of not taking into consideration SSI. The results of the peak accelerations are shown in Figure 5.17, where it shows that there is a significant impact of the shear wave velocity on the peak acceleration, moreover the softer the soil a grater the influence on the peak acceleration. Also, a tendency can be observed, where the influence of the shear wave velocity increases as the slenderness ratio increases. The stiffness range for the soft soils present in the Netherlands would correspond to a shear wave velocity of 100–200 and 200–400 m/s, which for high slenderness, the results show that the influence of the shear wave velocity can amount to around 30 to 50% difference in the estimated peak acceleration compared to the fixed base.

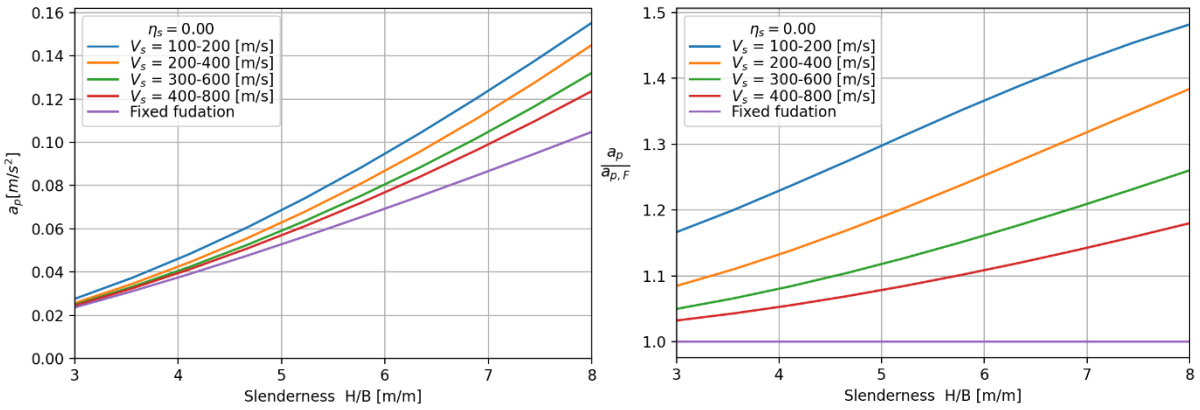

(a) (b)

Figure 5.17 Expected peak acceleration with respect to slenderness for the HF model with no soil material damping, in absolute terms (a) and relative terms compared to fixed foundation model (b).

In Figure 5.18, the damping ratio with respect to shear wave velocity is displayed, a general trend of the damping ratio to decrease is observed. Relative to the fixed foundation, two tendencies are observed, one with respect to the slenderness ratio and one with respect to shear wave velocity. Regarding the slenderness ratio, there is not only a general trend of the damping ratio to decrease but also a tendency to decrease in relative to the fixed base model. With respect to the shear wave velocity, a proportional tendency is observed, for lower shear wave velocity, a lower ratio of damping with respect to the fixed foundation is observed. This result seems counter intuitive since for softer soil a higher amount of radiation damping is expected. Therefore, it should be reiterated that the damping ratios compared are the global damping ratio of the system and for these results even though the material damping of the soil has been set to 0 the model still includes the structural damping of the building. Consequently, the change in the radiation damping of the soil cannot solely explain the tendencies observed over the overall damping of the system. This is addressed in further detail in subsequent results.

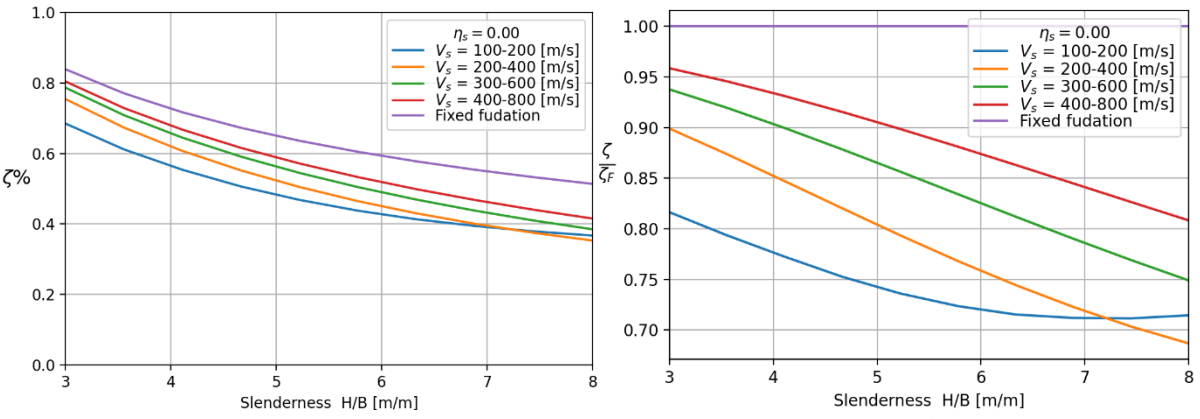

(a) (b)

Figure 5.18 Global damping ratio with respect to slenderness for the HF model with no soil material damping, in absolute terms (a) and relative terms compared to fixed foundation model (b).

Regarding the results presented in Figure 5.19 of the natural frequencies, the same tendencies as for the damping ratios are observed. With respect to slenderness ratio a general trend of the natural frequencies to decrease, this is expected since for this parametric study, the slenderness is modified only through the total height of the building, which would

proportionally increase the mass of the building and lever arm, both of which have an inversely proportional effect on the natural frequency of a system. The same argument can be used for the soil's stiffness both translation and rotational, are proportional to the natural frequency. The equation of the natural frequency of a single degree of freedom system $\omega_n = \sqrt{k_t/m}$ and $\omega_n = \sqrt{k_r/(m \cdot l^2)}$ translational and rotational, respectively, can display both tendencies.

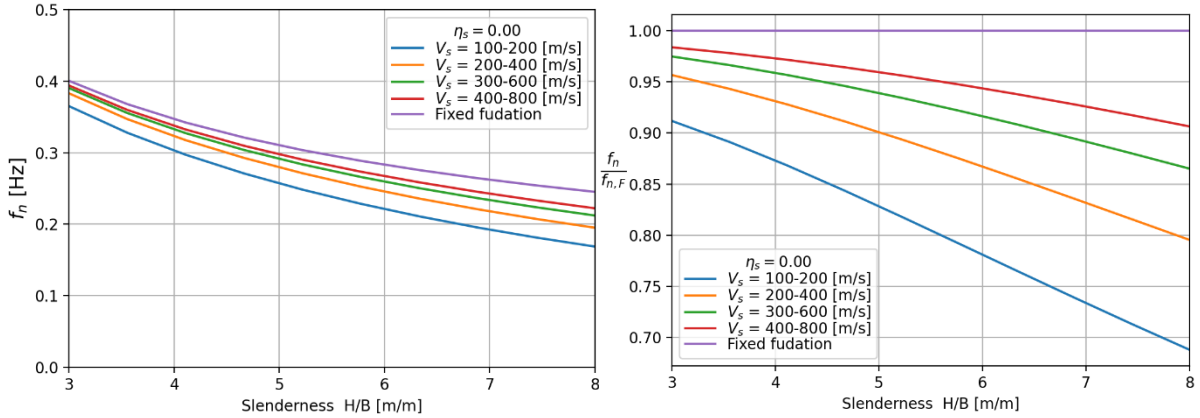

(a) (b)

Figure 5.19 First natural with respect to slenderness for the HF model with no soil material damping, in absolute terms (a) and relative terms compared to fixed foundation model (b).

The combination of the under prediction on natural frequency and damping ratio with respect to the fixed base corroborates the results of over-estimation of the peak acceleration compared to the fixed base. The shear wave velocity plays an important role in the calculation of the dynamic response of a high-rise building and the impact on the dynamic properties is larger at grater slenderness. Nevertheless, these results could not isolate the effect of radiation damping due to the presence of the buildings' structural damping.

With the current set of parameters the isolation of the radiation damping by removing the material damping form the structure, posed a significant problem. For the fixed foundation set up, the model has no source of damping so the dynamic response at the resonant frequency is infinite. Also for the models with soils stiffness the contribution of the radiation damping was so low that the resonance peak had a very sharp point, which meant that because of the resolution of the of the sampling frequencies not were not accurate enough to calculate the dynamic properties. The peak acceleration relies on the area under the curve of the acceleration PSD function and the global damping relies on accurate geometry to use the HPBW method. This lead to predictions that were not consistent and changed significantly when the sampling frequency was modified.

To overcome this problem the effect of radiation damping was investigated indirectly, were the parametric analysis of the shear wave velocity is repeated setting the imaginary part of the stiffness matrix to zero ($Im\left[\overline{\overline{K}}_d(\omega)\right] = 0$) to isolate the effect of the shear wave velocity with damping only from the structure. Comparing this result with the previous results with no soil material damping ($\eta_s = 0$) will offer an insight on the impact of radiation damping. On Figure 5.20 show on the left side the results of the previous results with no soil material damping, and on the right the results of no soil damping.

Comparing the results of the acceleration, it can be observed that the models with radiation damping have a significant reduction of acceleration, providing a greater influence for higher slenderness ratios and lower soil stiffness. The results of the natural frequency is the same for

both, which is expected since the real part of the system was unchanged. Comparing the results of the global damping ratio, it can be observed that the models with radiation damping have an increase on the global damping. In both cases, a proportional tendency is observed, for lower shear wave velocity, a lower ratio of damping with respect to the fixed foundation. Since both modes have the same tendency and one of the models does not have radiation damping it can be inferred that this tendency is not caused by radiation damping. Nonetheless, it can be concluded that the increase in soil stiffness reduces in the ability of the structure to dissipate energy by the structures material damping.

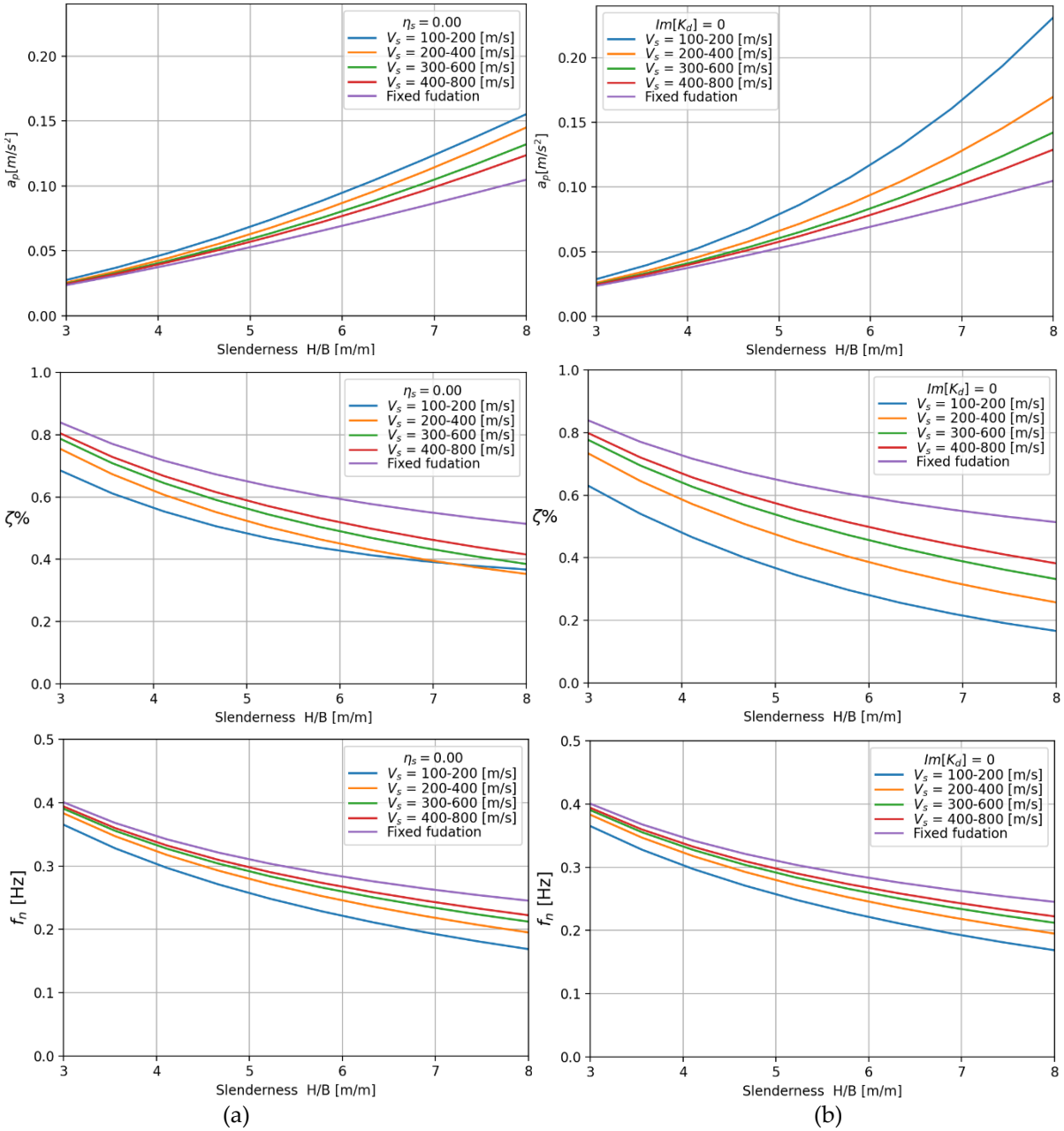

Figure 5.20 Dynamic properties with respect to slenderness for the HF model, (a) with no soil material damping, and (b) with imaginary part of the stiffness matrix to zero ($Im\left[\overline{\overline{K}}_d(\omega)\right] = 0$).

5.4 Main Findings

5.4.1 Comparison between models

In all results for the varying soil stiffness, soil material damping and building slenderness, the HF model predicts a higher peak acceleration than the EC model. Furthermore, the modifications the NIST model provides to the EC model significantly bridge the gap and made the peak acceleration predictions better resemble those from the HF model. From these results, the Parametric Study supports the results and tendencies presented in the Case Study and extends these conclusions for the New Orleans Tower to the wider array of building configurations engulfed under the ranges of the studied parameters.

Nevertheless, when looking at the other dynamic properties, such as the damping ratio and the first natural frequency, the modifications provided by the NIST model, present important inaccuracies in certain situations. At low slenderness ratios (3-4), there is around a 50% overestimation of the global damping ratio. Regarding the natural frequencies at low slenderness ratios (3-4) and high slenderness ratios (7-8), there is around 20% difference compared to the HF model. This can be due to the oversimplified estimation for the base natural frequency from the Eurocode (46/H).

The only exception where the NIST modification is not providing a clear closer resemblance to the HF model in the peak accelerations was for very high soil material damping ($\eta_s = 0.06$), where the EC model resembles better the HF model, even though the EC model was still around 25% lower. There is a clear tendency for the EC and HF models to have closer predictions for high soil material damping. From this tendency it is reasonable to infare that at higher material damping soil properties, the EC and HF models can match. With this said the reason this study did not investigate higher material damping soil properties is that $\eta_s = 0.06$ is already well in the range of nonlinear soil behaviour and for this study a linear soil behaviour model was used; so, it is beyond the limits of validity of the model.

5.4.2 Effect of soil material properties

On all studies on the impact of the soil stiffness, soft soils presented between 5% to 30% reduction of the natural frequency compared to the fixed base model. Given that a lower natural frequencies would lead to higher loads, not including the flexibility of the soil would lead to a underestimation in the loads. Furthermore, the Eurocode formula (46/H) for estimating the first natural frequency would give the same approximation to a structure with foundations on rock and in soft soil.

The results on the exploration into the impact of the material damping on dynamic properties using the HF model showed that even at low soil material damping levels ($\eta = 0.02$), not considering the effect of soil material damping led to up to 30% overestimation of peak acceleration and up to 50% underestimation of the overall damping ratio. On the other hand, modelling the soil with higher soil material damping ($\eta = 0.06$) led to up to 40% underestimation of peak acceleration and up to 120% overestimation of the overall damping ratio. This difference was observed to be highest for higher slender ratios.

The results on the exploration into the impact of the soil stiffness on dynamic properties using the HF model with no material or radiation damping from the soil ($Im\left[\overline{\overline{K}}_d(\omega)\right] = 0$) showed a for the soft soils present in the Netherlands, there was up to 50% lower damping ratio with

respect to the fixed foundation, for very slender structures (slenderness ratio 7-8). This shows that there is an impact on the global damping due to the soil stiffness, regardless of including the damping contribution of the soil. This important reduction on the influence of the tower structure damping on the global damping due to the soil stiffness, implies that auxiliary damping such as friction and Visco-elastic dampers which increase the damping of the tower structure might not be as effective for situations with softer soil. The result on the peak acceleration for the softest soil showed up to 40% in increase with respect to the fixed foundation for very slender structures (slenderness ratio 7-8).

The same study when repeated with the inclusion of radiation damping showed a reduction on the differences when compared to the fixed foundation, but still had a significant impact. The influence of the shear wave velocity amounted to around 30% to 50% difference in the estimated peak acceleration compared to the fixed base for very slender structures (slenderness ratio 7-8). But the impact is lower for low slenderness structures (slenderness ratio 3-4) around 10 to 20%.

Nevertheless, this impact was only observed when there was no soil material damping. For the case where the material damping was the one from the baseline system parameters ($\eta = 0.02$), the shear wave velocity did not have a great impact on the predicted peak acceleration relative to the fixed foundations. This difference compared to the fixed base model was less than 5%, even though it had a 5%-35% impact on the first natural frequency and 5%-60% impact global damping ratio. This is because the effect of soil stiffness on the natural frequency and the global material damping can lead to certain conditions where they cancel out each other's effects. Even though in this specific set of soil and structure properties studied, there was a small variation in peak acceleration, it cannot be assumed that the other dynamic properties of the system would have small variations as well, nor that for other sets of soil and structure properties there would be a low effect of SSI on the acceleration.

6

Conclusion

This study analysed how soil material damping and soil stiffness affect the dynamic response of high-rise buildings under wind loading in the Netherlands. For this the HF (High Fidelity) model was developed, which was first validated with a case study of the New Orleans Tower and then implemented as part of a parametric study on soil material damping and soil stiffness. For both the Parametric Study and the Case Study, the predictions of expected peak acceleration, global damping ratio and first natural frequency where compered to SDOF models such as the one in the Eurocode (EC model) and the NIST model. The NIST model follows the same procedure as the EC model but includes the effects of SSI on the calculation of natural frequency and modal damping.

The HF model consists of 3 sub-models: the foundation model that provides the influence of SSI through a foundation dynamic stiffness matrix; wind model that provides the stochastic approximation for the loading; and the tower structure model that is a Euler-Bernoulli beam, with material damping and fully populated, frequency dependant, dynamics stiffness matrix as the support of the beam from the foundation model. The stochastic dynamic response of the system is computed in the frequency domain. In this model the effect of the gravitational component due to the tilt of the structure is taken into account into the calculation of the total dynamic response of the system.

6.1 Answers for research questions

The main findings of chapter 4 and 5 have already been presented at the end of their respective chapters. This section will, in a concise manner, provide the specific answers to the research questions presented in the introduction.

1. Is the HF model an accurate model for predicting the dynamic response of high-rise buildings under wind loading?

Through the use of the case study it was shown that the HF model provides an accurate prediction of the dynamic characteristics and dynamic response of the New Orleans Tower. Compared to the measurements the error was less than 7% for all the evaluated dynamic properties. Also there was a good match between the acceleration density functions of the HF model and that from the measurements.

2. How do simplified methods such as the EC model and NIST model compare with the measurements?

The results of Case Study showed that the EC model provided a 30%-35% underestimation of the peak acceleration compared to the measurements, when using the natural frequency recommended by the Eurocode (46/H). When using the natural frequency used in design it

results is an 50% overestimation of the peak acceleration, which is on the safe side. This underestimation of natural frequencies in the design phase of the building is common.

For the NIST model the peak acceleration results were also underestimated, but at a lesser degree than the standard EC model, with 13%-19% underestimation of the peak acceleration compared to the measurements. The better performance of the NIST model compared to the EC model, resides in the influence of the SSI: the reduction of natural frequencies and damping results in a larger peak acceleration.

The results from the Parametric Study support the results and tendencies presented in the Case Study and extend these conclusions for the New Orleans Tower to the broader array of building configurations engulfed under the ranges of the studied parameters and the limitations of the model.

3. How much impact does the soil material damping have on the dynamic properties of the system?

The parametric study showed that the soil material damping had an important impact on the dynamic properties of the system, specifically on the overall damping of the system and the peak acceleration. Specially for very slender structures since the results show that with the increase of slenderness the soil material damping had a greater impact in determining the dynamic response of the structure. Not considering the effect of soil material damping led up to 20% overestimation of peak acceleration. Moreover, modelling the soil with a higher soil material damping ($\eta = 0.06$) led up to 40% underestimation of peak acceleration. This effect was observed to be highest for higher slender ratios (7-8). For lowers slenderness ratios the same tendencies of overestimation and underestimation where observed but at a lesser degree.

4. How much impact does the soil stiffness have on the dynamic properties of the system?

Similar to soil material damping the soil stiffness had an important impact on the dynamic properties of the system, where this impact became grater for structures with high slenderness. But the soil stiffness had more intricate effects since it affected the natural frequency and the amount of energy dissipated by the soil radiation damping, the soil material damping and the structure material damping. But there was not a global trend with respect to the effect of the soil stiffness on the global damping, since it depended on the amount of material damping. This meant that depending on the soil material damping the softest soil showed up to 40% in increase in the peak accelerations with respect to the fixed foundation in one case ($\eta = 0.00$) and almost no effect (5%) in another case ($\eta = 0.02$). When there was almost no effect it was identified that there were still an important effects on the overall damping and the natural frequency but they had opposite effects on the peak accelerations, effectively cancelling out each other effects. By comparing the results with and without the radiation damping it was shown that radiation damping accentuates the difference of global damping at the different soil stiffnesses, but maintains the same tendencies.

5. How do simplified methods such as the EC model and NIST model compare with the more rigorous HF model, with respect to the overall damping, the resonance frequency and the dynamic response?

From the results in the parametric study the EC model, compared to the HF model, overestimates both the natural frequency and the overall damping of the system leading to an underestimation of peak acceleration. The greatest discrepancy between the EC and the HF models happens at high slenderness.

The modifications the NIST model provides a reduction of natural frequencies and damping on the EC model which result in a larger peak acceleration. These modifications significantly bridge the gap and made the peak acceleration predictions better resemble those from the HF model. Even though the acceleration resembles the HF model much better the other studied dynamic properties, such as the damping ratio and the first natural frequency, still present important inaccuracies in certain situations. Specially the damping at low slenderness ratios (3-4), and the natural frequencies at high slenderness ratios (7-8). From this results it seems that the NIST modifications to include the effect of SSI on a SDOF system, has the desired effect on the wind induced dynamic response of high-rise buildings, but some modifications on the procedure shown on this study might be needed. For example when choosing parameters such as the fixed base natural frequencies or the different components of damping.

6.2 Recommendations for future research

This section provides recommendations for future research that can help expand the current knowledge on the dynamic response of high-rise buildings under wind loading in the Netherlands.

I. Building instrumentation

A. More buildings should be instrumented with pressure sensors. For this study there was pressure measurements available only for one building so the validation procedure was limited. Include buildings with other structural systems (braced still frames, outriggers).

B. Wind speed measurements of undisturbed wind speed data.

1. Sensors should be placed farther away from the building structure to reduce the influence wind flow around the building on the measurements of the undisturbed mean wind speed.

2. If possible more than one wind speed sensor should be used.

3. Use of LIDAR to calculate the wind speed data.

C. Locate the acceleration sensors close to the top of the building. This will make sure to be able to detect the second natural frequency and reduce the assumptions on the process of scaling SFOF acceleration results to the measured height.

II. Corroborations of assumptions

A. Corroborate the assumption that the model validated from wind events with low magnitudes can be used without any modification for SLS wind event magnitude events.

1. Measurement data of stronger events to validate the model.

2. Implement stick-slip model to investigate the influence of amplitude dependant damping.

B. Corroborate the assumption that the deformation of the soil are still linear under dynamic response of high-rise buildings under wind loading.

1. Model the tower, wind, foundation and soil in the same 3D FEM model and quantify the amplitude of the strains in the soil.

2. Use a model like the HF model to compute the deformations at the base of the structure and in a separate 3D FEM model of the soil and foundations, introduce the deformation of the base.

Both of this solutions can be done with linear models. If the results would show that the magnitudes of soil strain are in the non-linear range, the conclusion would still be that the nonlinear strains occur under these conditions even though the magnitude might not be accurate.

III. Other uses and modifications of the HF model

A. Study the effects and viability of auxiliary damping. This study showed that there is an important reduction on the influence of the tower structure damping on the global damping due to the soil stiffness. From this it can be implied that auxiliary damping such as friction and Visco-elastic dampers which increase the damping of the tower structure might not be as effective for situations with softer soil.

B. Modify FH model to be able to model structures with Outriggers, allowing to investigate effects at higher slenderness.

C. Include shear deformation to FH model to be able to model structures with lower slenderness.

D. Include tortional deformation to the HF model. This would allow to model both directions of movements, for non-symmetric structures.

E. Further investigate the influence of the tilt component on the global response of the structure, especially for what set of system properties can the tilt become an important component of the predicted acceleration.

IV. Further investigate the NIST model

A. Study the use of other natural frequency approximations for the fixed base natural frequency, and investigate its performance against measurements of the New Orleans and other buildings, as well as against analytical models such as the HF model.

B. Explore the possibility of separating the radiation and material damping from the soil stiffness matrix, and investigate how this effects the results of the NIST model.

V. Others

A. For this study the EC model followed all approximations provided in the Eurocode, but in practice several of this assumptions are refined with help of a FEM model of the structure. A script to create a modular parametric FEM model of a building would allow to extract the properties needed to update the EC model as it would be done in practice.

6.3 Closing remarks

The results of this study show that for the ranges of properties relevant to the Netherlands, the soil stiffness and soil material damping, have significant influence for accurate predictions of the dynamic response of high-rise buildings under wind loading. Specially, there was found a higher influence on the dynamic response for the extreme cases of high slenderness ratio structures on very soft soils.

Both properties of the soil as well as the slenderness ratio have significant effects on the first natural frequency and global damping ratio of the system, which lead to numerous combinations of effects on the peak acceleration of the structure. In summary, SSI interaction not only has an important impact, on the dynamic response of the system but it is also intricate, so any simplified method that wishes to calculate accurate dynamic properties of the system needs to include accurate predictions of natural frequencies and equivalent damping ratios.

The methodology of including the effect of SSI presented by the NIST, has been developed for seismic conditions. The results show that the methodology presented by the NIST when used to refine the first natural frequency and global damping ratio, is effective in including the effect of SSI in the EC model for wind loading, for the range of high-rise building configurations investigated in this study. The results of the Case Study show that the NIST modifications improve the prediction of the wind induced acceleration measurements of the New Orleans Tower. Additionally, it also improves the wind induced acceleration predictions compared to the HF model for the different slenderness ratios, soil stiffnesses and material damping relevant to the Netherlands. Nevertheless, this NIST model shows that there can be significant improvement in the calculations of the natural frequency as well as the overall damping ratio at lower slenderness ratios. The NIST model as presented in this study, always leads to a decrease in natural frequency and in damping which in turn increase the peak acceleration. So, the NIST model always increases the predicted peak acceleration.

The HF Model developed for this study, resulted as a useful tool to explore the effects of SSI on the dynamic response of high-rise buildings under wind loading. It provided insight into the intricacies of the full stochastic dynamic response of the system. The inclusion of the dynamic matrix as the base of the HF model, computed through Dynaplile provided a closer look into the impact specific soil material properties, had on the dynamic system, not having to sacrifice the oversimplification of pile foundations or soil layers. The addition of the effect of the tilt component of the acceleration provided an extra level of detail to the dynamic response results, at a low set up and computational cost.

References

[1] TKI Deltatechnologie, "Dynamisch gedrag van hoge gebouwen in Deltasteden," 2022. https://tkideltatechnologie.nl/project/dynamisch-gedrag-van-hoge-gebouwen-in-deltasteden/.

[2] The European Union Regulation, *EN 1991-1-4 Eurocode 1: Actions on structures - Part 1-4: General actions - Wind actions*, vol. 1, no. 2005. 2011.

[3] A. J. Bronkhorst, C. A. Van Bentum, and S. S. Gomez, "Wind-induced vibrations and damping in high- rise buildings," 2018.

[4] Y. Tamura, "Amplitude Dependency of Damping in Buildings and Critical Tip Drift Ratio," *Int. J. High-Rise Build.*, vol. 1, no. 1, pp. 1–13, 2012.

[5] R. Smith and M. Willford, "Damping in Tall Buildings – Uncertainties and Solutions," no. January, pp. 66–67, 2008.

[6] S. Sanchez Gómez, "Energy Flux Method For Identification Of Damping In High-Rise Buildings Subject To Wind," TU Delft, 2019.

[7] S. Sanchez Gómez, C. P. W. Geurts, and A. Metrikine, "On the importance of soil damping for tall buildings loaded by wind," *Eng. Struct.*, vol. 163, no. November 2017, pp. 426–435, 2018.

[8] C. Cruz and E. Miranda, "Insights Into Damping Ratios Buildings," *Earthq. Engng Struc Dyn.*, pp. 1–19, 2020.

[9] NEHRP Consultants Joint Venture, "Soil-Structure Interaction for Building Structures," *Nist Gcr*, vol. 12, pp. 917–21, 2012.

[10] A. C. W. M. Vrouwenvenvelder, "Lecture notes CIE5145 Random Vibrations TU Delft." 2004.

[11] Y. Paauwe, "Obtaining Insight into the Influence of the Main Parameters in the Preliminary Structural Design on the Wind-Induced Dynamic Response Including Soil-Structure Interaction Effects of High-Rise Buildings in the Netherlands," Delft University of Technology, The Netherlands, 2020.

[12] R. E. R. Aquino and Y. Tamura, "On stick-slip phenomenon as primary mechanism behind structural damping in wind-resistant design applications," *J. Wind Eng. Ind. Aerodyn.*, vol. 115, pp. 121–136, 2013.

[13] B. R. Ellis, "Significance Dynamic Soil-Structure Interaction in Tall Buildings," *Proc. Instn Civ. Engrs.*, vol. 81, no. 2, pp. 221–242, 1986.

[14] J. A. Mercado, L. G. Arboleda-Monsalve, and K. R. Mackie, "Period Lengthening Characteristics of Tall Buildings," *17th World Conf. Earthq. Eng. 17WCEE*, no. September, 2020.

[15] I. Venanzi, D. Salciarini, and C. Tamagnini, "The effect of soil-foundation-structure interaction on the wind-induced response of tall buildings," *Eng. Struct.*, vol. 79, pp.

117–130, 2014.

[16] N. Satake, K. Suda, T. Arakawa, and A. Sasaki, "Damping evaluation using full-scale data of buildings in Japan," *J. Struct. Eng.*, vol. 129, no. 4, pp. 470–477, 2003.

[17] M. Sonneveld, "Sensitivities and prerequisites of the application of the Energy Flux Analysis to high-rise structures excited by wind using in situ measurements," Delft University of Technology, The Netherlands, 2020.

[18] R. D. J. M. Steenbergen, A. C. W. M. Vrouwenvelder, and C. P. W. Geurts, "The use of Eurocode EN 1991-1-4 procedures 1 and 2 for building dynamics, a comparative study," *J. Wind Eng. Ind. Aerodyn.*, vol. 107–108, pp. 299–306, 2012, doi: 10.1016/j.jweia.2012.03.025.

[19] R. D. J. M. Steenbergen, "Super Elements in High-Rise Buildings under Stochastic Wind Load," Delft University of Technology, The Netherlands, 2007.

[20] T. E. U. Regulation, "National Annex to En 1991-1-4 + a1 + C2 / Nb," no. december 2011, 2011.

[21] A. Jeary, *Designer's Guide to the Dynamic Response of Structures*. 1997.

[22] A. Simone, *An Introduction to the Analysis of Slender Structures*, no. Spetember. 2011.

[23] A. J. Bronkhorst and C. P. W. Geurts, "Long-term vibration and wind load monitoring on a high-rise building," *Proc. ISMA 2020 - Int. Conf. Noise Vib. Eng. USD 2020 - Int. Conf. Uncertain. Struct. Dyn.*, pp. 1541–1552, 2020.

[24] C. P. W. Van Bentum, C.A., Kalkman, I.M., Geurts, "Field tests to study the pressure equalization on air permeable façade elements," *ICBEST 2014 Build. a Chang. World*, 2014.

[25] C. P. W. Van Bentum, C.A., Geurts, "Full scale measurements of pressure equalization on air permeable façade elements," *14th Int. Conf. Wind Eng.*, 2015.

[26] Nederlandse Organisatie voor Toegepast-natuurwetenschappelijk Onderzoek, "DINOloket, Data and Information from the Dutch Subsurface." https://www.dinoloket.nl/ondergrondgegevens.

[27] M. B. Darendeli, "Development of a new family of normalized modulus reduction and material damping curves," 2001.

[28] J. Roesset and L. Vasquez, "Dynamic analysis of pile and drilled shafts under dynamic loading Technical manual," no. August, 2016.

[29] S. H. U. Q. Chowdhury, "Damping Characteristics of Reinforced and Partially Prestressed Concrete Beams," *Engineering*, no. April, 1999.

[30] A. J. Bronkhorst, D. Moretti, and C. P. W. Geurts, "Identification of the dynamic properties of the residential tower New Orleans," vol. 1, pp. 1–8, 2021.

[31] T. N. O. Bouw and O. Informatie, "Nen 6702 Technical principles for building structures - TGB 1990 - Loadings and deformations," 2005.

[32] NAM Deltares, "Geological schematisation of the shallow subsurface of Groningen.," 2015.

[33] I. Towhata, *Geotechnical Earthuake Engineering*. Springer, 2008.

[34] R. M. Chung, F. Y. Yokel, and V. P. Drnevich, "Evaluation of dynamic properties of sands by resonant column testing," *Geotech. Test. J.*, vol. 7, no. 2, pp. 60–69, 1984.

[35] G. Lefebvre and D. LeBoeuf, "Rate effects and cyclic loading of sensitive clays," *J. Geotech. Eng., ASCE*, vol. 113, no. 5, pp. 476–489, 1987.

[36] B. O. Hardin and V. P. Drnevich, "Shear modulus and damping in soils design equation and curves," *Proc. ASCE*, vol. 98, no. SM7, pp. 667–692, 1972.

[37] A. Ciancimino *et al.*, "Dynamic characterization of fine-grained soils in Central Italy by laboratory testing," *Bull. Earthq. Eng.*, vol. 18, no. 12, pp. 5503–5531, 2020.

[38] Z. Khan, M. H. El Naggar, and G. Cascante, "Frequency dependent dynamic properties from resonant column and cyclic triaxial tests," *J. Franklin Inst.*, vol. 348, no. 7, pp. 1363–1376, 2011.

[39] G. Mylonakis, "Contributions to Static and Seismic Analysis of Piles and Pile-Supported Bridge Piers," *Phd Thesis*, no. February 1996, pp. 1–316, 1995.

[40] M. El-Marsafawi, "Dynamic Experiments on Two Pile Groups," *J. Geoteck. Engrg*, vol. 118, no. 4, pp. 576–692, 1992.

[41] F. Pizano, "Course CIE5340-18 Soil Dynamics TU Delft." 2021.

[42] A. Elgamal, Z. Yang, E. Parra, and A. Ragheb, "Modeling of cyclic mobility in saturated cohesionless soils," *Int. J. Plast.*, vol. 19, no. 6, pp. 883–905, 2003.

[43] T. Benz, *Small-Strain Stiffness of Soils and its Numerical Consequences*. University of Stuttgart, Mitteilung 55, 2007.

[44] R. B. J. Brinkgreve, M. H. Kappert, and P. G. Bonnier, "Hysteretic damping in a small-strain stiffness model," *Proc. 10th Int. Symp. Numer. Model. Geomech. NUMOG 10 - Numer. Model. Geomech. NUMOG 10*, no. January, pp. 737–742, 2007.

[45] M. R. Riaz, H. Motoyama, and M. Hori, "Review of soil-structure interaction based on continuum mechanics theory and use of high performance computing," *Geosci.*, vol. 11, no. 2, pp. 1–22, 2021.

[46] J. P. Wolf and A. J. Deeks, "Foundation vibration analysis: a strength-of-materials approach," *Choice Rev. Online*, vol. 42, no. 01, pp. 42-0328-42–0328, 2004.

[47] J. P. Wolf, "Simple physical models for foundation dynamics," *Dev. Geotech. Eng.*, vol. 83, no. C, pp. 1–70, 1995.

[48] H. G. Poulos and E. . Davis, *Pile Foundation Analysis and Design*. The University of Sydney, Rainbow-Bridfe Book Co., 1980.

[49] D. Salciarini and C. Tamagnini, "A hypoplastic macroelement model for shallow foundations under monotonic and cyclic loads," *Acta Geotech.*, vol. 4, no. 3, pp. 163–176,

2009.

[50] Z. Li, P. Kotronis, S. Escoffier, and C. Tamagnini, "A hypoplastic macroelement for single vertical piles in sand subject to three-dimensional loading conditions," *Acta Geotech.*, vol. 11, no. 2, pp. 373–390, 2015.

[51] Z. Jin, Z. Y. Yin, P. Kotronis, Z. Li, and C. Tamagnini, "A hypoplastic macroelement model for a caisson foundation in sand under monotonic and cyclic loadings," *Mar. Struct.*, vol. 66, no. December 2018, pp. 16–26, 2019.

[52] C. P. W. Geurts, "Wind-induced pressure fluctuations on building facades," Technische Universiteit Eindhoven, Nethelads, 1997.

[53] R. l. J. van de Berg and R. D. J. M. Steenbergen, "Identifying the Damping Contribution of Building," *4th ECCOMAS Themat. Conf. Comput. Methods Struct. Dyn. Earthq. Eng.*, 2013.

[54] F. Matichard and M. Evans, "Review: Tilt-free low-noise seismometry," *Bull. Seismol. Soc. Am.*, vol. 105, no. 2, pp. 497–510, 2015, doi: 10.1785/0120140200.

[55] K. Venkateswara, C. A. Hagedorn, M. D. Turner, T. Arp, and J. H. Gundlach, "A high-precision mechanical absolute-rotation sensor," *Rev. Sci. Instrum.*, vol. 85, no. 1, p. 015005, 2014, doi: 10.1063/1.4862816.

[56] K. Venkateswara, C. A. Hagedorn, J. H. Gundlach, B. Lantz, and R. Schofield, "Subtracting tilt from a horizontal-seismometer using a," *Bull. Seismol. Soc. Am.*, pp. 1–37, 2015.

Annexes

Overview of idealized common types of damping mechanisms

A damping mechanism is the term for those actions that dissipate energy from a mechanical system. This dissipation of energy can come in many forms: heat, plastic deformation, wave radiation (light, sound, ground waves) and others. Another important characteristic of damping mechanisms is what fiscal property of the system drives the dissipation some of the main types of damping mechanisms are introduced. Some of the most common types of damping mechanism are introduced on this section.

A.1 Coulomb damping

Also known as dry friction, energy is absorbed at a constant rate by the sliding friction between surfaces. It only takes into account that the contact forces between the surfaces creates a constant resistance force in the opposite defection of the relative motion between the surfaces. This damping mechanisms presents constant dissipation of energy. For single degree of freedom (SDOF) system it can be mathematically expressed in the equation:

$$m\ddot{x} + kx + N\mu \operatorname{sign}(\dot{x}) = F$$

with,

m = Mass
k = Stiffness
F = Force
N = Contact force between surfaces
μ = Coefficient of kinetic friction
x = Displacement
$\dot{x}$ = Velocity
$\ddot{x}$ = Acceleration
$\operatorname{sign}(\dot{x})$ = takes the ±1 with the same sign as the velocity

A.2 Viscous damping

This type of damping mechanisms can be exemplified by a fluid flowing through an opening and creating heat because of friction between particles and the container. This friction is driven by the velocity of the flow, which means that it is dependent a rate change in displacement. For continues systems it is described by the rate of change in strain.

The paring of a viscous damper with an elastic spring in paralleled or viscoelastic formulation is known as the Kelvin–Voigt model. For a SDOF system it can be mathematically expressed in the equation:

$$m\ddot{x} + c_d\dot{x} + kx = F$$

with,

c_d = Viscous damping coefficient

A.3 Fluid-structure damping

The damping caused by drag force of a fluids passing through structure is referred to as fluid-structure damping. It is similar to Coulomb damping but since the contact force between the fluid and the structure depends on the square of the velocity this damping mechanism is velocity dependent. For a SDOF system it can be mathematically expressed in the equation:

$$m\ddot{x} + \alpha\, \dot{x}^2 \text{sign}(\dot{x}) + kx = F$$

most commonly written:

$$m\ddot{x} + \alpha\dot{x}|\dot{x}| + kx = F$$

with,

$\alpha =$ Drag force coefficient $\left(\text{example: } \frac{1}{2}A\rho C\right)$

A.4 Plastic deformation damping

Plastic deformation is a complex mechanism were the particles reached a stress state where they move relative each other so much that the particles rearrange into different and permanent positions. There are two energy loses components, one related to the friction between moving particles and a second related to "work hardening".

The friction between moving particles is related here transfer from the kinetic energy of the particles It might seem that this component could be simply modelled as Coulombe damping, but complications arise when taking into account that the contact forces of the particles relate to the stresses inside the material and the friction coefficient between particles both of which have to do with intermolecular forces and other complex interactions.

The dissipation of energy due to work hardening comes from the rearrangement of particles from a lower to a higher energy configuration in the material lattice, where it absolves strain energy from the system. This also a complex process, it depends on the specific material molecular properties, its particle lattice distribution and similar to the last mechanisms, it also has to do with intermolecular forces and other complex interactions.

As it is evident damping due to plastic deformation is complex and cannot be accurately simplify to a simple physical model. For this reason, most of the time the energy dissipation due to plastic deformation has been models using other damping models and fitted to laboratory measurements.

Using a viscoelastic approach by calibration the area under the hysteretic viscus ellipsis to the area under the hysteretic laboratory measurements create an equivalent energy dissipation model. The shortcomings of this method are that the amount of energy dissipated only is valid for the amplitude and strain rate were it was calibrated. For simple elements like rods or beams this can be overcome by choosing the first natural frequency of the structure and the maximum allowed deformation as the parameters to formulate your viscous damping coefficient. If deformations are over the allowed maximum, the prediction might not be as accurate but the deformations are out of the allowable range anyways. Having defined the deformation, using the natural frequency the strain rate can be defined. Since on a structure most of the displacements occurs in the first natural frequency it is an adequate approximation.

The coulomb model is able to create hysteretic behaviour but it hysteretic loop is a rectangle. It has potential use for perfectly linear plastic materials were the elastic deformation is small compared to the total deformations. This limitation can be overcome by introducing paralleled, stick and slip components in series with springs, which creates an artificial discrete nonlinear spring. This recreates very similar hysteretic curves but because of its non-linearity no analytical solutions are possible and time step approaches need to be taken into account.

A way around some of this drawbacks of this methods is to use a complex stiffness or complex stress-strain model [33]. This model introduces an extra imaginary term to the stiffness, the real term has a completely linear behaviour in the force displacement curve, while the imaginary component has an elliptical behaviour in the force displacement curve. The result is a force displacement curve which resembles really well the form of the hysteretic curves. For a SDOF system it can be mathematically expressed in the equation:

$$m\ddot{x} + k(1 + i2\eta)x = F$$

with,

$i = \sqrt{-1}$

$\eta =$ Damping coefitient

Damping coefficient η is not the same as critical damping ratio ζ or vicious damping coefficient c. Damping coefitient η corresponds to the energy loss per cycle. When loaded in harmonically in the natural frequency the damping coefitent η is the same as the critical damping ratio ζ.

$$\eta = \frac{\nabla W(\omega = \omega_0)}{4\pi W} = \frac{c}{2\sqrt{mk}} = \zeta$$

In the same way as the viscoelastic approach the area under the complex stiffness curve and the area under the hysteretic laboratory measurements are calibrated to have an equivalent energy dissipation model. A limitation of this approach is that if deformations get to much into the plastic regime the complex stiffness curve does not resemble the real hysteretic stress, in fact model does not show a completely plastic regime, since it always increase with increasing deformations. Maximum deformations and strains reached are needed to be checked to ensure no over-stiffness on the plastic regime has occurred. A benefit of this approach over the viscoelastic approach is that the form of the hysteretic loop does not depend on the velocity or strain rate, which means that damping is applied more uniformly over all amplitudes.

A.5 Geometric attenuation

This form of damping has to do with how the wave front increases in size as it travels away from the source. With the increase size of wave front the energy is spread and the energy density of the wave decreases. In other words, the total energy in the system is constant and it is not transforming but the local energy density at the wave front decreases and the wave amplitude decays. In fact, since wave front is in 3D, the wave front is a growing sphere and its area increases proportional to r^2 (r being the distance from the source), because the total energy is constant the energy decreases proportional to $1/ r^2$. In this case the energy is stored in elastic strain which is proportional to the square root of the energy. This means that the amplitude of the strain is proportional to 1/r for waves propagating in a 3D medium. Using

the same logic, a 2D where its wave front is a growing circle, so its energy density is proportional to 1/r and the strain amplitude is proportional to $1/r^{0.5}$.

In soils, body wave propagation on a 3D medium is a dispersive system, which means that waves of different wavelengths travel at different speeds so they also dissipate the energy ate different rates. Because of this difference in speeds and also soil can be idealized as a half space which presents a boundary that reflect and polarize waves, they interact in constructive and destructive interference creating surface waves. This surface waves can be seen as propagating in 2D.

Both of these different types of waves attenuate with a different tendency because of their propagation dimension: surface waves with a coefficient of $1/r^{0.5}$ and body waves with a 1/r coefficient. This means that surface waves are expected to display much higher amplitudes at farther distance.

Foundation modelling background and theory

B.1 Relevant soil properties for its dynamic behaviour

There are many different types of soils and the have a wide range of dynamic properties. Depending on the location the types of soils can be narrowed down significantly. This section focus on describing the relevant dynamic properties of soils in the Netherlands. First a description of the types of soil and how they are specially distributed are introduced, to narrow down the types of soils that were considered. Then properties like material damping, nonlinear stiffness and radiation damping are addressed. Other dynamic properties like permeability and pore pressure build up are not be included because the vibrations induced by win loading are sufficiently slow that undrained behaviour can be assumed.

B.1.1 Soil profile description

This section presents a broad overview of the soil profiles commonly found in the Netherlands, specifically from the cities in the Netherlands that have the most high-rise buildings: Amsterdam, Rotterdam and The Hague. Some of the most important characteristics to consider are the types of soil, their layer distribution and their stiffness.

With respect to soil types it is common to find soft clays and sand, as well as soil with a mixture of both. Y. Paauwe [11], using DINOloket made sections through these three major cities and compiled the information to find representative soil profiles. Providing also equivalent properties of the first 30m of soil. These representative soil profiles and their equivalent properties are presented on Figure B.1.

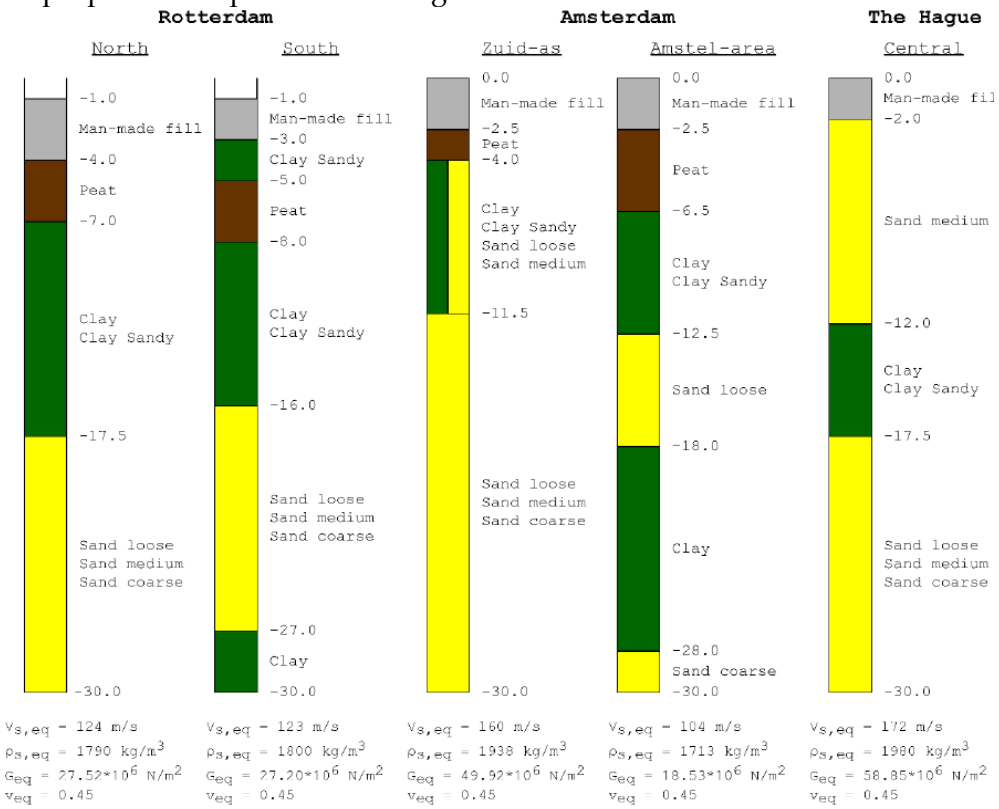

Figure B.1Representative soil profiles of cities in the Netherlands. Taken from Y. Paauwe [11].

B.1.2 Material damping and Nonlinear stiffness

The nonlinear stiffness of soils when subjected to cyclical deformation dissipate energy. This energy dissipation is high driven by plastic deformations in the soil, but some soils also show strain rate energy dissipation dependency which would correspond to a viscous damping mechanism. How much of this mechanism is present in soil, is dependent on the soil composition. The most relevant characteristic of a soil, with respect to its dynamic properties, are how hard it is and how fine or coarse are the grains. This topic is thoroughly explained by Towhata [33], some of the most important characteristics are summarised in the next paragraphs.

Towhata [33] uses the term discreteness to as a parameter of how bonded the soil grains are to each other, where a discreet soil have low particle bonding. Where the higher the effective stress and plasticity index increases the bonding and reduces discreteness. The higher the discreetness the higher the nonlinearity. So, in this sense a loose sand would be most nonlinear and an overconsolidaded clay would be less nonlinear. Since non-linear plastic behaviour relates to energy dissipation, it is to be expected that at lower effective stress, more material damping occurs. Which is what Chung [34] recreated in a resonant column test of sand, the damping ratio decrease with higher effective stress.

Nonlinearity of soil becomes more significant at higher amplitudes of strain, which means hysteretic damping is in general more pronounced at higher amplitudes. This means that hysteretic damping in soils is amplitude dependent. In fact, at small strains ($\varepsilon < 10^{-6}$ for sands and $\varepsilon < 10^{-5}$ for clays) soil is idealized as elastic which theoretically would mean no hysteretic damping. But experimental results on low strain amplitudes show that at lowered amplitudes there is still significant damping. Figure B.2 illustrates this strain ranges where soil has district behaviour. But it is important to pion out that different soil types have some difference in behaviour, this can be seen from Figure B.3 where it is shown that sands display a non-linear behaviour at around an order of magnitude higher, as well as some difference in damping at higher strains.

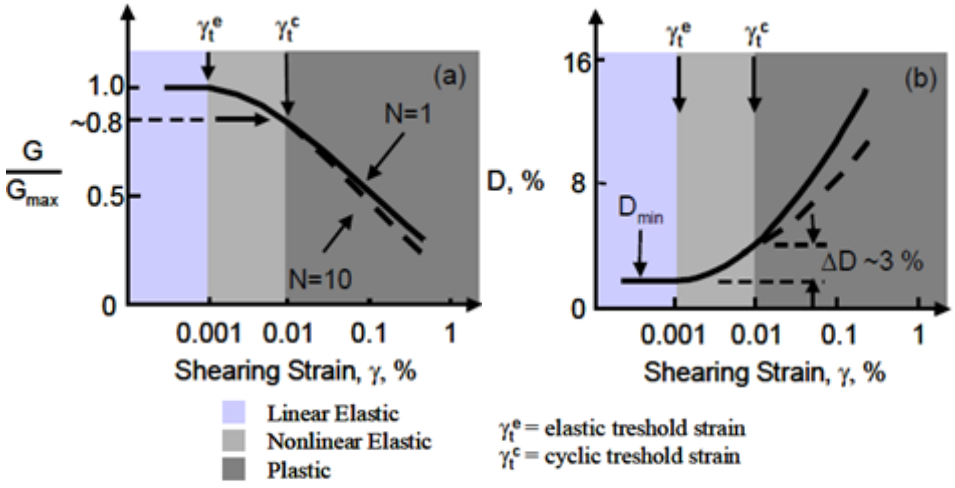

Figure B.2Linear elastic, nonlinear elastic and nonlinear plastic strain range. Taken from Mehmet Baris Darendeli [27]

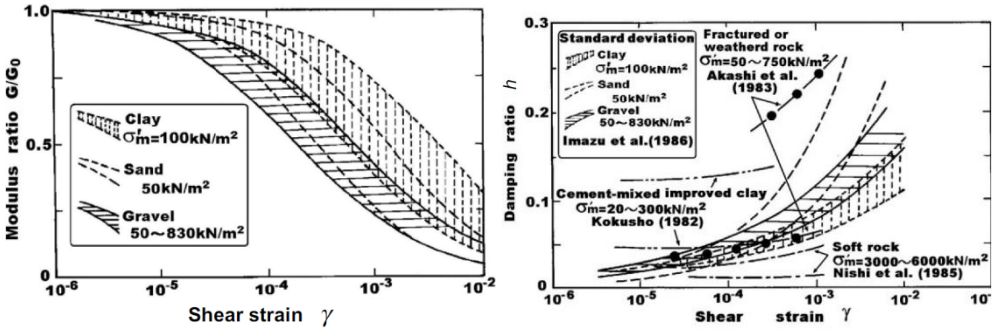

Figure B.3. G modulus nonlinearity and damping ratio, at different strain levels, for different soil types. Taken from Towhata [33]

Towhata [33] lists that the factors that affect shear modulus of sands are: Strain amplitude, effective stress, density and anisotropic consolidation. Whereas the factors that influence the damping ratio on sand are only: Strain amplitude and effective stress. Another phenomenon about soil is that cyclic tests show that with the increase of number of cycles the shear modulus increases and becomes more linear, therefore a decrease in the area of the stress-strain loops is expected with each cycle and with it the dissipation of energy decreases. This is especially important for wind induced vibrations where a wind storm can take place for hours and hundreds of cycles can take place. Dynamic tests such as Resonant Colum tests are rarely done for high number of cycles.

For clay Towhata [33] lists that the factors that affect shear modulus: Strain amplitude, effective stress, density, pre-straining, over-consolidation and consolidation time. Whereas the factors that influence the damping ratio are only: Strain frequency and effective stress. With respect to the number off cycles the opposite effect of sands happens, the stiffness decreased. This degradation can be attributed to a decrease in effective stress due to pore pressure build-up.

Clay stress-strain curve also varies with the stress rate, the faster the change in stress the greater shear modulus and greater strength, however this effect is small. In experimental tests conducted by Lefebvre and LeBoeuf [35] an increase of the stress rate by 132 times only increased 25% in shear modules and strength, which is not unexpected since a big part of the behaviour in clay comes from the friction and chemical bonding between grains, which is not rate dependent. This means that clay has both viscous and friction like properties.

In a study by Hardin and Drnevich [36] the tendency in silts to have greater damping ratios at bigger amplitudes of strain deformation. But they found practically the same values of damping for frequency's around 300 times lower. Silts having larger grains than clays have less of the vicious behaviour.

Because of the low dependency of soils on strain rate and more dependency on strain amplitude, Towhata [33] recommends using the complex stress-strain model to introduce damping, to achieve an independent from frequency damping ratio. This model would predict that at very small strains the damping ratio is zero, which is similar to the experimental behaviour for sands. But this model may present some challenges, especially if modelling the damping of clay at very small strain amplitudes. This is because experimental results on clays show damping does not go to zero, a constant minimum damping ratio is always precent at very small strains which is around 1%-2.5%. A. Ciancimino [37] proposed this minimum damping increase with Plasticity index, increase with loading frequency and decrease with

effective mean confining stress. In Ciancimino's [37] paper a formula using these parameters to find the minimum damping at small strains is proposed.

Another important aspect to explore is the frequency dependency. Khan et al.[38] compiled results from several studies using on dynamic properties and they show that cohesive soil has a small increase in shear modulus for frequencies ranging from 0.001 up to 1Hz. From 1 to 200 Hz the increase in shear modulus becomes more significant but also an increase in damping ratio is present. While, cohesionless soils showed no frequency dependant behaviour on frequencies ranging from 0.1 to 100 Hz.

The damping ratio, for the sands, with respect to frequency variation, was found to be unchanging. But there was a big change in damping ratio at degrees of bentonite water saturation, for the 32% saturation the damping ratio was around 10 times higher than the 0.5% damping ratio for dry sand. Which means that sands with small amounts of clay or silt have some degree of cohesive frequency dependant properties even though most of its composition is from sand. Since in the experimental tests performed by Khan et al.[38] even the addition of bentonite water to the sand was enough to see a difference in the tendency to increase in shear modulus as the frequency increased, at 1.5 Hz the shear modulus was the same for different degrees of bentonite water saturation but as the frequencies got higher the shear modulus deviated for each other, with the one with the higher degrees of bentonite water saturation having the biggest increase in shear modulus. It is important to mention that in this study a 17% decrease in damping ratio from 1.5Hz to 40Hz was measured for clays.

Cyclic soil behaviour can lead to pore pressure built up which in certain conditions can lead to complete loss of supporting capacity of the soil, also known as liquefaction. This pore pressure build-up changes the hysteretic behaviour of the soil and is normally treated as a two-phase model. This topic is not covered in depth since the wind induced vibrations are of low frequency and Netherland's soil is mainly soft sands so the behaviour is more akin to drained conditions where very little pore pressure build-up occurs.

B.1.3 Radiation damping

This source of damping comes from the energy caried away from the structure in the form of radiating waves, through geometric attenuation, that are never reflected back to the system. These radiating waves can be from both compression and shear deformation. For this to happen the medium (soil) needs to extend infinity in the radiating direction without change in density-stiffness. In reality if the soil properties maintain constant in a considerably long distance the infinite constant boundary can be considered.

When solving this analytically, radiation damping is achieved by giving a zero value to the constant that accompanies the terms of the wave equation that is moving away from the structure. For numerical methods real infinite boundary conditions cannot be modelled so artificial boundaries are using viscous springs to simulate the radiation or reflection of waves crossing the boundary. This is normally done by introducing dampers on the boundary, who absorbs the incoming wave. The problem with this method is that some waves such as surface waves are dispersive which means that waves of different wavelengths travel at different speeds. So, dampers placed on the boundary will only radiate all the energy of a specific wavelength.

B.1.4 Soil Pile Interaction

The inclusion of piles affects drastically how the foundation interacts with the soil. One of the biggest differences is vertical stiffness of the piles since the piles help both spread the load by increasing the surface area in contact with the soil, which allows the depth of the pies to reach stronger soil layers and even procure tension resistance of the foundation. Also, there is the group pile effect where the displacements imposed by one pile to the soil, overlaps between displacements imposed by the adjacent piles if they are close together. Depending on the distance between piles and the wavelength of the soil disturbance there can be constructive or destructive interference between the movement of the piles. This means that this phenomenon is frequency dependent, because different wavelengths have different amounts of amplification or damping of the movement. Which can translate to a considerable soil mass moving at important amplitudes and can have great effects on the inertia and in general the dynamic response of the building. Mylonakis [39] mentions that this interference between waves generated by different piles explains the peaks observed on the frequency domain in group pile measurements.

To include the group pile effect, the individual capacity of each pile are added up and multiplied by an efficiency factor. This efficiency factor depends on the frequency of the soil waves, the mechanical properties of the soil and the geometry of the foundation. This factor can increase or decrease the dynamic stiffness depending on the constructive or destructive interference. This is a factor that is hard to generalize since for a foundation of the building can have hundreds of piles, and not a homogeneous distribution. In NIST [9] it is taken into account through a dimensionless frequency which relates the size of the wavelength and the dimensions of the foundation. Y. Paauwe [11], points out from the result from NIST [9] on stiffness and damping of group piles, that for the soil properties expected in the Netherlands, and the low frequency expected from wind induced vibrations the stiffness was practically constant, and the damping ratio had a linear increase tendency. In NIST [9] some calculations for foundations with piles and shallow foundations are done and they found that the rocking and vertical dynamic stiffness with the inclusion of piles was around 50 times stiffer, the translational also increased but not as significant and maintained similar values but had important frequency dependent fluctuations.

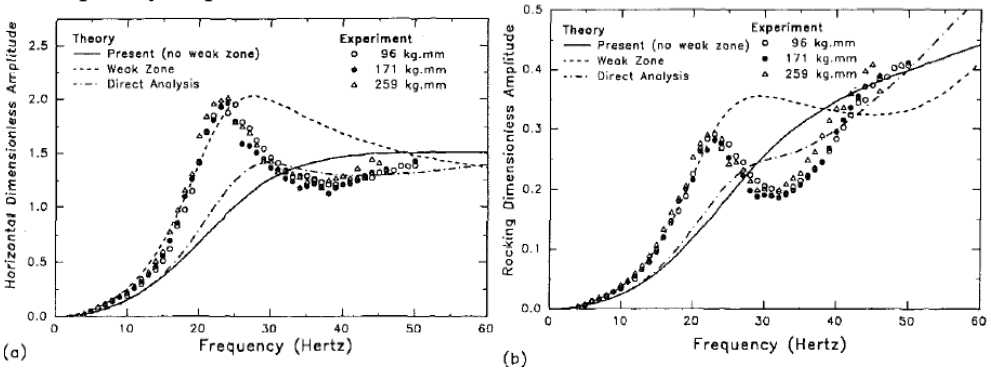

Figure B.4the response curve of 6 concrete piles under horizontal excitation. Left horizontal displacement, right rocking. Taken from El-Marafarwi [40].

It is important to point out that even though pile group effect is in general an important parameter to take into account, most of its extreme effects happen at much higher frequencies than the one expected from wind induced vibrations on higher rise buildings. El-Marafarwi [40] performed full scale tests on a group of 6 concrete piles on clay Figure B.4 shows the

response curve of 6 concrete piles under horizontal excitation is shown, and it is evident that most of the amplification happens at higher frequencies.

B.2 Soil Modelling approaches

This section presents several modelling approaches, their description, capabilities and limitations. The models can be divided into two big divisions, the linear and the nonlinear models. The linear models that are presented are the elastic, visco-elastic, and complex stress-strain. The nonlinear models are elastic-plastic, stress dependant stiffness and shear strain dependant. In general, the linear models can be solved both on the time and frequency domain while the nonlinear models need to be solved in the time domain though time history iterative schemes. In the next subsection the different models are presented in a somewhat increasing order of complexity.

SSI is most commonly used in seismic loading situations, where not only the response of the structure changes but also the ground motion input of the soil is different. This happens because the ground motion, instead of being the free field ground motion, is impacted by the presence of the structure. For wind induced motion the soil is not moving in the "free field" ground, which also means that compared to the seismic case, the applied wind force is the same as if the SSI was not taken into account. Because of this, often in practice when designing a high-rise building, SSI is taken into account in a static sense, but it has been shown that it also has an important effect on the dynamic response of the structure. For this reason it was important that in the section 2.5, it showcased the relevance of SSI in case of wind-induced vibrations on high-rise buildings.

B.2.1 Linear models

The linear model is first be introduced analytically and in general sense, this general formulation can be later used to on the rest of the models. First, we need to find the governing equation, where we combine the dynamic equilibrium, the compatibility equations and the constitutive relationships. The equations that express these 3 phenomena, in the same order as listed, are:

$$\rho \frac{\partial^2 u_i}{\partial t^2} = \frac{\partial \sigma_{ij}}{\partial i} + b_i \qquad \rightarrow \qquad \text{for} \qquad \Omega \text{ x } [0, T]$$

$$\varepsilon_{ij} = \frac{1}{2}\left(\frac{\partial u_i}{\partial j} + \frac{\partial u_j}{\partial i}\right)$$

$$\sigma_{ij} = D_{ijhk}\varepsilon_{ij}$$

where:

$i = x, y, z$
$j = x, y, z$
$\rho =$ density of the soil
$b_i =$ body forces
$D_{ijhk} =$ Stiffness matrix (4D matrix)

This expressions are completely analytical but using the Finite Element Method, through strong to weak formulation, it can be discretised in space to be solved numerically. The numerical formulation is:

$$\boldsymbol{M}\ddot{\boldsymbol{U}}(t) + \sum_{1}^{N_e} \int_{\Omega_e} \boldsymbol{B}^T \boldsymbol{D}\boldsymbol{B} d\,\Omega\, \boldsymbol{U}(t) = \boldsymbol{F}_{ext}(t)$$

This linear FE formulation is present in most soil dynamic and to solve this system the two most common ways of doing it is through the time domain and the frequency domain.

To solve the system through the time domain we need to discretize time and make use of a time integration scheme. There are many forms of time integration scheme but in general the equation is solved in succession for each time step where with the use of approximations such as Taylor series displacement, velocity and acceleration can be expressed in terms of each other. This means that we are left with only one variable and it is now a linear system where the most computationally heavy calculation is inverting a single matrix, which only needs to be performed once in the computation.

To solve the system through the frequency domain first a Fourier transform is performed on both sides of the equations transforming the differential equation to algebraic matrix equation that can be easily solved where, again, the most computationally heavy calculation is inverting the dynamic stiffness matrix. To find the solution in the time domain the inverse Fourier transform needs to be performed. Solving the system through the frequency domain gives a big advantage because in the process you also find the transfer function of the system which provides with a lot of information about the dynamic properties of the system.

B.2.1.1 Linear elastic

The simples soil modelling approach is that which only contains linear elastic soil behaviour. For this formulation the stiffness matrix, D_{ijhk} only contains real constant values, this matrix contains of diagonal terms that couples the stiffness in one principal direction with different DOFs. The formulation in the previous section is for the general case but be further simplified for the linear elastic case. Where the 4D stiffness matrix can be decomposed into:

$$\sigma_{ij} = D_{ijhk}\varepsilon_{ij} = \left(K_b - \frac{2}{3}G\right)\varepsilon_{vol}\delta_{ij} + G\varepsilon_{ij}$$

$$\varepsilon_{vol} = \frac{\partial u_j}{\partial j}$$

With:

K_b = Bulk modulus

G = Shear modulus

This is normally just done to ease analytical calculation because when using FE it is more convenient to have a single stiffness matrix.

From this formulation a lot of the soil's behaviour is able to be modelled. Some of the most important capabilities are: deformability of soil, period lengthening, flexible foundation, volumetric strain behaviour, radiational damping, wave reflection, influence of layers, soils inertia and group pile effects. It is able to include radiation damping through geometric attenuation of the propagating wave and finally dissipating boundaries. The wave reflection can be introduced through changes in stiffness in soil layers or from boundary conditions.

On the other hand, this formulation is not able to include: material damping, nonlinear behaviour, permanent deformations, pore pressure build up and gaping. The previous list of characteristics of soil that it is not able to reproduce are listed in order of how relevant they

are at low amplitudes of deformation of the soil. Since the expected amplitude of deformations on wind induced vibrations for high-rise buildings are small, characteristics such as material damping, nonlinear behaviour has some impact on the dynamic behaviour of the structure, while pore pressure build up and gaping might not even show up.

B.2.1.2 Linear visco-elastic

The simples linear soil modelling approach which includes damping is the viscoelastic approach. In this methodology, the stress constitutive relation includes both elastic and vicious damping parameters. The viscoelastic medium can be built with orthogonal and independent equations of motion a similar formulation as the viscoelastic idealization on the annex A.2 or they can be coupled through stress-strain law by the volumetric strain. For this formulation the stiffness matrix, D_{ijhk} contains real constant values and frequency dependant imaginary value, this matrix contains off diagonal terms that couples the stiffness in one principal direction with different DOFs. Ilaria Venanzi [15] mentions that commonly in practice the viscoelastic elements formulation used do not consider the coupling between the deformations on other degrees of freedom are prone to very low strain.

Similar to the linear elastic formulation it can be further simplified for the linear vico-elastic case. Where the 4D stiffness matrix can be decomposed into:

$$\sigma_{ij} = D_{ijhk}\varepsilon_{ij} = \left(K_b - \frac{2}{3}G\right)\varepsilon_{vol}\delta_{ij} + G\varepsilon_{ij} + \eta\frac{\partial\varepsilon_{ij}}{\partial t}$$

$$\varepsilon_{vol} = \frac{\partial u_j}{\partial j}$$

But in the same way as the elastic formulation This is normally just done to ease analytical calculation because using FE is more convenient to have a single stiffness matrix. But to avoid the frequency dependant values on the stiffness matrix the dynamic stiffness matrix is divided into the real stiffness D and viscous damping V. Which change the weak numerical formulation to:

$$\boldsymbol{M}\ddot{\boldsymbol{U}}(t) + \sum_{1}^{N_e}\int_{\Omega_e}\boldsymbol{B}^T\boldsymbol{V}\boldsymbol{B}d\,\Omega\,\dot{\boldsymbol{U}}(t) + \sum_{1}^{N_e}\int_{\Omega_e}\boldsymbol{B}^T\boldsymbol{D}\boldsymbol{B}d\,\Omega\,\boldsymbol{U}(t) = \boldsymbol{F}_{ext}(t)$$

This way by discretization it in space and integrating in time a Finite Element model with viscoelastic capabilities can be formulated.

This formulation contains the same capabilities and limitations as the linear elastic model with the only difference being that the addition of viscous damping can simulate the material damping. It is important to mention that it is only simulating the material damping because the damping introduced is frequency dependant. As it has been mentioned in the previous sections even though there is some frequency dependency of damping in clays, in general the damping is mostly amplitude dependant. The argument in favour of frequency dependant damping, reasons that this is a simple method to introduce damping and that even though it is frequency dependant, if the damping coefficient is chosen where the damping ratio is accurate for the natural frequency, ensuring an acuter damping at this frequency, which should have the biggest influence on the dynamic response. Even though there is some merit to this argument, a lot of time second and third natural frequency also carry significant energy as well as frequency content which also depends on the load. So, fixing the damping accuracy only to one frequency is not ideal.

B.2.1.3 Linear Complex Stress-Strain

Towhata [33] explains that a way of modelling the damping of soil that is not frequency dependant is to use a complex stiffness or complex stress-strain model. This model introduces an extra imaginary term to the stiffness, the real term has a completely linear behaviour in the force displacement curve, while the imaginary component has an elliptical behaviour in the force displacement curve. The result is a force displacement curve which resembles really well the form of the hysteretic curves. The simplest 1D, 1DOF it can be mathematically expressed in the equation:

$$\rho \frac{\partial^2 u_x}{\partial t^2} = G(1 + \mathrm{i}2\eta) \frac{\partial^2 u_x}{\partial x^2}$$

with,

$\mathrm{i} = \sqrt{-1}$

$\eta =$ Damping coefitient

Damping coefitient η is not the same as critical damping ratio ζ or vicious damping coefficient c. Damping coefitient η corresponds to the energy loss per cycle. Only in the specific situation of harmonic loading in the natural frequency the damping coefitient η is the same as the critical damping ratio ζ.

$$\eta = \frac{\nabla W(\omega = \omega_0)}{4\pi W} = \frac{c}{2\sqrt{mk}} = \zeta$$

Comparably as in the viscoelastic approach, the area under the complex stiffness curve and the area under the hysteretic laboratory measurements are calibrated to have an equivalent energy dissipation model. A limitation of this approach is that if deformations occur too much into the plastic regime the complex stiffness curve does not resemble the real hysteretic stress, in fact the model does not show a completely plastic regime, since it always increase with increasing deformations. Maximum deformations and strains reached are needed to be checked to ensure no over-stiffness on the plastic regime has occurred. A benefit of this approach over the viscoelastic approach is that the form of the hysteretic loop does not depend on the velocity or strain rate, which means that damping is applied more uniformly over all amplitudes.

To include this type of behaviour on the general linear model, the stiffness matrix, D_{ijhk} contains real constant values and frequency independent imaginary value, this matrix contains off diagonal terms that couples the stiffness in one principal direction with different DOFs.

This formulation contains the same capabilities and limitations as the linear elastic model with the only difference that the addition of complex stiffness can simulate the material damping and material nonlinearity. It is important to mention that even though it is a better simulation of the material damping and it introduces nonlinear stiffness, it can only be ensured that the amount of energy dissipated is accurate, but not that the shape of the stress strain curve can have difference. In fact, at different amplitudes the stress strain paths should not be the same. A problem with this amplitude dependency means that a very low amplitudes there is virtually no damping, and as it has been demonstrated in A. Ciancimino [37] there is a minimum damping always present at low amplitudes.

B.2.2 Nonlinear models

The formulation for the nonlinear models is the same as the linear models but with the difference that the introduction of material non-linearity changes the constitutive relationship since the stiffness matrix, D_{ijhk} is not constant. This also poses the problem where the convergence on internal forces equal to external forces is not as easy to fulfil and interactive methods such as Newton-Rapson algorithm which is needed to be used to reach a certain convergence tolerance. This means that at every step of the convergence algorithm the local tangent stiffness matrix needs to be recalculated and this matrix needs to be manipulated and eventually inverted for every interaction and for as many every time steps defined. This process is a very costly computation for systems with many DOFs, and in nonlinear systems it has to be done many times, while in linear systems it only needs to be done once. Other convergence algorithms can also be used to decrease the number of recalculation and inversion of the stiffness matrix at each time step. It is common to have problems with non-convergence or divergence while solving the problem, which requires tuning of the model.

The process described in the previous paragraph solves the system in the time domain. As presented previously for the linear system solving the system in the frequency domain was simpler and gave insight to several dynamic properties of the system. The nonlinear models are not able to be solved in the frequency domain, this is because in a nonlinear system the stiffness changes in time. Having a time dependency on the stiffness makes it so that when applying the Fourier Transform the we are not able to get rid of the time variable. This is a disadvantage of the method because the dynamic properties are not certain. These dynamic properties are so valuable that for the characterization of the structure that the system is often linearized to be able to have some value for the natural period or the frequency response function, even though it is known to be an oversimplification.

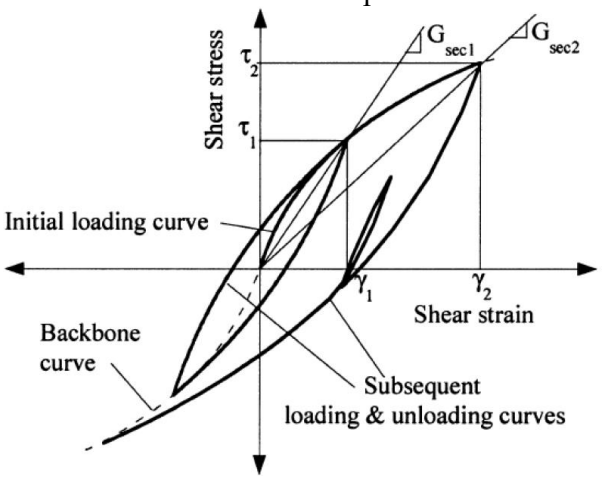

Figure B.5Idealized soil cyclic behaviour. Taken from F. Pizano [41]

B.2.2.1 Nonlinear elastic-plastic strain

For the formulation of the nonlinear elastic plastic the constitutive relationships used has a linear elastic initial phase and a linear plastic final phase. Since the stiffness is composed perfectly linear in the initial stage the solution can be found through linear means until any component of the systems reaches the bifurcation point in the strain stress relationship. The linear plastic phase can be either perfectly plastic, where the strain remains constant and has no stiffness, or it is linear but with a different stiffness than the initial one, normally called strain hardening. In Figure B.6 an illustration of the elastic plastic behaviour is presented.

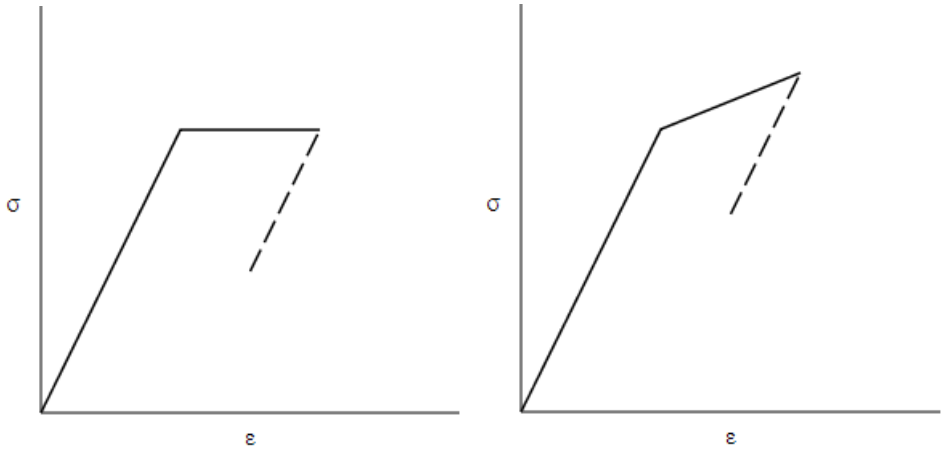

a) Perfect Plastic Model b) Plastic Kinematic Hardening (KH) Model

Figure B.6Illustration of the elastic plastic behaviour.

From a uniaxial (1D) perspective this material behaviour is introduce by the spring and slider model. The slider is an element with infinite rigidity that has a plastic deformation at a certain force. The models for perfect plastic (a), uniaxial KH plasticity (b) and multiaxial KH plasticity (c) are presented in Figure B.7. For the perfect plastic model, the elastic spring (with stiffness G) and the plastic slider (with capacity τ_f) are in series. The stiffness and plastic capacity relate one to one to the material behaviour. For the plastic hardening model, the elastic spring (with stiffness H) is added in parallel to the plastic slider, and this system is in series with the elastic spring (with stiffness G). In this case the stiffness of the spring in the elastic stage is given by G and for the plastic stage is the stiffness of both the springs in series. With the inclusion of more of this spring-slider a multiaxial KH plasticity model is constructed; this model can reproduce the gradual degradation of the secant stiffness.

This material model can model irreversible plastic differentiation which is depicted by the dash in Figure B.6 and the cyclic behaviour in Figure B.7. This characteristic is able to include permanent deformations and most importantly hysteretic damping. Other than the inclusion of nonlinear stiffness, hysteretic damping, and permanent deformations, it has the same capabilities as the linear elastic model previously presented. It is important to realize that the non-linearities included are an approximation of the real material properties, a multi-surface KH plasticity is the model that can get as close to the real stiffness nonlinearity of the soil, but its accuracy depends on how many spring-slider elements are added.

The hysteretic damping included in this formulation is dependent and proportional on the amplitude of the plastic strain. F. Pizano [41] illustrates this damping, total strain dependency on Figure B.8. From the figure it is clear that at very small strains no material damping is present so plastic strains do not dissipate energy. Including a high number of spring-slider elements, as presented in Figure B.8b makes the model capable of displaying hysteretic behaviour at smaller strain amplitudes. For all levels of complexity of the model the damping is rate independent.

a) Perfect Plastic Model

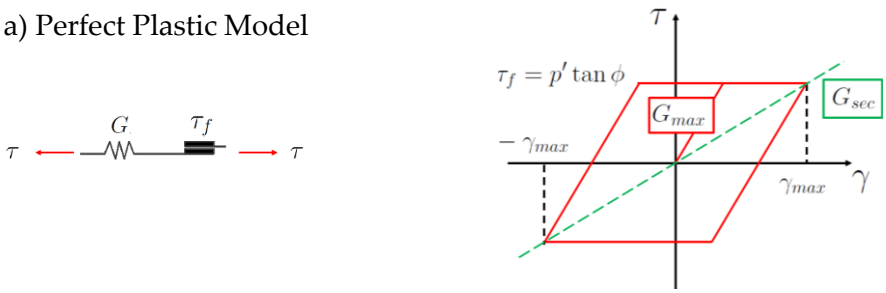

b) Uni-surface KH plasticity

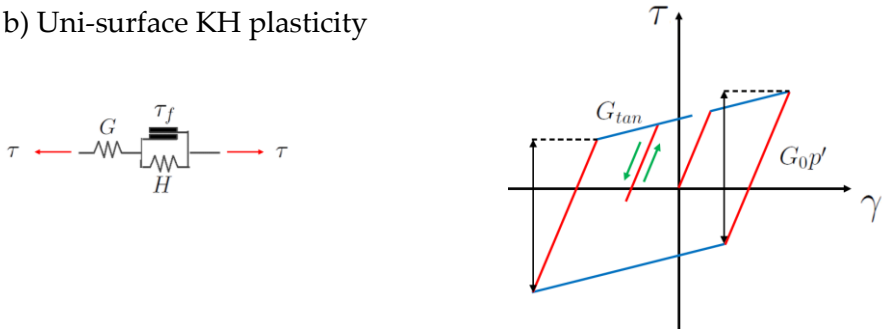

c) Multi-surface KH plasticity

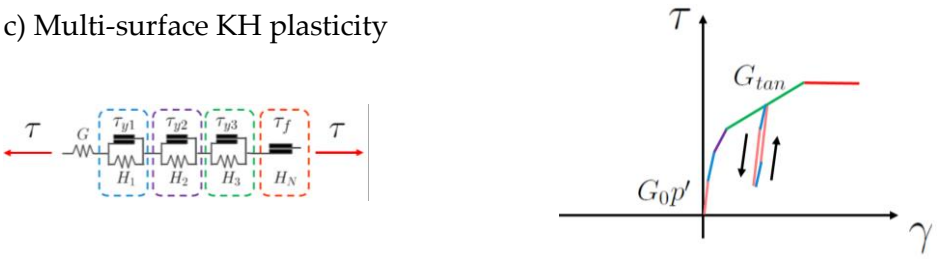

Figure B.7Cyclic elastic-plastic soil behaviour models. Taken from F. Pizano [41]

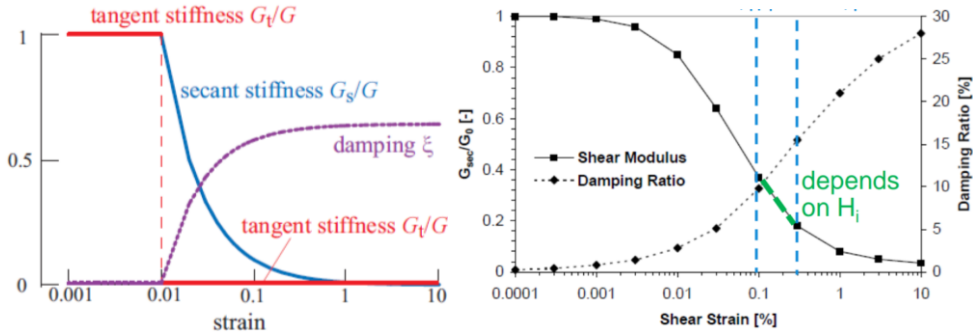

a) Perfectly plastic model c) Multi-surface KH plasticity

Figure B.8Nonlinear behaviour of stiffness and damping with respect to total strain. Taken from F. Pizano [41]

One of the biggest advantages of this model is that it has very low computational costs when the system is in the linear elastic range, because no iterations are needed to reach convergence of the stiffness. So, if an important part of the range of strains can be acutely represented by linear behaviour, this would decrease the computational effort to solve the system.

To pass from this 1D formulation to a 3D formulation several aspects need to be taken into account. Firstly, is the constitutive relations need to take into account the difference in stiffness behaviour between axial a shear deformation, as well as their coupling through the volumetric strain and the buck modules. As well defining yield a surface for every slider (on the 1D model it was a singe yield value for every slider).

Elgamal et al.[42] developed a 3D multi-surface KH plasticity model for sands known as the UCSD Sand Model. This method contains all the above characteristics mentioned, but also includes some extra characteristics of the soil. These additional behaviours are:

- Pleasure dependant elastic modulus for G and K
- Deviatoric flow rule
- Refined modelling of dilatancy
- Pore pressure build up

B.2.2.2 Nonlinear strain dependant stiffness

In the previous section the non-linearity was introduced through a combination of linear stiffness segments, other formulations aim to model a continuous definition of a stress dependant stiffness. One of these models is the Hardening Soil (HS) model developed by T. Schanz et al.in 1999. This model uses a hyperbolic stress-strain relationship for the soil, also taking into account the accumulation of plastic deviatoric strain. A summary of the governing equations taken from Benz, T. [43] is provided in Figure B.9a.

Elastic stiffness tensor:

$$D_{ijkl} = \frac{E_{ur}}{(1+\nu_{ur})(1-2\nu_{ur})}((1-2\nu_{ur})\delta_{ik}\delta_{jl} + \nu_{ur}\delta_{jk}\delta_{jl})$$

Yield functions:

$$\begin{aligned} f^s_{12} &= \frac{2q_a}{E_i}\frac{(\sigma_1-\sigma_2)}{q_a-(\sigma_1-\sigma_2)} - \frac{2(\sigma_1-\sigma_2)}{E_{ur}} - \gamma^{ps} \\ f^s_{13} &= \frac{2q_a}{E_i}\frac{(\sigma_1-\sigma_3)}{q_a-(\sigma_1-\sigma_3)} - \frac{2(\sigma_1-\sigma_3)}{E_{ur}} - \gamma^{ps} \text{ and} \\ f^c &= \frac{\tilde{q}^2}{\alpha^2} - p^2 - p_p^2 \text{ where} \\ \tilde{q} &= \sigma_1 + (\delta^{-1}-1)\sigma_2 - \delta^{-1}\sigma_3 \text{ with } \delta = \frac{3-\sin\varphi}{3+\sin\varphi} \end{aligned}$$

Plastic potentials:

$$\begin{aligned} g^s_{12} &= \frac{(\sigma_1-\sigma_2)}{2} - \frac{\sigma_1+\sigma_2}{2}\sin\psi_m \\ g^s_{13} &= \frac{(\sigma_1-\sigma_3)}{2} - \frac{\sigma_1+\sigma_3}{2}\sin\psi_m \text{ and} \\ g^c &= \frac{\tilde{q}^2}{\alpha^2} - p^2 - p_p^2 \text{ where} \\ \tilde{q} &= \sigma_1 + (\delta^{-1}-1)\sigma_2 - \delta^{-1}\sigma_3 \text{ with } \delta = \frac{3-\sin\varphi}{3+\sin\varphi} \end{aligned}$$

Mobilized dilatancy (modified Rowe):

$$\sin\psi_m = \frac{\sin\varphi_m - \sin\varphi_{cs}}{1-\sin\varphi_m\sin\varphi_{cs}} \geq 0, \text{ where}$$
$$\sin\varphi_{cs} = \frac{\sin\varphi-\sin\psi}{1-\sin\varphi\sin\psi}$$

Hardening laws:

$$\begin{aligned} d\gamma^{ps} &= d\lambda^s h_{\gamma^{ps}} \quad \text{with} \quad h_{\gamma^{ps}} = (\frac{\partial g}{\partial\sigma_1} - \frac{\partial g}{\partial\sigma_2} - \frac{\partial g}{\partial\sigma_3}) = 1 \\ dp_p &= d\lambda^c h_{p_p} \quad \text{with} \quad h_{p_p} = 2H\left(\frac{\sigma_3+c\cot\varphi}{p^{\text{ref}}+c\cot\varphi}\right)^m p, \text{ v} \\ H &= \frac{K_s K_c}{K_s-K_c} \quad \text{and} \quad K_s = \frac{E^{\text{ref}}_{ur}}{3(1-2\nu)} \end{aligned}$$

Stress dependent stiffness:

$$\begin{aligned} E_i &= E_i^{\text{ref}}(\frac{\sigma_3+c\cot\varphi}{p^{\text{ref}}+c\cot\varphi})^m \\ E_{ur} &= E_{ur}^{\text{ref}}(\frac{\sigma_3+c\cot\varphi}{p^{\text{ref}}+c\cot\varphi})^m \end{aligned}$$

(Para-)Elastic stiffness tensor:

$$D_{ijkl} = \frac{2G}{1-2\nu_{ur}}((1-2\nu_{ur})\delta_{ik}\delta_{jl} + \nu_{ur}\delta_{jk}\delta_{jl}) \text{ where}$$
$$G = \begin{cases} G_0\left(\frac{\gamma_{0.7}}{\gamma_{0.7}+a\gamma_{\text{Hist}}}\right)^2 & \text{for } \gamma_s < \gamma_c \\ \frac{E_{ur}}{2(1+\nu_{ur})} & \text{for } \gamma_s \geq \gamma_c \end{cases}$$

Yield functions:

$$\begin{aligned} f^s &= \frac{3}{2}\frac{q}{E_i}\frac{(\frac{1-\sin\varphi_m}{\sin\varphi_m})}{(\frac{1-\sin\varphi_m}{\sin\varphi_m})-R_f(\frac{1-\sin\varphi}{\sin\varphi})} - \frac{3}{2}\frac{q}{E_{ur}} - \gamma_s^{ps} \\ f^c &= \frac{q^2}{(\chi\alpha)^2} - p^2 - p_p^2 \text{ where} \\ \sin^2\varphi_m &= \frac{9-\frac{I_1 I_2}{I_3}}{1-\frac{I_1 I_2}{I_3}} \end{aligned}$$

Plastic potentials:

$$\begin{aligned} g^s &= q - (p + c\cot\varphi)\frac{6\sin\psi_m}{3-\sin\psi_m} \\ g^c &= \frac{q^2}{(\tilde{\chi}\alpha)^2} - p^2 - p_p^2 \text{ where} \\ \tilde{\chi} &= \chi(\theta_{\sigma_{Trial}}) \end{aligned}$$

Mobilized dilatancy (modified Rowe):

$$\sin\psi_m = \begin{cases} \frac{\sin\varphi_m-\sin\varphi_{cs}}{1-\sin\varphi_m\sin\varphi_{cs}} & \text{for } \sin\varphi_m - \sin\varphi_{cs} \geq 0 \\ \frac{1}{10}(Me^{\frac{1}{15}\ln(p_{cs}/p)} - \eta) & \text{for } \sin\varphi_m - \sin\varphi_{cs} < 0 \end{cases}$$
$$\sin\varphi_{cs} = \frac{\sin\varphi-\sin\psi}{1-\sin\varphi\sin\psi} \text{ and } \frac{p_{cs}}{p} = \frac{\eta\sin\varphi_{cs}(1-\sin\varphi_m)}{M\sin\varphi_m(1-\sin\varphi_{cs})}$$

Hardening laws:

$$\begin{aligned} d\gamma^{ps}_s &= d\lambda^s h_{\gamma^{ps}_s} \quad \text{with } h_{\gamma^{ps}_s} = \frac{3}{2} \\ dp_p &= d\lambda^c h_{p_p} \quad \text{with } h_{p_p} = 2H\left(\frac{\sigma_3+c\cot\varphi}{p^{\text{ref}}+c\cot\varphi}\right)^m p \\ H &= \frac{K_s K_c}{K_s-K_c} \quad \text{and } K_s = \frac{E^{\text{ref}}_{ur}}{3(1-2\nu)} \end{aligned}$$

Stress dependent stiffness:

$$\begin{aligned} E_i &= E_i^{\text{ref}}(\frac{\sigma_3+c\cot\varphi}{p^{\text{ref}}+c\cot\varphi})^m \\ E_{ur} &= E_{ur}^{\text{ref}}(\frac{\sigma_3+c\cot\varphi}{p^{\text{ref}}+c\cot\varphi})^m \\ G_0 &= G_0^{\text{ref}}(\frac{\sigma_3+c\cot\varphi}{p^{\text{ref}}+c\cot\varphi})^m \end{aligned}$$

Lode Matsuoka-Nakai dependency:

$$\chi(\theta) = \frac{\sqrt{3}\delta}{2\sqrt{\delta^2-\delta+1}}\frac{1}{\cos\vartheta} \text{ with}$$
$$\vartheta(\theta) = \begin{cases} \frac{1}{6}\arccos(-1 + \frac{27\delta^2(1-\delta)^2}{2(\delta^2-\delta+1)}\sin^2(3\theta)) & \text{for } \theta \leq 0 \\ \frac{\pi}{3} - \frac{1}{6}\arccos(-1 + \frac{27\delta^2(1-\delta)^2}{2(\delta^2-\delta+1)}\sin^2(3\theta)) & \text{for } \theta > 0 \end{cases}$$
$$\delta = \frac{3-\sin\varphi}{3+\sin\varphi}$$

a) Standard HS models c) HSsmall model

Figure B.9Governing equations. Taken from Benz, T. [43]

Benz, T. [43] explains that the HS model formulation neglects small strain stiffness since the base elastic stiffness is taken as the secant stiffness of large strains. Because of this a modification of the HS model with a Small-Strain Overlay model and including other failure

criteria is proposes. With the inclusion of this we have the formulation of the HSsmall model. This model includes all the parameters needed for the HS formulation with the addition of the stiffness of the soil at very small strains (G_0) and the threshold of shear strain ($\gamma_{0.7}$) at which G_0 is reduced by 70%. A summary of the governing equations taken from Benz, T. [43] is provided in Figure B.9b.

Brinkgreve [44] comments that this HSsmall model even though it is able to reproduce in general an accurate prediction of damping is soil, it often under predicts the damping at very low strain and over predicts the damping at higher amplitudes. Because of this Brinkgreve mentions that including a base kind of viscus damping (such as Rayleigh damping) can improve the model.

B.2.3 Direct modelling approach

As mentioned on the first section of this chapter, one of the approaches to SSI is the direct method. For this approach the structure, the foundation and the soil are all introduced in a single model and the analysis done in this sole model. The soil is normally model as a continuum through solid finite elements (FE), in a similar way the foundations and the structures are model with FE but often use beam elements, plane shear stress or others. A diagram of a 2D model using direct approach is shown in Figure B.10. The finite element method (FEM) is used to solve the governing equations, (usually in the time domain) where soil, foundation and structure are included in the same model and solved simultaneously.

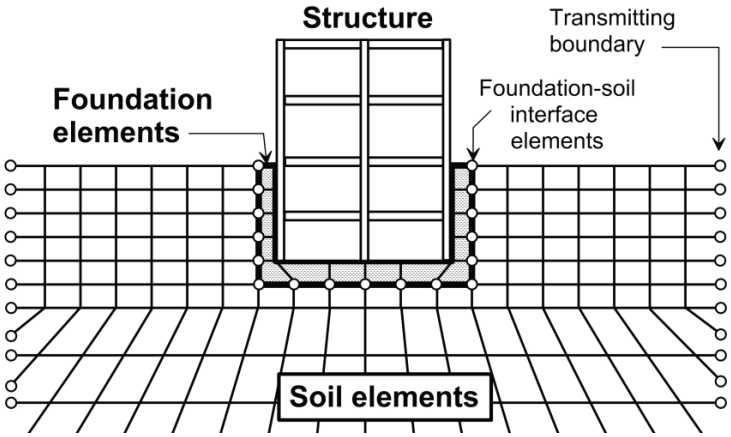

Figure B.10 Graphic representation of SSI using a direct analysis. Taken from NIST [9]

Other important features needed to be included on a direct approach are interface elements and soil boundaries. Most of the time the foundation elements and soil elements are of a different type and size so interface elements are used to appropriately link the elements. Interface elements are also used to introduce other phenomena such as gaping, which is when the soil and the foundation loose contact. The soil boundary is of outmost importance the direct approach, this topic is further exported on the section in soil modelling, but in a nut shell they are an artificial boundary introduced to simulate the radiation or reflection of waves crossing the boundary as they would if the soil continued indefinitely.

An advantage of the direct method is that from the model provides information of the displacements in the soil medium as well and not only from the structure. This is very helpful when trying to identify which components of the structure are the ones having a greater or lower impact in the damping and dynamic response of the building.

The direct approach of modelling SSI is in theory the most rigorous way to model the dynamic behaviour of the structure. Nevertheless, it come with several practical limitations for implementing it for real structures. The most important limitations are the computational demand, high modelling expertise requirement and the accuracy of material parameters.

With respect to the computational demand, M. Rizwan Raiz [45] shows that a full FE model taking into account accurate geometry, element representation and material non-linearities, is achievable with today's computing power, but it demands: an extreme amount of computations; as well as a lot of expertise, effort and time for the engineer making the model.

With respect to the material parameter, to accurately model the material non-linearities, a lot of material properties need to be known, for some materials such as steel this material properties might be well defined but for others like the soil it is more intricate. Taking soil as an example, in this report several nonlinear models were presented, all of which required large amount of dynamic soil parameters, and a lot of this parameters are not typically known from the testing done in practice. Furthermore, material properties are neither deterministic nor homogeneous, and some properties such as the ones from soil have a large scatter. For this reason, the author of this report questions the fidelity of a rigorous direct nonlinear time history analysis if so, much of the parameters are uncertain. M. Rizwan Raiz [45] mentions that to achieve the desired fidelity intended from this type of approach it would need to include a stochastic approach, which would further more increase the computational problem. This solution might be of interest academically but not a practical solution even with current high computing power.

B.2.4 Indirect modelling approach

The indirect approach, also known as substructure approach, is a practical way of simplifying the model, but also inducing SSI. It does this by introducing the foundation and soil as an equivalent set of springs and dashpots elements and a rigid interface in between these elements and the structure, as shown in Figure B.11. This system can be then easily solved in the frequency domain if nonlinearities are not included.

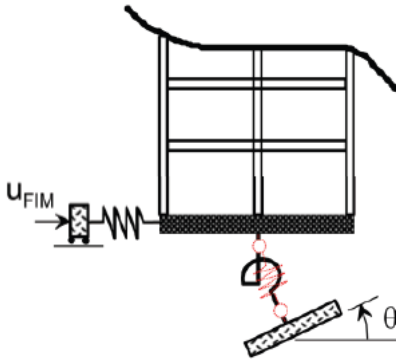

Figure B.11 Graphic representation of SSI using an indirect analysis. Taken from NIST [9]

This equivalent spring and dashpot elements are usually developed from analytical derivations and have to be calibrated with empirical results, so that they have the same effect on the structure as the foundation and soil. There are several foundation elements and several ways of introducing these elements, some of these technics are later explored in section 4.4. It is important to realize that a lot of the procedures developed for this methodology were made with earthquake motion in mind. NIST presents a procedure for the Substructure approach. It is important to mention that the NIST [9] document was redacted with seismic induced

vibrations in mind, which means some of the values and procedures might need some modification for the use in wind induced vibrations. For example in the model NIST [9] describes as the first steps of the procedure is to transfer the ground motion without the influence of the foundation to a motion of the foundation taking into account its influence. In the case of wind loading this would be different because the motion of the ground comes from the displacement of the foundation and not the other way around.

A limitation of the indirect approach is that foundations are considered rigid, this might be a more appropriate assumptions in some structures more than others. As well as, M. Rizwana Raiz [45] compared an indirect approach to a direct method. Rizwana points out that the dynamic impedance or inertia of the soil is neglected in the foundation equivalent element.

This approach has the flexibility of having various levels of complexity, both on the structure and the foundation (more on this in section 4.4), depending on the level of accuracy that is required. For example, a simple Timoshenko beam model for the structure, with concentrated mass at every storey height could be very useful at the preliminary design phase, where the general geometry is still being defined, but it is important to have a broad idea of how the structure should behave. Subsequently at later stages of the project, the structure can be modelled in a more accurate way showing results of hire fidelity and even being able to give member forces for element design.

B.3 Foundation modelling

B.3.1 Equivalent foundation models

As mentioned in section 2.3 there are different modelling approaches for SSI, the direct and indirect approach. The direct approach would make use the models presented in section 4.2 to model the soil, with the inclusion of interface elements to connect the different types of FE elements. But for the indirect approach there is a need to have simplified equivalent foundation models that incorporate the behaviour of the soil. There are several foundation models having various levels of complexity, some including more realistic behaviour of the interaction between the soil and foundation, this section presents the capabilities of several of the most used models. The various levels of complexity for modelling the foundation, give the engineer more flexibility to choose the modelling approach depending on the level of accuracy that is required.

A general limitation of this models is that incorporation of radiation damping through dashpots is limited on simulating one single interface of total radiation or with partial reflection but it cannot predict the internal reflection of several soil layers.

B.3.1.1 Winkler/Pasternak Models

The simplest model is the Winkler model which makes use of linear elastic independent and discrete springs to simulate the soil and over it, a foundation element, the springs are perpendicular to the surface, a diagram of this model is presented on Figure B.12. The only parameter needed from the soil is the Sub-Grade Reaction Modulus which is the pressure over the settlement. This type of foundation is able to include the deformability to the foundation and is able to change the stiffness of the entire system, which can lead to period lengthening effects. The Winkler model is normally used for shallow foundations but for piles the springs can be placed sounding the pile perpendicular to the surface. The foundation element can be

modelled by various types of elements, which means the foundation's rigidity can be taken into account. Some of the characteristics that it is not able to model with respect to soil are: nonlinear behaviour, shear capacity, material damping, radiation damping, pore pressure build-up, permanent deformations, gaping, soil inertia and group pile effects. Winkler's model with the use of nonlinear spring stiffnesses have also been developed as well, this can include energy dissipation from hysteric loops on the springs.

Pasternak Model shown on Figure B.12 is very similar to the Winkler model but it adds a shear beam model in between the soil and the foundation, to include the effects of the shear force between soil particles. The axial and shear elasticity are not coupled so they don't show the effect of bulk modulus in soils. An important shortcoming of both Winkler and Pasternak is that the deformations of the structure tends to be greater since they don't include damping but add the flexibility of the soil.

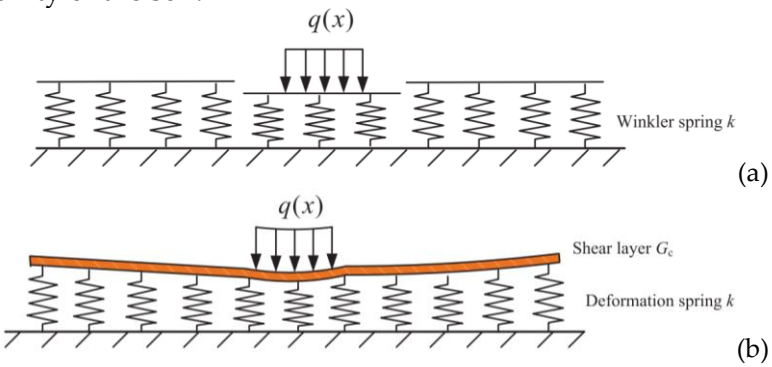

Figure B.12 (a) Winkler foundation model and (b) Pasternak foundation model. Taken from R. Liang 2019.

B.3.1.2 Wolfe's Cone Model

Another method looks to characterize the vertical, horizontal, rocking and torsional dynamic stiffnesses of the soil with the use of cone models. The cone model aims to substitute the 3D soil behaviour with a 1D infinite tapered rod that increases its cross-sectional area with depth, a 2D representation of this cone can be seen on Figure B.13. Through the increase in cross sectional area and infinite length the geometrical attenuation behaviour can be modelled. The angle of the cone is determined by the material properties of the soil. The most commonly used cone model is the one presented by Wolf and Deeks [46]. The degrees of freedom of this cone like rod are vertical, horizontal (2 directions), rocking (2 directions) and torsional. The result is an element where the vertical and tortional DOFs are uncoupled but the horizontal and rocking DOFs are coupled. Since the geometrical interaction of the soil is influenced by the wavelength, both the stiffness and the damping are frequency dependant. This frequency dependency is normalized to a dimensionless frequency (a_0) since what is important is the size of the wavelength in comparison to the size of the foundation.

The formulation of this model is introduce in Wolf and Deeks' [46] book. This formulation is able to introduce geometric attenuation through the increase in cross sectional area but eventually there needs to be a dashpot boundary that simulates the infinite boundary to model dissipation of energy to infinity. Because a rod is a non-dispersive system finding a dashpot boundary that does not reflect or refract waves is easier than for a 3D soil case. The introduction of the stiffness as viscoelastic also gives the opportunity to include material damping through the damping coefficient, even though it is a frequency dependant damping.

This Wolf cone formulation results on equations to build a dynamic stiffness matrix that can represent the foundation for the SSI model. The information needed to perform the wolf model are: Shear modulus of soil, Poisson's ratio of soil, density of the soil and geometry of the foundation. Other properties that appear in the formulas such as wave velocities and static stiffness can be derived from the previous material properties. Some of the characteristics that it is not able to model with respect to soil are: nonlinear behaviour, pore pressure build-up, permanent deformations, gaping and group pile effects. It is also important to mention that the cone model starts from an initial assumption of a stiff circular foundation which is not necessarily the case with most high-rise buildings.

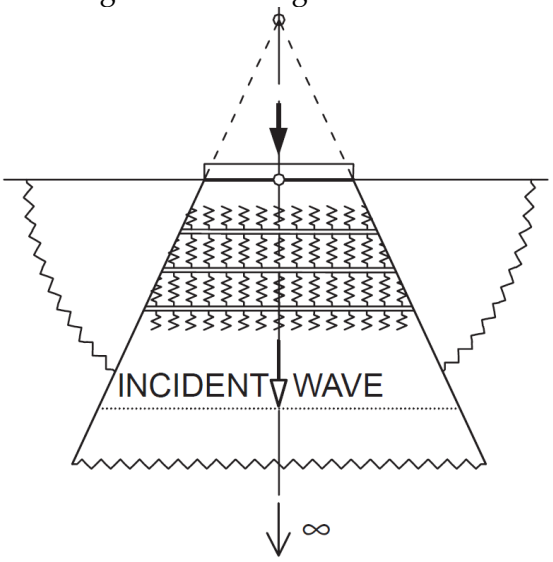

Figure B.13Illustration of Wave propagation in cone. Taken from Wolf and Deeks [46]

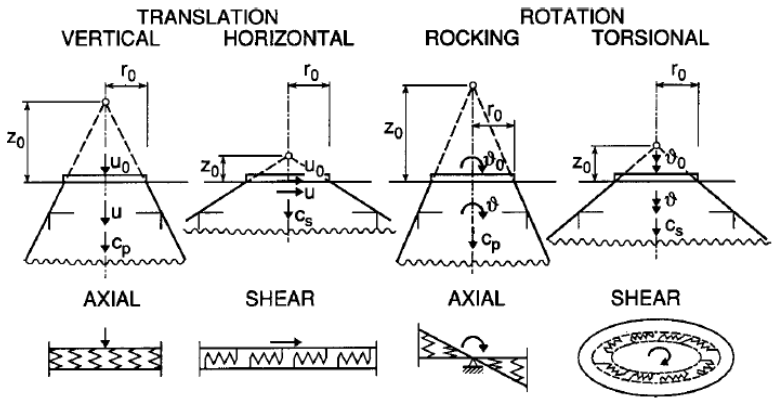

Figure B.14Representation of the different degrees of freedom in cones models. Taken from Wolf [47]

The cone model formulation is also able to capture reflection and refraction in soil layers, but this leads to solutions that are unique to each configuration of the problem so it cannot be generalized to a simplified set of formulas for the dynamic stiffness matrix of the foundation. For refracted waves it is done by a change in stiffness of the cone, the area at the interface has to be the same so the equivalent material property of the cone is what changes. Even though this new cone has the same cross-sectional area at the interface, because of the change in properties the slope of the cone changes. It is clear that the reaction would be the same as a continuous beam that has an abrupt change in stiffness, the reflection is a bit trickier. After the reaction we want the model to continue geometrically attenuate but if it is reflected to a beam which the cross-sectional area is decreasing there would be a concentration of the energy

rather than the attenuation, for this reason the rod needs to be swapped by an inverted cone rod with the same cross-sectional area at the interface but increasing cross sectional area in the direction of reflection. This process of reflection and reflection can be repeated for as many interfaces needed and each time it involves 2 new cones with matching cross-sectional area at the interface and increasing the cross-sectional area in the direction of wave propagation determined by the layer properties. At the end because the system is linear all the results can be supposed in space.

B.3.1.3 Rigid Foundation Empirical Models

The inclusion of damping is crucial, which lead several researchers to perform analytical soil half-space models which would be able to include the radiation and were embedded on the surface with constant soil properties. From the analytical models and finite element models, researchers came to approximate formulas that could accurately predict the static and dynamic properties of the foundation through material and geometrical properties of the foundation and soil, and present dynamic stiffness and damping values for the foundation. NIST [9] recommends equations from Pais and Kausel (1988), Gazetas (1991), or Mylonakis et al.(2006). The damping values come from radiation damping since what is evaluated in these models is the geometrical attenuation, which is introduced as vicious damping.

B.3.1.4 Pile Models

The small base of a high-rise building compared to its high causes the vertical load and the overrenting moment supported by the ground is considerably large. On soft soil this is a complication, which is solved by using pile raft type foundations. The inclusion of this piles helps both spread the load by increasing the surface area in contact of the soil, allows the depth of the pies allow to reach stronger soil layers and even provides tension resistance of the foundation. To increase the capacity of the foundation the piles can increase in diameter, depth or amount. From these options the most economical is normally to increase the number of piles, but as the piles get closer together the displacements imposed by one pile to the soil, start to significantly overlap between displacements imposed by the adjacent piles. This can lead to constructive or destructive interference between the pile movements, which is perceived as having an increase or decrease of dynamic stiffness compared to what would be expected on a single pile, due to having undisturbed soil surrounding the single pile. This change in the plie's impedance is known as lie group effect. At low frequencies such as the first natural periods of a high rise buildings the soil movements, somewhat resemble the transversal and rocking motions of the foundation, where the soil in between the pile moves fairly together. This means that a considerable mass is moving at important amplitudes and has great effects on the inertia and in general the dynamic response of the building. In fact, this extra soil mass contributes to the period lengthening effect mentioned previously. This effect has been vastly researched, Poulos [48] and several other experts agree that the pile group effects can lead to amplification of damping and a significant reduction of stiffness.

Another factor to take into account is that depending on the distance between piles and the wavelength of the soil disturbance there can be constructive or destructive interference acting of the piles. This means that this phenomenon is frequency dependent, because different wavelengths have different amount of amplification or attenuation of the pile movement. In NIST [9] it is taken into account through a dimensionless frequency which relates the size of the wavelength and the dimensions of the foundation. Y. Paauwe [11], modelled the stiffness

and damping of group piles for the soil properties expected in the Netherlands, and showed that at this low frequency expected from wind induced vibrations the stiffness was practically constant, and the damping ratio had a linear increase tendency. In NIST [9] some calculation for foundations with piles and shallow foundations are done and they found that the rocking and vertical dynamic stiffness with the inclusion of piles was around 50 times stiffer, the translational also increased but not as significant and maintain similar values but had important frequency dependent fluctuations. From these results it is clear that the pile group effect is an important SSI effect that needs to be taken into account to accurately predict the dynamic behaviour of high-rise buildings.

The equivalent foundations that have been introduced previously are all based on shallow foundations but most high-rise buildings are cemented on deep foundations, sometimes the shallow foundation approach can give a good estimation of the foundation with piles, but this generally is not the case. A procedure for determining the stiffness and damping of foundation with piles is provided in the NIST [9] document. Firstly, the static stiffness of a single pile is calculated from which the dynamic stiffness modifier is added. This dynamic stiffness is calculated for the vertical and horizontal stiffness at the base of the pile, for a single pile. To include the group pile effect, the individual capacity of each pile are added up and multiplied by an efficiency factor. In NIST [9] it is taken into account through a dimensionless frequency which relates the size of the wavelength and the dimensions of the foundation.

Using this procedure, the horizontal and vertical dynamic stiffness of the piles can be approximated and can be related directly to the horizontal and vertical dynamic stiffness of the total foundation. For the dynamic stiffness of rocking, it can be calculated with the geometry of the foundation (lever arm) and the vertical dynamic stiffness of the piles.

The information needed to include the pile impedance is: Shear modulus of soil, elasticity modulus of pile, Poisson's ratio of soil, density of the soil density of the pile and geometry of the foundation. Other properties that appear in the formulas such as wave velocities and static stiffness can be derived from the previous material properties. Some of the characteristics that it is not able to model with respect to soil are: nonlinear behaviour, pore pressure build-up, permanent deformations and gaping.

B.3.1.5 Macro-element Model

The Macro-element model was recently developed to tackle some of the limitations of the elastic models by including nonlinear material stiffness behaviour, different behaviour on loading and de loading. This is done by lumping the foundation behaviour onto a dynamic stiffness matrix derived from constitutive equations that relate the loads and moments to corresponding displacements and rotations. With these properties it could predict irreversibility of deformations and hysteretic behaviour. For this to be able to be modelled, the element needs to keep track of the past loading history, which means that the nonlinear dynamic stiffness matrix is both strain and time dependant. Salciarini and Tamagnini [49] describe formulation for macro element models using ether elastoplastic or hypoplastic behaviour. The elastoplastic formulation uses a linear stiffness with a Heaviside step function that activates the nonlinearity. The hypoplastic formulation modifies the tangential stiffness continuously accounting for previous loading, rate dependency and direction of loading. The hypoplastic formulation by Salciarini and Tamagnini [49] has 5 DOFs and requires a 5D matrix

and 2D matrix with the constitutive relations of the soil which take into account deformation, previous loading history and time dependency.

Ilaria Venanzi [15] points out that Macro-element system was developed to be able to model the coupling behaviour of stiffness on different DOFs, without the need of creating a FE of the inelastic soil continuum, by lumping the response of the foundation-soil interaction on one macro-element with a dynamic stiffness that matrix with coupling non diagonal terms, that in a way simulate the volumetric stress-strain behaviour of soil. This in combination with being able to account for nonlinearity and irreversibility behaviour of the soil makes for a foundation element that better represents the soil properties.

Recently there has been some macro element models developed for piles, in this review the focus is on the formulation by Zheng Li et al.[50] which is a formulation for a hypoplastic macro-element for single vertical piles in sand subject to 3D loading, which was calibrated using FE models and experimental results. The nonlinear hysteretic behaviour predicted on by the microelement compared to the experimental results on Figure B.15 show that the Macro-element is able to accurately showcase the nonlinear behaviour, and it is able to show progressive accumulation of irreversible displacements. The macro-element has the limitation that it is developed on homogeneous soil profile, Z. Li et al.[50] addressed this problem and showed that macro-element can be modelled without any significant deviations as a homogeneous soil if at least the top half of the effective length of the pile was one single soil layer. This was attributed to the pile deforming less as it gets deeper so the effect of the change in layer

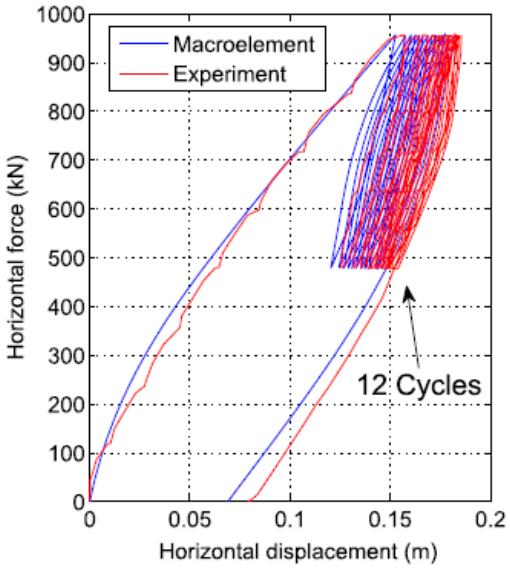

Figure B.15Vertical macro-element for singe pile nonlinear behaviour compared to experimental results. Taken from Li et al.[50]

The macro element approached has the drawback that it requires a lot of input parameters to construct the dynamic stiffness matrix, in Figure B.16 a table from formulation of hypoplastic Macro-element model foundation in sand by Zhuang Jin et al. [51] is presented. Because of the inclusion of these parameters and a more complete representation of the soil properties, the microelement model is able to perform a more realistic behaviour of the structure. From the studied literature, no information was found on the incorporation of pore pressure build up and pile grouped effects, to model. The field of study is very new so it may be that these

characteristics are currently being worked on or that they have just recently been developed and there is not much literature on the topic. Other limitation of the macro element model is: it does not take into account the flexibility of the foundation and the wave radiation modelling would all come from a point source. Finally, it is important to say that because of the stiffness non linearity the structure needs to be solved in the time domain. This can be considered a draw back since time integration is most often much more computationally demanding.

Parameters of the hypoplastic macroelement for a caisson foundation in sand.

Group	Parameters	Description	Value
Failure surface	V_0 (kN)	Vertical bearing capacity	90
	t_0 (−)	Tension factor	0.06
	e (−)	Eccentricity of the failure surface	0.91
	h_0 (−)	Dimension of the failure surface (horizontal)	0.068
	m_0 (−)	Dimension of the failure surface (moment)	0.045
	β_1, β_2 (−)	Shaping factors of the failure surface	0.96, 0.97
Pseudo-elastic stiffness	k_{vv} (kN/m)	Vertical stiffness	3100
	k_{hh} (kN/m)	Horizontal stiffness	3200
	k_{mm} (kN/m)	Rotational stiffness	1800
	k_{hm}, k_{mh} (kN/m)	Coupled translation-rotation stiffness	2500
Hardening parameter	κ (−)	Scaling function constant	1.1
Cyclic behaviour (internal displacement)	m_R (−)	Stiffness at load reversal point	10
	m_T (−)	Stiffness when neutral loading	2
	R (−)	Range of linearity	0.006
	β^r (−)	Rate of evolution of internal displacement	0.5
	x (−)	Transition of stiffness	0.5

Figure B.16Parameters needed to construct the dynamic stiffness matrix for macro-element. Taken from Zhuang Jin et al.[51]

Wind model

C.1 Wind velocity distribution

During a wind event, the wind speed it can be described as the sum of a constant mean value, $\bar{v}(z)$, in the primary direction and 3 zero-mean fluctuation components, one parallel to the mean value $\tilde{v}_{\parallel}(z,t)$ and two orthogonal, $\tilde{v}_{\perp,1}(z,t)$ and $\tilde{v}_{\perp,2}(z,t)$.

$$\underline{v}(z,t) = \begin{bmatrix} \bar{v}(z) \\ 0 \\ 0 \end{bmatrix} + \begin{bmatrix} \tilde{v}_{\parallel}(z,t) \\ \tilde{v}_{\perp,1}(z,t) \\ \tilde{v}_{\perp,2}(z,t) \end{bmatrix}$$

For a 1D model looking at loads only in the along-wind directions, the wind speed model can be simplified to only the mean wind speed and parallel component or the fluctuations.

$$\underline{v}(z,t) = \bar{v}(z) + \tilde{v}_{\parallel}(z,t)$$

These wind events has a time duration of around 10 minutes to an hour, and are offten segmented form a continues streem of date, as depicted in Figure C.1.

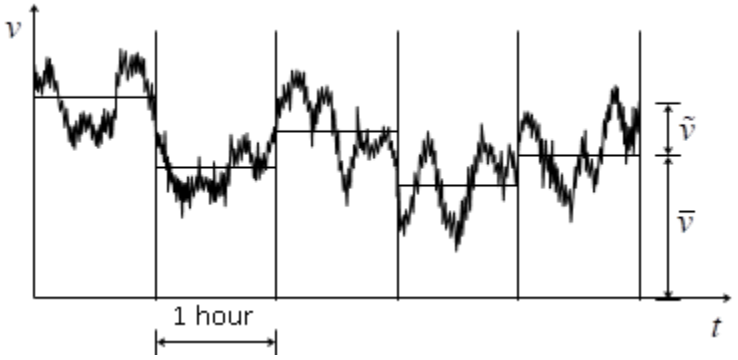

Figure C.1 Wind speed vitiation and segmentation of events. [10]

The average wind profile has a can be approximated through different models, the most well-known models which fit a logarithmic and exponential function [10]. Following the Eurocode EN 1991-1-4 [2], for this study the logarithmic velocity profile was used which is approximation using a logarithmic function and taking into account the roughness of the terrain.

$$\bar{v}(z) = v_b \cdot k_r \cdot \ln\left(\frac{z}{z_0}\right)$$

$$k_r = 0.19\left(\frac{z_0}{0.05}\right)^{0.07}$$

with:

v_b = reference wind speed at 10 m of height
$\bar{v}(z)$ = the mean wind speed at z
z_0 = terrain roughness length

The flutuations can be expresed in terms if the standard derivation of this wind velocity fluctuations. The Eurocode uses the next formula to calculate the standard deviation,

$$\sigma_v = v_b \cdot k_r = v_b \cdot 0.19\left(\frac{z_0}{0.05}\right)^{0.07}$$

with:

σ_v = standard deviation of the fluctuating component of the wind.

The characterization of these fluctuations with respect to frequency content distribution is of outmost importance. Researchers have developed several spectra that fit measurements.The modified Kaimal reduced spectrum, $S_L(z,f)$, recommended by the EN 1991-1-4 [2], uses the following equation,

$$S_L(z,f) = \frac{6.8 \cdot f_L(z,f)}{\left(1 + 10.2 \cdot f_L(z,f)\right)^{\frac{5}{3}}}$$

$$f_L(z,f) = \frac{f \cdot L(z)}{v_m(z)}$$

$$L(z) = L_t \cdot \left(\frac{z}{z_t}\right)^{\alpha}$$

$$\alpha = 0.67 + 0.05 \ln(z_0)$$

with:

$L_t = 300$ *[m]*
$z_t = 200$ *[m]*
$z_0 = ter$rain roughness length
f = frequency

The eurocode uses this modified Kaimal spectrum, but since it uses a wite noise spectrum, it evaluates the equation just the natural frequency instead of maintaining the frequency as a running variable.

From the distribution of the standard deviation of the wind speed and the reduced spectrum, the wind speed variance spectrum for every height, $S_{vv}(f,z)$, can be found with the next equation.

$$S_{vv}(z,f) = \frac{S_L(z,f){\sigma_v}^2}{f}$$

Later the a representative auto-variance spectrum for the entire area, will be needed. For this spectrum is evaluated at the reference hight (z_s), providing,

$$S_{vv}(f) = \frac{S_L(z = z_s,f){\sigma_v}^2}{f}$$

with:

z_s = Reference height of the structure ($z_s = 0.6H$)

C.2 Mean wind pressure and the associated spectrum

The wind is applying pressure on all exterior surfaces of the building. This pressure distribution for each area, can be calculated through the wind speed through the next equation.

$$p_w(z,y,t) = \frac{1}{2} C_p(y) \rho \left(\underline{v}(z,t)\right)^2$$

With:

$\rho_a = 1.25\ kg/m^3$ = air density
C_p = local dynamic pressure coefficient

This previous equation is making the assumption that the pressure at the surface of the building directly depends on the undisturbed wind velocity ($\underline{v}(z,t)$). This is important to mention because undisturbed wind velocity is not the same as the local wind velocity at the surface of the building, this local dynamic pressure coefficient (C_p) takes into account the geometry of the building and the direction of the wind flow to relate the undisturbed wind velocity to the pressure at different points of the cross-section. The structure was simplified to a rectangular cross-section and constant in height. The wind direction was assumed as perpendicular to the largest cross-sectional dimension. The last assumption is that the C_p coefficient was simplified to a constant coefficient along each face, which is the average from the real distribution. From the figure below its evident that the C_p coefficient for the front, back and sides are 0.8, -0.4, -0.8 respectively.

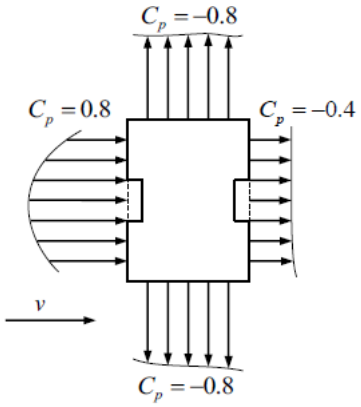

Figure C.2 Pressure coefficients (plan view) [2]

There are four surfaces from which we should add up their separate contributions, but because of the building geometry the contribution the pressure forms the perpendicular sides have no force component in the wind direction and in the perpendicular direction they cancel each other. Furthermore, since we are plaining on using the pressure on a global scale, it is suitable assume a constant width (B) and simplify the force from pressure per area to a distributed drag force per height. This also means that full correlation between wind velocities at the same height is assumed, even at different sides of the cross-section. This assumption is valid since from the beginning the pressure formula is from the global undisturbed flow and not the local wind velocity at the surface, also for the of the geometry of high-rise building the width of the building is much smaller than the height, so the variations of the wind in the width are negligible.

$$q(z,t) = \frac{1}{2} B \cdot C_D \cdot \rho_a \cdot \left(\underline{v}(z,t)\right)^2$$

$$C_D = C_{pF} - C_{pB} = 1.2$$

with:

$C_{pF} = 0.8$ = Front pressure

$C_{pB} = -0.4$ = Back pressure

C_D = Drag coefficient

In the previous sections the wind velocity was described as a sum of the a time independent mean wind velocity and a time dependant speed fluctuations. Introducing this separation of wind components to the force of the wind we obtain,

$$q(z,t) = \frac{1}{2} B \cdot C_D \cdot \rho_a \cdot (\bar{v}(z) + \tilde{v}_{\parallel}(z,t))^2$$

$$q(z,t) = \frac{1}{2} B \cdot C_D \cdot \rho \cdot (\bar{v}(z)^2 + 2 \cdot \bar{v}(z) \cdot \tilde{v}_{\parallel}(z,t) + \tilde{v}_{\parallel}(z,t)^2)$$

The wind fluctuations are typically of much smaller value than the mean wind velocity, so it can be assumed that the contribution of the fluctuations squared are negligible. Finally, taking into account that this is a linear system the problem can be solved as superposition of the static and the dynamic response.

$$q(z,t) = q_{St}(z) + q_{Dy}(z,t)$$

$$q_{St}(z) = \frac{1}{2} B \cdot C_D \cdot \rho_a \cdot \bar{v}(z)^2$$

$$q_{Dy}(z,t) = B \cdot C_D \cdot \rho_a \cdot \bar{v}(z) \cdot \tilde{v}_{\parallel}(z,t)$$

The static load can be solved directly, while the dynamic load is of stochastic nature and needs further manipulation. Also, as it is explain in further detail on the procedure of finding the dynamic response of the building, only the dynamic loading is of relevance to calculate the accelerations of the structure.

Since the dynamic stochastic load is an algebraic linear system with only one time dependent stochastic term, this allows to expressed this function in the frequency domain through the auto-variance spectra (S_{qq}) of the distributed wind drag force.

$$S_{qq}(z,f) = \left(B \cdot C_D \cdot \rho_a \cdot \bar{v}(z)\right)^2 \cdot S_{vv}(z,f)$$

This formula holds true for a single point, but since is needed for a large surfaces, we need to take into account that wind fluctuation peaks do not always happen at the same time, but they are also not completely independent processes. In other words, if taken the combined load the individual fluctuating wind loads, the result are in-between a fully corelated events (all peaks happening at the same time) and completely uncollated events (al the fluctuations would average out to zero). One way of taking this into account is to look for a reduction factor that takes the fully corelated event and reduces its magnitude to the expected value for its correlation levels.

To calculate this reduction factor, first the force acting a small section (dF) of the structure needs to be formulated. For this the equation for the dynamic pressure derived previously is used and multiplied by an infinitesimal height (dz) and width (dy),

$$dF(f) = C_D \cdot \rho_a \cdot \bar{v}(z) \cdot \tilde{v}_{\parallel}(z,t)\, dz$$

Integrating it to the entire structure to find the total force,

$$S_{FF}(f) = \iint_0^B \iint_0^H \left(C_D \cdot \rho_a \cdot \bar{v}(z_1)\right) \cdot \left(C_D \cdot \rho_a \cdot \bar{v}(z_2)\right) \cdot S_{v_1 v_2}(z_1, z_2, y_1, y_2, f)\, dz_1 dz_2 dy_1 dy_2$$

Introducing the formula the cross-variance spectrum ($S_{v_1 v_2}$) of the fluctuations [52],

$$S_{v_1 v_2}(z_1, z_2, y_1, y_2, f) = coh_{v_1 v_2} \sqrt{S_{v1v1}(z,f) \cdot S_{v2v2}(z,f)} = \frac{S_{vv}(f) {\sigma_v}^2}{f} e^{-f \cdot \frac{\Delta_{12}}{v_b}}$$

With Δ_{12} as:

$$\Delta_{12} = \sqrt{C_z^2 (z_1 - z_2)^2 + C_Z^2 (y_1 - y_2)^2}$$

From this simplifications and also takin out of the integral all z and y independent values,

$$S_{FF}(f) = (C_D \cdot \rho_a)^2 \cdot S_{vv}(f) \iint_0^B \iint_0^H \bar{v}(z_1) \cdot \bar{v}(z_2) \cdot e^{-f \cdot \frac{\Delta_{12}}{v_b}}\, dz_1 dz_2\, dy_1 dy_2$$

Calculating the response from the fully correlated, with the assumption that the wind velocity and fluctuations is the same for the entire building a reference height (z_h),

$$\tilde{S}_{FF}(f) = \left(H \cdot B \cdot C_D \cdot \rho_a \cdot \bar{v}(z_s)\right)^2 \cdot S_{vv}(f)$$

with:

z_s = Reference height of the structure ($z_s = 0.6H$)

This reference hight comes from the hight of the wind stagnation point which is an appropriate reference point for the overall admittance.

Introducing the reduction factor (χ^2), that makes both forces equal,

$$S_{FF}(f) = \chi^2 \tilde{S}_{FF}(f)$$

$$\chi^2 = \frac{S_{FF}(f)}{\tilde{S}_{FF}(f)}$$

Substituting for both total force variances.

$$\chi(f)^2 = \frac{1}{\bar{v}(z_s)^2} \iint_0^B \iint_0^H \bar{v}(z_1) \cdot \bar{v}(z_2) \cdot e^{-f \cdot \frac{\Delta_{12}}{v_b}} \, dz_1 dz_2 \, dy_1 dy_2$$

It is important to mention that this factor is frequency dependant since correlation its dependant on the wavelength. Going back to the auto-variance spectrum of the distributed wind drag force at the reference height, yields its equivalent cross-spectra.

$$S_{q_e q_e}(f) = S_{qq}(z_s, f) \cdot \chi(f)^2$$

$$S_{q_e q_e}(f) = S_{vv}(z_s, f) \cdot \left(B \cdot C_D \cdot \rho_a \cdot \bar{v}(z_s) \cdot \chi(f)\right)^2$$

It is common to group all the components multiplying the wind velocity spectra, into an aerodynamic admittance.

$$H_a^2(f) = \left(B \cdot C_D \cdot \rho_a \cdot \bar{v}(z_s) \cdot \chi(f)\right)^2$$

$$S_{q_e q_e}(f) = S_{vv}(z_s, f) \cdot H_a^2(f)$$

Bur for this study, for ease of further algebraic manipulation of the equivalent spectra of the distributed wind drag force was segmented into 3 different multiplying coefficients. First a constant coefficient that can be calculated from system parameters. Second a coefficient that varies with z coordinate. Third a frequency dependant coefficient.

$$S_{q_e q_e}(z, f) = Q_c^2 \cdot Q_z(z)^2 \cdot Q_{ff}(f)$$

$$Q_c = B \cdot C_D \cdot \rho_a \cdot \sigma_v^2$$

$$Q_z(z) = \ln\left(\frac{z}{z_0}\right)$$

$$Q_{ff}(f) = \frac{F_D(f) \cdot \chi(f)^2}{f}$$

Tower structure model

To model the dynamic behaviour of the high-rise building, a 1D continuous representation of the main load bearing structure as a cantilever beam was used. This model was assembled by means of a segmented Euler-Bernoulli beam, with the addition material damping of the beam as well as fully populated, frequency dependant, complex valued dynamics stiffness matrix as the support of the beam.

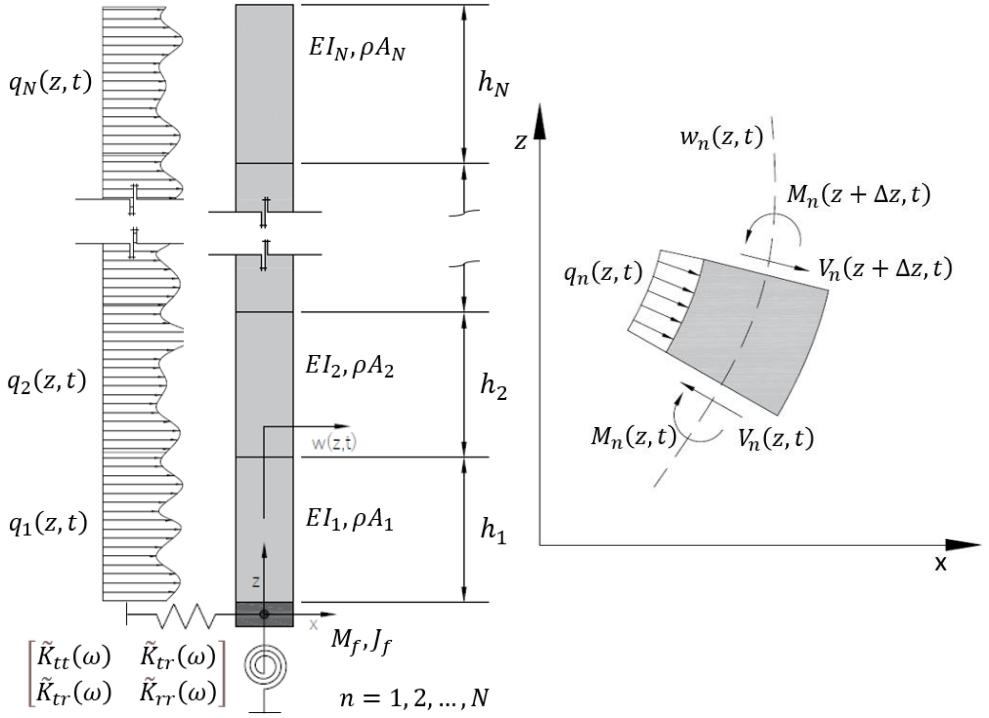

Figure D.1 Diagram of HF Tower structure model, showcasing the reference and coordinate systems.

D.1 Euler-Bernoulli beam governing equations

Each segment of the beam is modelled using the Euler-Bernoulli beam formulation. A graphical representation of the model is shown in Figure D.1. where the coordinate system and sign convention are depicted. Bending is descibed by $w(z,t)$, with in the positive x direction of the beam at a point in its length (z) and in time (t). The Properties of the beam are its density (ρ) $[kg/m^3]$, flexural stiffness (EI) $[Nm^2]$ and cross sectional area (A) $[m^2]$.

With the assumption that perpendicular sections of the beam remain perpendicular after deformation the angle of rotation (ϕ) can be calculated as well as the rate of change of the ϕ or curvature (κ):

$$\phi(z,t) = -\frac{d}{dz}w(z,t) \quad ; \quad \kappa(z,t) = \frac{d}{dz}\phi(z,t)$$

Assuming a linear distribution of strains and small deformation angles over the cross section of the beam the strain can be related to couverture by the following equation:

$$\varepsilon(z,t,x) = \kappa(z,t) \cdot x$$

Using the Hooke's law the linear material stress strain behaviour can be introduced as,

$$\sigma(z,t,x) = \varepsilon(z,t,x) \cdot E$$

Finally the moment can be described as the integral over the cross section of the stress times its lever arm.

$$M(z,t) = \iint_{\Omega} x \cdot \sigma(z,t,x) dA = E \cdot I(z) \cdot \kappa(z,t)$$

From the equilibrium of external forces $q(z,t)$ and inertial forces the following second order PDE is derived:

$$\frac{\partial^2}{\partial z^2} M(z,t) + q(z,t) = \rho A \frac{\partial^2}{\partial t^2} w(z,t)$$

When substituting for the previous relationships and assuming a constant inertia over the Equation of motion (EOM) of the beam can be rewritten as the 4th order PDE:

$$EI \frac{\partial^4}{\partial z^4} w(z,t) + \rho A \frac{\partial^2}{\partial t^2} w(z,t) = q(z,t)$$

Since the model is made of N number of beam segments with different distributed properties there is an equation of motion for each beam, such as,

$$EI_n \frac{\partial^4}{\partial z^4} w_n(z,t) + \rho A_n \frac{\partial^2}{\partial t^2} w_n(z,t) = q_n(z,t)$$

with,

$n = 1, 2, \dots, N$

but the result of w_n is only relevant on the location of each segment. For this reason this equations can also be rewritten without the subscript as,

$$w(z,\Omega) = \begin{cases} w_1(z,\Omega), & z_0 \geq z_1 \\ w_2(z,\Omega), & z_1 \geq z_2 \\ \vdots & \\ w_{n-1}(z,\Omega), & z_{n-2} \geq z_{n-1} \\ w_n(z,\Omega), & z_{n-1} \geq z_n \end{cases}$$

with,

z_{n-1}= starting z coordinate of beam segment n

z_n= ending z coordinate of beam segment n

D.2 Material damping

To model the material damping of the beam a stress dependant Kelvin-Voigt model can be used. (Berg, Steenbergen, 2013) Since both structural and non-structural elements interact by relative movements between each other. This is introduced in the form a rate dependent stress, which can be represented as a rate dependent term in the elasticity modulus:

$$\sigma(z,t,x) = \varepsilon(z,t,x) \cdot \left(E + E^* \frac{\partial}{\partial t}\right)$$

with $\eta = \frac{E^*}{E}$,

$$\sigma(z,t,x) = \varepsilon(z,t,x) \cdot E \left(1 + \eta \frac{\partial}{\partial t}\right)$$

Rewriting the EOM including the time dependent term in the elasticity modulus:

$$\rho A_n \frac{\partial^2 w_n(z,t)}{\partial t^2} + EI_n \left(\frac{\partial^4 w_n(z,t)}{\partial z^4} + \eta_n \frac{\partial^5 w_n(z,t)}{\partial t \partial z^4}\right) = q_n(z,t)$$

D.3 Boundary and interface conditions

For this model of we need to describe the boundary and interface conditions that describe a cantilever, segmented Euler-Bernoulli beam, with a fully populated dynamics stiffness matrix as the support of the beam. In this section the boundary and interface conditions are presented from the bottom to the top.

On the base the beam supported by the frequency dependant dynamic stiffness, from which shear forces and moments need to be balanced including the inertial forces from the foundation slab. As introduced on the chapter on foundation modelling, this dynamic stiffness matrix is complexed valued, so it has both an imaginary and a real part:

$$\overline{\overline{K}}_d(\omega) = \begin{bmatrix} \widetilde{K}_{tt}(\omega) & \widetilde{K}_{tr}(\omega) \\ \widetilde{K}_{tr}(\omega) & \widetilde{K}_{rr}(\omega) \end{bmatrix} = Re\begin{bmatrix} \widetilde{K}_{tt}(\omega) & \widetilde{K}_{tr}(\omega) \\ \widetilde{K}_{tr}(\omega) & \widetilde{K}_{rr}(\omega) \end{bmatrix} + i \cdot Im\begin{bmatrix} \widetilde{K}_{tt}(\omega) & \widetilde{K}_{tr}(\omega) \\ \widetilde{K}_{tr}(\omega) & \widetilde{K}_{rr}(\omega) \end{bmatrix}$$

This dynamic stiffness matrix relate force and displacement in the frequency domain. To express the this stiffness matrix in the time domain the inverse Fourier transform need to be applied the stiffness matrix in the frequency domain,

$$\mathcal{F}^{-1}\left(\overline{\overline{K}}_d(\omega)\right)\right) = \mathcal{F}^{-1}\left(Re\begin{bmatrix} \widetilde{K}_{tt}(\omega) & \widetilde{K}_{tr}(\omega) \\ \widetilde{K}_{tr}(\omega) & \widetilde{K}_{rr}(\omega) \end{bmatrix}\right) + \mathcal{F}^{-1}\left(i \cdot Im\begin{bmatrix} \widetilde{K}_{tt}(\omega) & \widetilde{K}_{tr}(\omega) \\ \widetilde{K}_{tr}(\omega) & \widetilde{K}_{rr}(\omega) \end{bmatrix}\right)$$

with,

$\mathcal{F}^{-1}$ = inverse fourier transfrom operator

Furthermore, formulating the system in the time domain with complex stiffness is a problem that can be solved by assimilating the imaginary part as dashpot,

$$\mathcal{F}^{-1}\left(\overline{\overline{C}}_d(\omega)\right) = \mathcal{F}^{-1}\left(Re\left(\frac{\overline{\overline{K}}_d(\omega)}{i\omega}\right)\right)$$

$$\begin{bmatrix} \mathcal{F}^{-1}(C_{tt}(\omega)) & \mathcal{F}^{-1}(C_{tr}(\omega)) \\ \mathcal{F}^{-1}(C_{tr}(\omega)) & \mathcal{F}^{-1}(C_{rr}(\omega)) \end{bmatrix} = \begin{bmatrix} \mathcal{F}^{-1}\left(Im\left(\frac{\widetilde{K}_{tt}(\omega)}{\omega}\right)\right) & \mathcal{F}^{-1}\left(Im\left(\frac{\widetilde{K}_{tr}(\omega)}{\omega}\right)\right) \\ \mathcal{F}^{-1}\left(Im\left(\frac{\widetilde{K}_{tr}(\omega)}{\omega}\right)\right) & \mathcal{F}^{-1}\left(Im\left(\frac{\widetilde{K}_{rr}(\omega)}{\omega}\right)\right) \end{bmatrix}$$

and the real part as a spring,

$$\begin{bmatrix} \mathcal{F}^{-1}(K_{tt}(\omega)) & \mathcal{F}^{-1}(K_{tr}(\omega)) \\ \mathcal{F}^{-1}(K_{tr}(\omega)) & \mathcal{F}^{-1}(K_{rr}(\omega)) \end{bmatrix} = \begin{bmatrix} \mathcal{F}^{-1}\left(Re\left(\frac{\widetilde{K}_{tt}(\omega)}{\omega}\right)\right) & \mathcal{F}^{-1}\left(Re\left(\frac{\widetilde{K}_{tr}(\omega)}{\omega}\right)\right) \\ \mathcal{F}^{-1}\left(Re\left(\frac{\widetilde{K}_{tr}(\omega)}{\omega}\right)\right) & \mathcal{F}^{-1}\left(Re\left(\frac{\widetilde{K}_{rr}(\omega)}{\omega}\right)\right) \end{bmatrix}$$

In this formulation the numbering of the EOMs starts also from the bottom so for the base the $n = 1$.

BC1: Shear force equilibrium at $z = 0$:

$$Ma = \sum F$$

$$M_f \frac{\partial^2 w_1(z,t)}{\partial t^2}\bigg|_{z=0} = V_1(z,t)|_{z=0} - F_{ktt} \otimes w_1(z,t)|_{z=0} + F_{ktr} \otimes \frac{\partial}{\partial z} w_1(z,t)\bigg|_{z=0}$$

$$\left(\boldsymbol{EI_1} + \boldsymbol{E^* I_1}\frac{\boldsymbol{\partial}}{\boldsymbol{\partial t}}\right)\frac{\boldsymbol{\partial^3 w_1(z,t)}}{\boldsymbol{\partial z^3}} + \boldsymbol{\mathcal{F}^{-1}}\left(\boldsymbol{K_{tt}(\omega)}\right)\otimes\boldsymbol{w_1(z,t)} + \boldsymbol{\mathcal{F}^{-1}}\left(\boldsymbol{C_{tt}(\omega)}\right)\otimes\frac{\boldsymbol{\partial w_1(z,t)}}{\boldsymbol{\partial t}} + \boldsymbol{M_f}\frac{\boldsymbol{\partial^2 w_1(z,t)}}{\boldsymbol{\partial t^2}} - \boldsymbol{\mathcal{F}^{-1}}\left(\boldsymbol{K_{tr}(\omega)}\right)\otimes\frac{\boldsymbol{\partial w_1(z,t)}}{\boldsymbol{\partial z}} - \boldsymbol{\mathcal{F}^{-1}}\left(\boldsymbol{C_{tr}(\omega)}\right)\otimes\frac{\boldsymbol{\partial^2 w_1(z,t)}}{\boldsymbol{\partial t \partial z}}\Bigg|_{\boldsymbol{z=0}} = \boldsymbol{0}$$

with,

$\otimes$ = Convolution operator

BC2: Moment equilibrium at $z = 0$:

$$J\alpha = \sum M$$

$$J_f\frac{\partial^3 w_1(z,t)}{\partial t^2 \partial z}\Bigg|_{z=0} = M_1(z,t)|_{z=0} + M_{krr}\otimes\frac{\partial}{\partial z}w_1(z,t)\Big|_{z=0} - M_{ktr}\otimes w_1(z,t)|_{z=0}$$

$$\left(\boldsymbol{EI_1} + \boldsymbol{E^* I_1}\frac{\boldsymbol{\partial}}{\boldsymbol{\partial t}}\right)\frac{\boldsymbol{\partial^2 w_1}}{\boldsymbol{\partial z^2}}\Bigg|_{\boldsymbol{z=0}} - \boldsymbol{\mathcal{F}^{-1}}\left(\boldsymbol{K_{rr}(\omega)}\right)\otimes\frac{\boldsymbol{\partial w_1(z,t)}}{\boldsymbol{\partial z}} - \boldsymbol{\mathcal{F}^{-1}}\left(\boldsymbol{C_{rr}(\omega)}\right)\otimes\frac{\boldsymbol{\partial^2 w_1(z,t)}}{\boldsymbol{\partial t \partial z}} - \boldsymbol{J_f}\frac{\boldsymbol{\partial^3 w_1(z,t)}}{\boldsymbol{\partial t^2 \partial z}} + \boldsymbol{\mathcal{F}^{-1}}\left(\boldsymbol{K_{tr}(\omega)}\right)\otimes\boldsymbol{w_1(z,t)} + \boldsymbol{\mathcal{F}^{-1}}\left(\boldsymbol{C_{tr}(\omega)}\right)\otimes\frac{\boldsymbol{\partial w_1(z,t)}}{\boldsymbol{\partial t}}\Bigg|_{\boldsymbol{z=0}} = \boldsymbol{0}$$

The formulation of BC1 and BC2, which includes convolution operations and inverse Fourier transforms are cleaner in the frequency domain.

Next the interface conditions between beams is described. An interface condition occurs for every connection between beam segments. In this case continuity of displacement, angle, shear and moment is expected in all the connections between segments so one general set of 4 interface conditions can be used to describe all possible interface conditions.

IC$_{m,1}$: Displacement continuity at $z = z_m$:

$$\boldsymbol{w_m(z,t)}|_{\boldsymbol{z=z_m}} = \boldsymbol{w_{m+1}(z,t)}|_{\boldsymbol{z=z_m}}$$

IC $_{m,2}$: Rotation continuity at $z = z_m$:

$$\frac{\boldsymbol{d}}{\boldsymbol{dz}}\boldsymbol{w_m(z,t)}\Big|_{\boldsymbol{z=z_m}} = \frac{\boldsymbol{d}}{\boldsymbol{dz}}\boldsymbol{w_{m+1}(z,t)}\Big|_{\boldsymbol{z=z_m}}$$

IC $_{m,3}$: Moment continuity at $z = z_m$:

$$M_m(z,t)|_{z=z_m} = M_{m+1}(z,t)|_{z=z_m}$$

$$\boldsymbol{EI_m}\frac{\boldsymbol{d^2}}{\boldsymbol{dz^2}}\boldsymbol{w_m(z,t)}\Big|_{\boldsymbol{z=z_m}} = \boldsymbol{EI_{m+1}}\frac{\boldsymbol{d^2}}{\boldsymbol{dz^2}}\boldsymbol{w_{m+1}(z,t)}\Big|_{\boldsymbol{z=z_m}}$$

IC $_{m,4}$: Shear continuity at $z = z_m$:

$$V_m(z,t)|_{z=z_m} = V_{m+1}(z,t)|_{z=z_m}$$

$$\boldsymbol{EI_m}\frac{\boldsymbol{d^3}}{\boldsymbol{dz^3}}\boldsymbol{w_m(z,t)}\Big|_{\boldsymbol{z=z_m}} = \boldsymbol{EI_{m+1}}\frac{\boldsymbol{d^3}}{\boldsymbol{dz^3}}\boldsymbol{w_{m+1}(z,t)}\Big|_{\boldsymbol{z=z_m}}$$

where:

$m = 1, 2, \ldots, (N-1)$

Finally the boundary conditions for the free end are moment and shear equal to zero for the final beam ($n = N$).

BC3: Zero Moment at $z = H$:

$$M_N(z,t)|_{z=H} = 0$$

$$\boldsymbol{EI_N \frac{d^2}{dz^2} w_N(z,t)\Big|_{z=H} = 0}$$

BC4: Zero Shear at $z = H$:

$$V_N(z,t)|_{z=H} = 0$$

$$\boldsymbol{EI_N \frac{d^3}{dz^3} w_N(z,t)\Big|_{z=H} = 0}$$

At the end the system of equation ends up with $4 \cdot N$ equations from the boundary conditions.

D.4 Modal properties of the system

The modal characteristics of the undamped system such as natural frequencies and mode shapes are computed by solving the system described above but with no forces and no material damping. This results in the set of homogeneous set of PDEs,

$$\rho A_n \frac{\partial^2 w_n(z,t)}{\partial t^2} + EI_n \frac{\partial^4 w_n(z,t)}{\partial z^4} = 0$$

This allows use to use the method of separation of variables, where $w_n(z,t)$ is assumed that can be described as the real part of the multiplication of a function of time $\Psi(t)$ and a function of space $W(z)$.

$$w_n(z,t) = W_n(z) \cdot \Psi_n(t)$$

Substituting into EOMs and dividing by $W_n(z) \cdot \Psi_n(t)$:

$$\frac{1}{\Psi_n(t)} \frac{\partial^2 \Psi_n(t)}{\partial t^2} + \frac{1}{W_n(z)} \frac{EI_n}{\rho A_n} \frac{\partial^4 W_n(z)}{\partial z^4} = 0$$

This leads to an equation where the equality to zero can only hold if the space dependent part and the time dependent part are equal to a same magnitude but opposite sign constant. This constant is equal to ω^2.

$$\frac{1}{\Psi_n(t)} \frac{\partial^2 \Psi_n(t)}{\partial t^2} = -\omega^2$$

$$\frac{1}{W_n(z)} \frac{EI_n}{\rho A_n} \frac{\partial^4 W_n(z)}{\partial z^4} = \omega^2$$

In the time domain it can be rewritten as, a 2nd order homogeneous ODE with a known solution.

$$\frac{\partial^2 \Psi_n(t)}{\partial t^2} + \omega^2 \Psi_n(t) = 0$$

$$\Psi_n(t) = E_n \sin(\omega t) + F_n \cos(\omega t)$$

In the space domain it can be rewritten as, a 4th order homogeneous ODE with a known solution.

$$\frac{\partial^4 W_n(z)}{\partial z^4} - \frac{\rho A_n}{EI_n} \omega^2 W_n(z) = 0$$

$$\beta_n^4 = \frac{\omega^2 \rho A_n}{EI_n}$$

$$W_n(z) = A_n \cdot \cosh(\beta_n z) + B_n \cdot \sinh(\beta_n z) + C_n \cdot \cos(\beta_n z) + D_n \cdot \sin(\beta_n z)$$

Substituting the solutions of $W_n(z)$ and $\Psi_n(t)$ to the BC and IC we get.

BC1:

$$EI_1 \frac{\partial^3 W_1(z)}{\partial z^3}\bigg|_{z=0} + \left(\mathcal{F}^{-1}\left(K_{tt}(\omega)\right) - \omega^2 M_f\right) W_1(z)\big|_{z=0} - \mathcal{F}^{-1}\left(K_{tr}(\omega)\right) \frac{\partial W_1(z)}{\partial z}\bigg|_{z=0} = 0$$

BC2:

$$EI_1 \frac{\partial^2 W_1(z)}{\partial z^2}\bigg|_{z=0} - \left(\mathcal{F}^{-1}\left(K_{rr}(\omega)\right) - \omega^2 J_f\right) \frac{\partial W_1(z)}{\partial z}\bigg|_{z=0} + \mathcal{F}^{-1}\left(K_{tr}(\omega)\right) W_1(z)\big|_{z=0} = 0$$

$IC_{m,1}$:

$$W_m(z)|_{z=z_m} = W_{m+1}(z)|_{z=z_m}$$

$IC_{m,2}$:

$$\frac{d}{dz} W_m(z)\bigg|_{z=z_m} = \frac{d}{dz} W_{m+1}(z)\bigg|_{z=z_m}$$

$IC_{m,3}$:

$$EI_m \frac{d^2}{dz^2} W_m(z)\bigg|_{z=z_m} = EI_{m+1} \frac{d^2}{dz^2} W_{m+1}(z)\bigg|_{z=z_m}$$

$IC_{m,4}$:

$$EI_m \frac{d^3}{dz^3} W_m(z)\bigg|_{z=z_m} = EI_{m+1} \frac{d^3}{dz^3} W_{m+1}(z)\bigg|_{z=z_m}$$

BC3:

$$EI_N \frac{d^2}{dz^2} W_N(z)\bigg|_{z=H} = 0$$

BC4:

$$EI_N \frac{d^3}{dz^3} W_N(z)\bigg|_{z=H} = 0$$

The result is a set of $4 \cdot N$ algebraic equations. That can be written in matrix form with $\bar{\bar{M}}$ as a matrix size ($4N$ x $4N$) for the coefficients and $\bar{C}$ as a vector of the constants of size ($4N$ x 1):

$$\bar{\bar{M}}\bar{C} = \begin{pmatrix} BC1 & 0 & 0 & & & & \\ BC2 & 0 & 0 & & & & \\ IC_{1,1} & IC_{1,1} & 0 & & & & \\ IC_{1,2} & IC_{1,2} & 0 & & & & \\ IC_{1,3} & IC_{1,3} & 0 & & & & \\ IC_{1,4} & IC_{1,4} & 0 & \cdots & & 0 & \\ 0 & IC_{2,1} & IC_{2,1} & & & & \\ 0 & IC_{2,2} & IC_{2,2} & & & & \\ 0 & IC_{2,3} & IC_{2,3} & & & & \\ 0 & IC_{2,4} & IC_{2,4} & & & & \\ & \vdots & & \ddots & & \vdots & \\ & & & & IC_{N-2,1} & IC_{N-2,1} & 0 \\ & & & & IC_{N-2,2} & IC_{N-2,2} & 0 \\ & & & & IC_{N-2,3} & IC_{N-2,3} & 0 \\ & & & & IC_{N-2,4} & IC_{N-2,4} & 0 \\ & 0 & & \cdots & 0 & IC_{N-1,1} & IC_{N-1,1} \\ & & & & 0 & IC_{N-1,2} & IC_{N-1,2} \\ & & & & 0 & IC_{N-1,3} & IC_{N-1,3} \\ & & & & 0 & \mathrm{I}IC_{N-1,4} & IC_{N-1,4} \\ & & & & 0 & 0 & BC3 \\ & & & & 0 & 0 & BC4 \end{pmatrix} = 0$$

where,

$$\bar{C}_n = \begin{bmatrix} A_n \\ B_n \\ C_n \\ D_n \end{bmatrix}$$

and $\bar{C}$ is the vector of stacked $\bar{C}_n$, such as,

$$\bar{C} = \begin{bmatrix} \bar{C}_1 \\ \bar{C}_2 \\ \vdots \\ \bar{C}_{n-1} \\ \bar{C}_n \end{bmatrix}$$

This homogeneous set of algebraic equations has valid solutions when the determinant of the confident matrix is equal to zero.

$$det\left|\bar{\bar{M}}\right| = 0$$

This equation is also known as the characteristic equation. The characteristic equation is transcendental so it has an infinite set of solutions. Since we are only interested on the first few modes this values can be solved numerically.

Having found the natural frequencies, and setting one of the constant to an arbitrary value the other constants can be calculated. Then substituting the arbitrary constant and the natural frequency to the space domain shape function solution:

$$W_n(z, \omega_i) = A_{n,i} \cdot \cosh(\beta_i z) + B_{n,i} \cdot \sinh(\beta_i z) + C_{n,i} \cdot \cos(\beta_i z) + D_{n,i} \cdot \sin(\beta_i z)$$

Finally the mode shapes can be computed by normalizing the previous function with respect to the end of the beam ($z = H$).

$$\Phi_n(z) = \frac{W_n(z, \omega_i)}{W_n(H, \omega_i)}$$

D.5 Dynamic response in the frequency domain

D.5.1 System setup

For this section the EOMs, BC and IC presented in the sections D.1 and D.3 were used. They were all formulated in the time domain. First they need to be transformed to the frequency domain through the Forward Fourier Transform (FFT):

$$G(z,\Omega) = \int_{-\infty}^{\infty} g(z,t) \cdot e^{-i\Omega t} dt$$

Using the of the FFT on the EOMs, BC and IC the system can be reformulated on the frequency domain as,

$$\frac{\partial^4 \widetilde{W}_n(z,\Omega)}{\partial z^4} - \frac{\Omega^2 \rho A_n}{\widetilde{EI}_n} \cdot \widetilde{W}_n(z,\Omega) = \frac{\tilde{Q}_n(z,\Omega)}{\widetilde{EI}_n}$$

BC1: $\widetilde{EI}_1 \frac{\partial^3 \widetilde{W}_1(z,\Omega)}{\partial z^3}\Big|_{z=0} + \left(\widetilde{K}_{tt}(\Omega) - \Omega^2 M_f\right)\widetilde{W}_1(z,\Omega)\Big|_{z=0} - \widetilde{K}_{tr}(\Omega)\frac{\partial \widetilde{W}_1(z,\Omega)}{\partial z}\Big|_{z=0} = 0$

BC2: $\widetilde{EI}_1 \frac{\partial^2 \widetilde{W}_1(z,\Omega)}{\partial z^2}\Big|_{z=0} - \left(\widetilde{K}_{rr}(\Omega) - \Omega^2 J_f \frac{\partial^2}{\partial t^2}\right)\frac{\partial \widetilde{W}_1(z,\Omega)}{\partial z}\Big|_{z=0} + \widetilde{K}_{tt}(\Omega) \cdot \widetilde{W}_1(z,\Omega)\Big|_{z=0} = 0$

IC$_{m,1}$: $\widetilde{W}_m(z,\Omega)\Big|_{z=z_m} = \widetilde{W}_{m+1}(z,\Omega)\Big|_{z=z_m}$

IC$_{m,2}$: $\frac{d}{dz}\widetilde{W}_m(z,\Omega)\Big|_{z=z_m} = \frac{d}{dz}\widetilde{W}_{m+1}(z,\Omega)\Big|_{z=z_m}$

IC$_{m,3}$: $\frac{d^2}{dz^2}\widetilde{W}_m(z,\Omega)\Big|_{z=z_m} = \frac{d^2}{dz^2}\widetilde{W}_{m+1}(z,\Omega)\Big|_{z=z_m}$

IC$_{m,4}$: $\frac{d^3}{dz^3}\widetilde{W}_m(z,\Omega)\Big|_{z=z_m} = \frac{d^3}{dz^3}\widetilde{W}_{m+1}(z,\Omega)\Big|_{z=z_m}$

BC3: $\frac{d^2}{dz^2}\widetilde{W}_N(z,\Omega)\Big|_{z=H} = 0$

BC4: $\frac{d^3}{dz^3}\widetilde{W}_N(z,\Omega)\Big|_{z=H} = 0$

with:

$$\widetilde{EI}_n = (E_n + i\Omega E_n^*) I_n$$

FFT of the loading ($\tilde{Q}_n(z,\Omega)$) assumes that this loading function can be written as a superposition of time-dependent harmonic function with space-dependent complex amplitude function. To understand the implications of this assumption, the forcing function needs to be defined. Since the only result of interest of the response of the structure is the acceleration only the dynamic wind loading presented in section C.2, is of relevance. This is because, static loading only provides the static deformation on the structure and since the model is linear it will not have any impact on the dynamic properties.

$$q_n(z,t) = q_{Dy}(z,t) = B \cdot C_D \cdot \rho \cdot \bar{v}(z) \cdot \tilde{v}_{\parallel}(z,t)$$

This formulation for the wind loading contains the term corresponding to the stochastic gusts amplitude, this term is both space and time dependent. But, as presented on section C.2, the gusts can be assumed to have no spatial dependence, from assuming that the gusts are fully correlated spatially,

$$\tilde{v}_{\parallel}(z,t) \approx \tilde{v}_{\parallel}(t)$$

$$q_n(z,t) \approx [B \cdot C_D \cdot \rho \cdot \sigma_v] \cdot \ln\left(\frac{z}{z_0}\right) \cdot \tilde{v}_{\parallel}(t)$$

With this formulation of the loads, expressed only as a function in time, also provides the possibility on expressing this function as a superposition of sinusoidal loads with random phase angle. Which provides easier manipulation on the frequency domain.

This is a big assumption, since this means that wind fluctuation peaks always happen at the same time. By using the aerodynamic admittance, introduced on the previous chapter, we take into account a reduction factor since wind fluctuation peaks do not always happen at the same time. This reduction factor (χ^2) was derived in section C.2, and in this same section it is shown how it is included in $Q_\Omega(\Omega)$, which ultimately ensures that collective wind load acting on large area has less variations compared to the fully corelated counterpart.

The FFT of the loads with this assumptions is expressed as,

$$\tilde{Q}_n(z,\Omega) = [B \cdot C_D \cdot \rho \cdot \sigma_v^2] \cdot \ln\left(\frac{z}{z_0}\right) \cdot Q_\Omega(\Omega)$$

The Solutions for the EMOs in the frequency domain can be found as a summation of the homogenous solution and the particular solution.

$$\widetilde{W}_n(z,\Omega) = \widetilde{W}_{h(n)}(z,\Omega) + \widetilde{W}_{p(n)}(z,\Omega)$$

The homogeneous solution being the same one used in the previous section.

$$\widetilde{W}_{h(n)}(z,\Omega) = \tilde{A}_n \cdot \cosh(\beta_n z) + \tilde{B}_n \cdot \sinh(\beta_n z) + \tilde{C}_n \cdot \cos(\beta_n z) + \widetilde{D}_n \cdot \sin(\beta_n z)$$

$$\beta_n = \sqrt[4]{\frac{\Omega^2 \rho A_n}{\widetilde{EI}_n}}$$

In a similar way as for the equivalent spectra of the distributed wind drag force, the wind force can segmented into 3 multiplying coefficients. First a constant coefficient that can be calculated from system parameters. Second a coefficient that varies with z coordinate. Third a frequency dependant coefficient. Using the same coefficient previously introduced for the constant term, the forcing function can be rewritten as,

$$\tilde{Q}_n(z,\Omega) = Q_c \cdot Q_\Omega(\Omega) \cdot \ln\left(\frac{z}{z_0}\right)$$

with:

$$Q_c = B \cdot C_D \cdot \rho_a \cdot \sigma_v^2$$

Furthermore, Van den Berg [53] proposes a way to simplify the calculations by fitting the logarithmic function with an exponential function,

$$\ln\left(\frac{z}{z_0}\right) \approx \left(a + b \cdot e^{-\frac{z}{c}}\right)$$

$$\tilde{Q}_n(z,\Omega) = Q_c \cdot Q_\Omega(\Omega) \cdot \ln\left(\frac{z}{z_0}\right) \approx Q_c \cdot Q_\Omega(\Omega) \cdot \left(a + b \cdot e^{-\frac{z}{c}}\right)$$

where a, b and c are constants that are used to approximate the logarithmic tendency of the wind distribution. Leaving as an unknown the frequency dependency, $Q_\Omega(\Omega)$.

To condense the equation even further the constant term, which depends on the wind and building properties, and the frequency dependant term, which contains the frequency content of the wind force, are grouped into a single term,

$$Q_W(\Omega) = Q_c \cdot Q_\Omega(\Omega)$$

so that,

$$\tilde{Q}_n(z,\Omega) \approx Q_w(\Omega)\left(a + b \cdot e^{-\frac{z}{c}}\right)$$

The particular solution that was used is,

$$\widetilde{W}_{p(n)}(z,\Omega) = Q_{a(n)}(\Omega) + Q_{b,c(n)}(\Omega) \cdot e^{-\frac{z}{c}}$$

which has the same form as the forcing function.

Now, by substituting the particular solution and the approximation for the forcing function in the EOMs on the left had side, it follows that,

$$\frac{1}{c^4} Q_{b,c(n)}(\Omega) \cdot e^{-\frac{z}{c}} - \beta_n^4 \left(Q_{a(n)}(\Omega) + Q_{b,c(n)}(\Omega) \cdot e^{-\frac{z}{c}}\right) = \frac{Q_w(\Omega) \cdot \left(a + b \cdot e^{-\frac{z}{c}}\right)}{\widetilde{EI}_n}$$

Both sides of the equality can be separated into exponential part and constants part, colour coded for clarity,

$$\left(\frac{1}{c^4} - \beta_n^4\right) Q_{b,c(n)}(\Omega) \cdot e^{-\frac{z}{c}} \quad - Q_{a(n)}(\Omega)\beta_n^4 \quad = \quad \frac{Q_w(\Omega) \cdot b}{\widetilde{EI}_n} \cdot e^{-\frac{z}{c}} \quad + \frac{Q_w(\Omega) \cdot a}{\widetilde{EI}_n}$$

Therefore, the values for the constants $Q_{a(n)}(\Omega)$ and $Q_{b,c(n)}(\Omega)$ are found as,

$$Q_{a(n)}(\Omega) = -Q_w(\Omega) \frac{a}{\widetilde{EI}_n \beta_n^4}$$

$$Q_{b,c(n)}(\Omega) = Q_w(\Omega) \frac{b}{\widetilde{EI}_n \left(\frac{1}{c^4} - \beta_n^4\right)}$$

With both constants being proportional to $Q_w(\Omega)$.

The solution can be rewritten as:

$$\widetilde{W}_n(z,\Omega) = \tilde{A}_n \cdot \cosh(\beta_n z) + \tilde{B}_n \cdot \sinh(\beta_n z) + \tilde{C}_n \cdot \cos(\beta_n z) + \tilde{D}_n \cdot \sin(\beta_n z) + Q_a(\Omega) + Q_{b,c}(\Omega) e^{-\frac{z}{c}}$$

D.5.2 Transfer function

By substituting the solution to the boundary and interface conditions, a set of $4 \cdot N$ algebraic equations is obtained. This equation can be manipulated by separating all terms that contain the constants to one side of the equation and the one with no constants to the other side. Furthermore, it can be written in matrix form with $\bar{\bar{M}}$ as a matrix size ($4N$ x $4N$) for the coefficients multiplied by $\bar{C}$ as the vector of the constants of size ($4N$ x 1) equal to $\bar{F}$ as the forcing vector of size ($4N$ x 1):

$$\bar{\bar{M}}(\Omega)\bar{C}(\Omega) = \bar{F}(\Omega)$$

where,

$$\bar{C}_n = \begin{bmatrix} A_n \\ B_n \\ C_n \\ D_n \end{bmatrix}$$

and $\bar{C}$ is the vector of stacked $\bar{C}_n$, such as,

$$\bar{C} = \begin{bmatrix} \bar{C}_1 \\ \bar{C}_2 \\ \vdots \\ \bar{C}_{n-1} \\ \bar{C}_n \end{bmatrix}$$

In the forcing vector there are all components from the boundary and interface conditions that do not have one of the unknown constants from the solution. Also the boundary and interface conditions only contains linear combinations of the solution and its derivatives. Because of this characteristics of the algebraic equation it is certain that the forcing vector is proportional to $Q_{\mathrm{w}}(\Omega)$. This means that from the forcing vector the $Q_{\mathrm{w}}(\Omega)$ can be factored out and can be rewritten it terms of a general forcing vector ($\bar{F}_0$) as,

$$\bar{F}(\Omega) = \bar{F}_0(\Omega) \cdot Q_{\mathrm{w}}(\Omega)$$

Using liner algebra the values of the constants can be solved.

$$\bar{C}(\Omega) = \bar{\bar{M}}(\Omega)^{-1}\bar{F}_0(\Omega) \cdot Q_{\mathrm{w}}(\Omega)$$

From this last equation it is clear that the constants are also proportional to $Q_{\mathrm{w}}(\Omega)$, so in the same way it can also be factored out, which means it can be written as,

$$\bar{C}(\Omega) = \bar{C}_0(\Omega) \cdot Q_{\mathrm{w}}(\Omega)$$

and consequently,

$$\bar{C}_n(\Omega) = \bar{C}_{0,n}(\Omega) \cdot Q_{\mathrm{w}}(\Omega)$$

Writing the sinusoidal terms of the homogeneous solution in vector format,

$$\bar{R}(z,\Omega) = \begin{bmatrix} \cosh(\beta_n z) \\ \sinh(\beta_n z) \\ \cos(\beta_n z) \\ \sin(\beta_n z) \end{bmatrix}$$

The solution can be written as,

$$\widetilde{W}_n(z,\Omega) = \bar{C}_n(\Omega) \cdot \bar{R}(z,\Omega)^T + Q_{a(n)}(\Omega) + Q_{b,c(n)}(\Omega)e^{-\frac{z}{c}}$$

The $Q_{\mathrm{w}}(\Omega)$ which engulfs all the components related to the frequency dependency and magnitude of the wind at a certain height can be seen as the forcing function. Also, from previous argumentation it is clear that all terms are proportional to $Q_{\mathrm{w}}(\Omega)$. Because of this proportionality, a transfer function (H_w) between displacement and force amplitude ($Q_{\mathrm{w}}(\Omega)$) can be found with,

$$H_{w(n)}(z,\Omega) = \bar{C}_{0,n}(\Omega) \cdot \bar{R}(z,\Omega)^T - \frac{a}{\widetilde{EI}_n\beta_n^4} + \frac{b}{\widetilde{EI}_n\left(\frac{1}{c^4} - \beta_n^4\right)}e^{-\frac{z}{c}}$$

$$\widetilde{W}_n(z,\Omega) = H_{w(n)}(z,\Omega) \cdot Q_{\mathrm{w}}(\Omega)$$

Taking into account that it was previously defined that, $Q_{\mathrm{w}}(\Omega) = Q_c \cdot Q_\Omega(\Omega)$, it can be written as,

$$\widetilde{W}_n(z,\Omega) = H_{w(n)}(z,\Omega) \cdot Q_c \cdot Q_\Omega(\Omega)$$

This transfer function $H_{w(n)}$ has a subscript n since every segment of the beam has its own solution for the deformation ($\widetilde{W}_n$), but the result of both $H_{w(n)}$ and $\widetilde{W}_n$ are only relevant on the location of each segment. For this reason this equations were rewritten without the subscript as,

$$\widetilde{W}(z,\Omega) = \begin{cases} \widetilde{W}_1(z,\Omega), & 0 \geq z_1 \\ \widetilde{W}_2(z,\Omega), & z_1 \geq z_2 \\ \vdots & \\ \widetilde{W}_{n-1}(z,\Omega), & z_{n-2} \geq z_{n-1} \\ \widetilde{W}_n(z,\Omega), & z_{n-1} \geq z_n \end{cases}$$

$$H_w(z,\Omega) = \begin{cases} H_{w(1)}(z,\Omega), & 0 \geq z_1 \\ H_{w(2)}(z,\Omega), & z_1 \geq z_2 \\ \vdots & \\ H_{w(n-1)}(z,\Omega), & z_{n-2} \geq z_{n-1} \\ H_{w(n)}(z,\Omega), & z_{n-1} \geq z_n \end{cases}$$

This frequency response transfer function (H_w) is noted by the subscript w since it is associated to the displacement and this is commonly called Mechanical Admittance. From the mechanical admittance, the transfer functions associated to velocity ($H_{\dot{w}}$, Mechanical Mobility) and to the acceleration ($H_{\ddot{w}}$, Mechanical Accelerance), can be computed from,

$$H_{\dot{w}}(z,\Omega) = i\Omega \cdot H_w(z,\Omega)$$
$$H_{\ddot{w}}(z,\Omega) = -\Omega^2 \cdot H_w(z,\Omega)$$

Furthermore, transfer function for the rotation angle can also be calculated through, the same procedure but using the first derivative of the displacement,

$$\phi(z,\Omega) = -\frac{\partial}{\partial z}\widetilde{W}_n(z,\Omega)$$

so,

$$H_\phi(z,\Omega) = \frac{-\frac{\partial}{\partial z}\widetilde{W}_n(z,\Omega)}{Q_c \cdot Q_\Omega(\Omega)}$$

This frequency response transfer functions are complexed valued and had to visualize in a complex decomposition, so it is common to calculate the amplitudes ($|H(z,\Omega)|$) and phase angles ($\theta_H(z,\Omega)$),

$$|H(z,\Omega)| = \sqrt{Im\big(FRF(z=H,\Omega)\big)^2 + Re\big(FRF(z=H,\Omega)\big)^2}$$

$$\theta_H(z,\Omega) = \arg\big(FRF(z=H,\Omega)\big) = \arctan2\left(\frac{Im\big(FRF(z=H,\Omega)\big)}{Re\big(FRF(z=H,\Omega)\big)}\right)$$

To visualize the mechanical properties of the system values for z need to be chosen. For example at the highest point of the building.

The Mechanical Accelerance that has been previously calculated is from the acceleration on the z direction algin the w degree of freedom, in other words the lateral component of the motion. But this is not the total apparent acceleration that someone would be subjected to on the surface of the structure in its local frame of reference. Since the structure also rotates the component of the acceleration due to gravity needs also to be included, this is depicted in Figure D.2. This effect would be also measured by the accelerometers since they are fixed paralleled to the story floor and rotate with it. The acceleration component due to this tilt would be,

$$H_{tilt}(z,\Omega) = -g \cdot \sin\Big(H_\phi(z,\Omega)\Big)$$

with,

g = gravitational constant (9.81 [m/s^2])

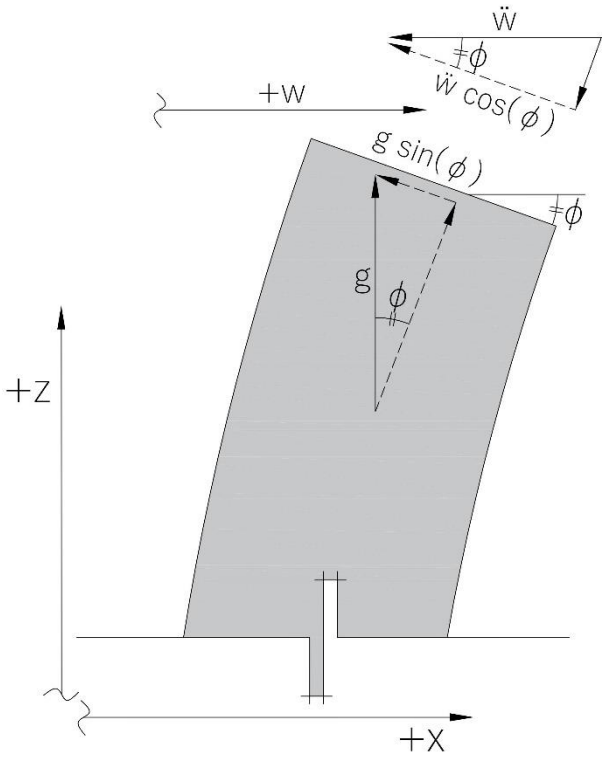

Figure D.2 Depiction of lateral and tilt acceleration component

Even though the acceleration components of the lateral movement and rotation are of stochastic nature, since the rotation comes from the derivative of the deformation both quantities are fully corelated leading to simple addition of their amplitudes, to find the overall apparent acceleration in a frame of reference fixed to the surface of the beam.

$$|H_a(z,\Omega)| = |-\Omega^2 \cdot H_w(z,\Omega)| + \left|-g \cdot \sin\left(H_\phi(z,\Omega)\right)\right|$$

Additionally, the trigonometric small angle approximations can be made since the rotation angles are expected to be small,

$$\sin(\phi) \approx \phi$$
$$\cos(\phi) \approx 1$$

Finally, this apparent acceleration can be approximated with,

$$|H_a(z,\Omega)| = |-\Omega^2 \cdot H_w(z,\Omega)| + \left|-g \cdot H_\phi(z,\Omega)\right|$$

The effect of tilt has been studied by [54]–[56] for the Laser Interferometer Gravitational-Wave Observatory (LIGO). The studies conducted by this observatory need to subtract the effects of tilt from the measurements since they are only interested on the lateral component of the acceleration.

D.5.3 Response Spectral Density Function

The deformation is calculated through the multiplication of transfer function and the forcing function. This forcing function is described in terms of a frequency dependent function (Q_Ω) which was obtain threw the Fourier transform of the time dependant component of the wind load. The stochastic wind load, $Q_\Omega \cdot Q_c$, is the single sided variance spectrum of the distributed wind drag force. But, to find the Dynamic Response Spectral Density Function (RSD) for a non-fully correlated stochastic system, the equivalent auto-variance spectrum is needed. In the wind model chapter in section C.2, the relation between the single sided and cross-spectra

was introduced. From this relation and introducing the transfer function the RSD function can be computed as,

$$S_{ww}(\mathrm{z},\Omega) = |H_w(z,\Omega)|^2 \cdot Q_c^2 \cdot Q_{\Omega\Omega}(\Omega)$$

Where the Q_c has been previously defined in the wind modelling chapter, and $Q_{\Omega\Omega}(\Omega)$ was defined in terms frequency $Q_{ff}(f)$ instead of angular frequency (Ω) in section C.2.

$$Q_c = B \cdot C_D \cdot \rho \cdot \bar{v}_b \cdot k_r \cdot \sigma_v$$

$$Q_{\Omega\Omega}(\Omega) = Q_{ff}\left(f = \frac{\Omega}{2\pi}\right) = \frac{F_D(f) \cdot \chi(f)^2}{f}$$

D.5.4 Dynamic Response

The dynamic response can be characterized by the acceleration Since this are stochastic processes, the mean value and the standard deviation of the acceleration are the relevant dynamic properties of interest. It is obvious that the mean acceleration of the building has to be equal to zero. The standard deviation can be computed through the integral of the RSD function,

$$\sigma_a(z)^2 = \int_0^\infty S_a(\mathrm{z},\Omega)d\Omega = \int_0^\infty |H_a(z,\Omega)|^2 \cdot Q_c^2 \cdot Q_{\Omega\Omega}(\Omega)d\Omega$$

$$\sigma_a(z) = Q_c \sqrt{\int_0^\infty |H_a(z,\Omega)|^2 \cdot Q_{\Omega\Omega}(\Omega)d\Omega}$$

Having the stochastic properties of the system, allows the expected peak value of the response to be approximated. The dynamic response can be characterized as a gaussian narrow banded process, if RSD functions has most of its density around the a single frequency. It is common that the motion at the top of the high rise building under wind loading, is mostly influenced by the first natural frequency (f_{n1}). So, it can be assumed as a gaussian narrow banded process. It is important to mention this verification of this assumption by looking at the RSD functions, since it does not need to be true in all cases. For example, for results that are shown on the case study, for accelerations at other heights of the building such as the ground floor there are more than one dominant frequency.

For the case of gaussian narrow banded process, when knowing this predominant frequency as well as the period (T) of the event, the expected peak response of high-rise buildings can be calculated with the next formula,

$$a_e(z,T) = \sigma_a(z)\left(\sqrt{2\ln(T \cdot f_0)} + \frac{0.6}{\sqrt{2\ln(T \cdot f_0)}}\right)$$

where,

$a_e(z,T)$ = expected peak acceleration at a certain z for an event of a period T
T = Duration of the event [s]
f_0 = central frequency [Hz]

This formula comes from calculating the expected amount of peaks that will occur during the event in question, and using the Gaussian normal distribution standard deviation to predict from that amount of peaks what would be the expected maximum acceleration.